Numerical simulations of continuum field theories and exotic quantum phase transitions.

Dissertation zur Erlangung des naturwissenschaftlichen Doktorgrades der Julius-Maximilians-Universität Würzburg

vorgelegt von:
Zhenjiu Wang
aus Dongping, Shandong, China
Würzburg 2020

Eingereicht am: .....
bei der Fakultät für Physik und Astronomie
1. Gutachter: .....
2. Gutachter: .....
3. Gutachter: .....
der Dissertation

Vorsitzender.....
1. Prüfer: .....
2. Prüfer: .....
3. Prüfer: .....
im Promotionkolloquiums

Tag des Promotionskolloquiums: .....

Doktorurkunde ausgehändigt am: .....

Abstract

In this thesis, we investigate several topics pertaining to emergent collective quantum phenomena in the domain of correlated fermions, using the quantum Monte Carlo method. They display exotic low temperature phases as well as phase transitions which are beyond the Landau–Ginzburg theory. The interplay between three key points is crucial for us: fermion statistics, many body effects and topology. We highlight the following several achievements: 1. Successful modeling of continuum field theories with lattice Hamiltonians, 2. their sign-problem-free Monte Carlo simulations of these models, 3. and numerical results beyond mean field descriptions.

First, we consider a model of Dirac fermions with a spin rotational invariant interaction term that dynamically generates a quantum spin Hall insulator. Surprisingly, an s-wave superconducting phase emerges due to the condensation of topological defects of the spin Hall order parameter. When particle-hole symmetry is present, the phase transition between the topological insulator and the superconducting phase is an example of a deconfined quantum critical point(DQCP). Although its low energy effective field theory is purely bosonic, the exact conservation law of the skyrmion number operator rules out the possibility of realizing this critical point in lattice boson models. This work is published in Ref. [1].

Second, we dope the dynamically generated quantum spin Hall insulator mentioned above. Hence it is described by a field theory without Lorentz invariance due to the lack of particle-hole symmetry. This sheds light on the extremely hot topic of twisted bilayergraphene: Why is superconductivity generated when the repulsive Coulomb interaction is much stronger than the electron-phonon coupling energy scale? In our case, Cooper pairs come from the topological skyrmion defects of the spin current order parameter, which are charged. Remarkably, the nature of the phase transition is highly non-mean-field-like: one is not allowed to simply view pairs of electrons as single bosons in a superfluid-Mott insulator transition, since the spin-current order parameter can not be ignored. Again, due to the aforementioned skyrmions, the two order parameters are intertwined: One phase transition occurs between the two symmetry breaking states. This work is summarized in Ref. [2].

Third, we investigate the $2 + 1$ dimensional O(5) nonlinear sigma model with a topological Wess-Zumino-Witten term. Remarkably, we are able to perform Monte Carlo calculations with a UV cutoff given by the Dirac Landau level quantization. It is a successful example of simulating a continuous field theory without lattice regularization which leads to an additional symmetry breaking. The Dirac background and the five anti-commuting Dirac mass terms naturally introduce the picture of a non-trivial Berry phase contribution in the parameter space of the five component order parameter. Using the finite size scaling method given by the flux quantization, we find a stable critical phase in the low stiffness region of the sigma model. This is a candidate ground state of DQCP when the O(5) symmetry breaking terms are irrelevant at the critical point. Again, it has a bosonic low energy field theory which is seemingly unable to be realized in pure boson Hamiltonians. This work is summarized in Ref. [3].

Zusammenfassung

In dieser Arbeit untersuchen wir verschiedene Themen über emergente kollektive Quantenphänomene im Bereich der korrelierten Fermionen unter Verwendung der Quanten-Monte-Carlo-Methode. Sie zeigen sowohl exotische Tieftemperaturphasen als auch Phasenübergänge, die jenseits der Landau-Ginzburg-Theorie liegen. Das Zusammenspiel von drei Schlüsselpunkten ist für uns entscheidend: Fermionenstatistik, Vielteilcheneffekte und Topologie. Es sind bemerkenswerte Erfolge erzielt worden: 1. Erfolgreiche Modellierung mehrerer kontinuierlicher Feldtheorien über Gitter-Hamiltonians. 2. Vorzeichenproblem-freie Monte-Carlo-Simulation von ihnen. 3. Numerische Ergebnisse jenseits des Molekularfeld-Verständnisses.

Zunächst betrachten wir ein Modell von Dirac-Fermionen mit einem spinrotationsinvarianten Wechselwirkungsterm, der dynamisch einen Quanten-Spin-Hall-Zustand erzeugt. Überraschenderweise entsteht eine s-Wellen-supraleitende Phase durch die Kondensation von topologischen Defekten des Spin-Hall-Ordnungsparameters. Wenn Teilchen-Loch-Symmetrie vorhanden ist, ist dieser Phasenübergang zwischen topologischem Isolator und Supraleiter ein Beispiel für einen dekondefinierten quantenkritischen Punkt (DQCP). Obwohl seine niedrigenergetische effektive Feldtheorie rein bosonisch ist, schließt der exakte Erhaltungssatz des Skyrmionenzahloperators die Möglichkeit aus, diesen kritischen Punkt in Gitter-Boson-Modellen zu realisieren. Diese Arbeit ist veröffentlicht in Ref. [1].

Zweitens dotieren wir den dynamisch erzeugten Quanten-Spin-Hall-Isolator von oben. Er wird aufgrund der fehlenden Teilchen-Loch-Symmetrie durch eine Feldtheorie ohne Lorenzt-Invarianz beschrieben. Dies wirft ein Licht auf das extrem heiße Thema des verdrehten Doppelschichtgraphens: Warum wird Supraleitung erzeugt, wenn die abstoßende Coulombwechselwirkung viel stärker ist als die Elektron-Phonon Kopplungsenergie? In unserem Fall kommen Kupferpaare aus den topologischen Skyrmiondefekten der Parameter der Spinstromordnung, die geladen sind. Bemerkenswerterweise ist die Art des Phasenübergangs in hohem Maße nicht molekularfeldartig: Es ist nicht erlaubt, ein Elektronenpaar einfach als einzelnes Boson in einem Superfluid-Mott-Isolator-Übergang zu betrachten, da der Parameter der Spin-Strom-Ordnung nicht ignoriert werden kann. Wiederum aufgrund der oben erwähnten Skyrimionen, sind zwei Ordnungsparameter miteinander verbunden: ein Phasenübergang findet zwischen den beiden Zuständen mit gebrochener Symmetrie statt. Diese Arbeit ist in Ref. [2].

Drittens untersuchten wir das 2 + 1-dimensionale nichtlineare O(5)-Sigma-Modell mit einem topologischen Wess-Zumino-Witten-Term. Bemerkenswerterweise sind wir in der Lage, Monte-Carlo-Berechnungen durchzuführen, mit UV-Cutoff gegeben durch die Quantifizierung der Dirac-Landau-Ebenen. Es ist ein erfolgreiches Beispiel für die Simulation einer kontinuierlichen Feldtheorie ohne Gitterregularisierung, die zu zusätzlichen Symmetriebrechungen führt. Der Dirac-Hintergrund und die 5 antikommutiernenden Dirac-Massenterme führen natürlich das Bild eines nicht-trivialen Berryphasen Beitrags im Parameterraum des Ordnungsparameters mit fünf Komponenten ein. Unter Verwendung der Methode der endlichen Größenskalierung, die durch Flussquantisierung gegeben ist, fanden wir eine stabile kritische Phase im Bereich der niedrigen Steifigkeit des Sigma-Modells. Dies ist ein Kandidat für den Grundzustand des DQCP, wenn die O(5)-Symmetrie brechenden Terme am kritischen Punkt irrelevant sind. Auch hier handelt es sich um eine niedrigenergetische bosonische Feldtheorie, die scheinbar durch reine Boson-Hamiltonians nicht realisiert werden kann. Diese Arbeit ist in Ref. [3].

Contents

1 Introduction

Landau–Ginzburg-Wilson theory (LGW)[4], established in 1957, has been viewed as a useful picture to understand phase transitions. One can construct the field theory considering a general function of fluctuating complex order parameters[1]: if the fluctuations are ignored, a nonzero, space and time independent order parameter indicates a spontaneous broken symmetry. The nature of transitions into a conventional superconducting state[5] or a number of magnetic systems are successfully described by this theory. Soon people got interested in looking for the universal behavior when the phase transition is continuous: the different transitions turned out to be classifiable into families called 'universality class' based on the symmetries as well as the physical dimensions of the system. The 'universal' reason why this always works originates from a symmetry: renormalization group invariance [6]. Approaching the critical point the characteristic length scale ξ diverges, and the system is invariant under scaling transformations.

Generally, LGW phase transitions can be driven by not only temperature but also quantum fluctuations [7]. Crossing a quantum critical point, normally there is a characteristic energy gap which closes, accompanied by the divergence of the correlation length. Thanks to the picture of path integral, one is allowed to map a D dimensional quantum system to a $D+1$ dimensional classical system where the inverse temperature of the quantum system plays the role of 'length' in the additional direction. Hence a wide range of quantum critical points have classical analogs. However, this sounds too good to be true: when one want to write a field theory with clean mathematics in $D+1$ dimension, certain approximations are required (apart from few simple examples).

On the other hand, the notion of path integral also introduces a new way of numerically solving the problem of many body physics. Trying to diagonalize numerically a many body Hamiltonian is a NP-hard problem, since the dimension of Hilbert space grows exponentially. However a path integral formulation in $D+1$ dimensional space time allows us to sample certain 'field' (where its definition depends on how the path-integration is formulated) configurations by a Markov process: the Monte Carlo method. The possibility of using Markov processes is based on the assumption that the field configuration have a certain Boltzmann weight. Crucially, it does not mean that a classical model with local interaction is found in $D+1$ dimension, although the number of fields (operators) that we need to sample scale linearly as a function of classical volume (βL^D). Especially in fermionic Monte Carlo, after integrating out variables with fermion statistics, the classical weight for an auxiliary field configuration can not be computed locally but necessarily involves the total information of single particle propagator which diverges as a function of dimension of fermionic single particle Hilbert space.

The LGW picture may break down in certain cases, e.g. when Fermi-statistics plays a role. A famous example for both QCD and condensed matter communities is the dynamical generation of massive Dirac fermions introduced by Gross and Neveu[8]. Opening of the fermionic mass gap necessarily involves a spontaneous symmetry breaking. But it can not be described by a LGW theory of only bosonic order parameters: fermion statistics is necessarily involved. The failure of the LGW picture in this case is very similar to the breaking down of classical analog in QMC simulation, in the sense that trying to integrate out fermions will lead to a infinite complicated non-analytic function of order parameters. We investigate an example of this critical point in $2+1$D

[1]Here we explicit mean theories described by commuting c-numbers in path integrals.

in Chapter. 3.

Another case where breaking down the LGW picture happens is when topology plays a role. The idea goes back to certain classical system: Kosterlitz–Thouless transition at 2 dimensional XY model[9]. Vortex-antivortex unbinding process explains the nature of infinite order transition. Unlike Goldstone modes, 'vortex' as a topological object is a local minimum in configurations in the sense of free energy: any smooth variation process of vectors fields in order to destroy the vortex must cross energy barriers. The zero temperature phenomena driven by quantum fluctuation is more exotic, and in many cases the notion of topology is also related to the aforementioned failure of simple quantum-classical analog in path integration: there is a phase factor contribution to the classical Boltzmann weight, namely the Berry phase. The Berry phase may lead to an additional global contribution which only depends on how the 'classical spin' configurations winds in space time. An example would be the one-dimensional $SU(2)$ spin chain[10]. It turns out that its ground state strongly depends on the spin quantum number: it is either gaped with two-fold degeneracy in the integer spin case, or critical when the spin is half integer. The underlining story is based on the role played by a topological theta term to the action of 1+1D: it is not only a theory where the gradients of local order parameters contribute to the Boltzmann weight, but also depends on how the order parameter winds in space-time. We write down the effective action of 1D spin chain as an example:

$$S = \int d^2x \frac{1}{g}(\partial_\mu \vec{n})^2 + \frac{i\theta}{8\pi}\epsilon_{\mu\nu}\epsilon_{abc}n^a\partial_\mu n^b\partial_\nu n^c. \tag{1}$$

It is easy for a mathematician to generalize the theory from 1D to 2D quantum systems. Take the theta term as an example, it simply means a generalization of $\pi_2(S_2)$ in $1+1$D to $\pi_3(S_3)$ in $2+1$D. One can view the topological invariant as a 'magnetic monopole' in a sphere of arbitrary dimension. However, this may not be enough for a student of condensed matter physics: generally we need to search for a many body Hamiltonian. We briefly discuss the underlining questions here.

Relation between lattice Hamiltonian and continuous field theories. For many designed Hamiltonian based on studying quantum phase transition, some pre-assumption is needed. One may need to know the phase diagram first by a mean field study; or a Monte Carlo simulation. Very often, venturing an educated guess makes sense. For example, a 'coupled dimer' model[11] on a 2D square lattice describes a Neel-paramagnetic transition which is described by the field theories of 3D non-linear sigma model: one is allowed to make this guess due to the known ground state in limiting cases. However, there are dangerous points.

Usually we work in a $2+1$D Euclidean space-time where we take the quantized lattice spacing a as the regulator. In the conventional case the continuum limit is approached in the limit of $a \longrightarrow 0$. For example, we can approximate the action of free scalar field[12] theory from partial derivatives of fields in continuous space into finite difference of fields in a cubic lattice. After path-integration over lattice fields of number which is proportional to $V/(a^D)$ (V denotes the volume) the continuous limit is reproduced. However a problem arises when we change to fermion statistics: generally we will encounter the so called 'fermion doubling' if we put local fermions on a lattice. If we perturb the lattice fermions by interaction, the doubling problem would introduce fundamental correlation effects. For example, if one wants to work with an effective 1D field theory which reproduces the edge physics of 2D quantum spin Hall insulator, certain technique of non-local fermions is needed to realize a single Dirac cone.

Mapping from a lattice Hamiltonian to local field theories with clean mathematics is generally not exact. Taking again the 1D Heisenberg chain as an example, higher order corrections during long wave length expansion are dropped during the derivation of Eq. 1. We show in Chapter. 7 a similar derivation of effective field theory based on integrating out gaped fermionic degrees of freedom. However a small but RG relevant correction may drive the system to another fixed point: the 'gaped spin liquid' state found in the 2D honeycomb lattice Hubbard model[13] may be an example, although a simple field theory based on magnetic order parameter coupled to free Dirac fermions would lead to a direct phase transition between Dirac semi-metal and anti-ferromagnetic state, which is described by a Gross-Neveu Heisenberg universality class.

Normally, the minimal request is that the symmetries of the continuous field theory are not explicitly broken by the lattice Hamiltonian. (Apart from the Poincare symmetry of space-time) However this condition is often relaxed when considering 'emergent' degrees of freedom: e.g. the gauge degrees of freedom after coarse-graining a lattice model with 'gauge fixing'[14], in the studies of lattice gauge theories. We show in Sec. 3 a quantum phase transition with an emergent non-compact U(1) gauge symmetry. Global symmetries are also subtle, since in some cases they are not exactly realized by the lattice Hamiltonian. More seriously, this symmetry breaking is often relevant under renormalization. Hence in many studies of interesting phase transitions, 'emergence' of global symmetries is required. In another words, the symmetry breaking field induced by the lattice discretization is relevant in a phase but irrelevant around the critical point. An interesting example is the thermal phase transition of 3D clock model with Z_4 anisotropy[15]: an emergent U(1) symmetry is found under renormalization at the critical point. This Z_4 symmetry is built in the internal degrees of freedom regardless of lattice, but several counterparts are found in 2D quantum phase transition: the semimetal-Valence bond solid (VBS) transition via interacting fermions which is believed to be a Gross-Neveu U(1) critical point[16]; the 'deconfined quantum critical point' based on AFM-VBS transition[17]. Both cases have VBS ordering in terms of lattice-induced Z_4 symmetry breaking, and surprisingly in the vicinity of both critical point Z_4 gives way to a $U(1)$ symmetry after coarse-graining. However it is crucial to mention that, neither of above two critical points (despite the similarity of symmetry) are described by the field theory of 3D clock model.

All of our studies are based on numerical investigation of correlated fermions. However, most of them are described by 'bosonic' field theories (apart from the SM-insulator transition in Chapter 3). This is because we are mainly interested in the low energy behavior, where the energy scales are much lower than the excitation energy of single fermions. In these cases, the low lying excitations are collective mode based on particle-hole(particle-particle) operators (e.g, goldstone modes). Note that the above argument does not necessarily mean that the correlated insulators in fermionic model are well described by simple bosonic second quantized Hamiltonian with 'local' interaction. For example, it is not possible to describe magnetic systems and superconductors in Hubbard-like models by a simple Heisenberg model: the nonzero local particle number fluctuation in Hubbard-like system introduces a different ground state as well as excited states. However, when we turn our attention to quantum critical points, they share the same universal behavior in most cases. Take the well-known $SU(2)$ symmetric Kondo lattice model[18] as an example: the magnetic property of the anti-ferro magnetic state driven by the effective RKKY interaction is different from any Heisenberg system of local interaction. However, in the vicinity of the transition point between

AFM state and Kondo insulator, the magnetization scales proportionally to δ^β: the universal number β is equivalent to the one of 2D bilayer Heisenberg model. That is why in many cases we can simply integrate out the fermionic degrees of freedom and get an effective field theory with just bosons (e.g. generalization of Eq. 1 to higher dimension).

Why don't we just simulate continuum field theory of c-numbers (e.g action of Eq. 1) by a classical Monte Carlo? Two killers exist. First, as aforementioned, the topological θ term in the example of Eq. 1 contributes a global sign factor of ± 1 to the Boltzmann weight of certain configurations. This is the notorious negative sign problem in Monte Carlo simulation. Second, after discretizing the field theory on a lattice, a specific engineering step is needed during the sampling process to keep a well-defined notion of 'topology'. The magic of a QMC approach based on our lattice Hamiltonian is that our c-numbers in $2+1$D is coupled to fermion degrees of freedom with certain symmetry (particle-hole, time reversal, etc.), such that the Boltzmann weight of all configurations after integrating out fermions are real and positive. On the other hand, the spacial-time distributions of our c-number configurations have no direct link to the topology: for example, we can not observe 'skyrmions' directly in Monte Carlo simulations.

Numerical efficiency. We focus on correlated fermions in this thesis, and our main method is auxiliary field quantum Monte Carlo (AFQMC) [19]. Its efficiency generally scales proportional to βL^{3d}; while the stochastic series expansion(SSE) [20] method based on bosonic models generally scales as βL^d. Followed by numerical simulation, our method of 'renormalization' on the lattice problem is finite size scaling (FSS). In the vicinity of a quantum critical point we assume that the free energy density as well as other dimensionless quantities scale as a function of ξ/L. One expect the correlation length ξ to be universal as a function of the distance to the critical point. Large system sizes are generally needed to acquire good scaling, since there are corrections to scaling: either from the fields which are irrelevant under RG, or from the non-singular part of the free energy, which is normally due to the short distance behavior of lattice Hamiltonian. Hence generally it is not efficient to study a quantum critical point with a bosonic effective field theory using fermionic Monte Carlo.

Summary of our results

During the thesis, we mainly studied two classes of lattice Hamiltonian, which are all based on correlated fermions. In Chapter. 2 we briefly review the basic structure of AFQMC method. The AFQMC has two approaches: fermion with thermal fluctuations at certain temperature (FTQMC) in a grand canonical ensemble; the ground state approach at a given particle number sector (PQMC), which does not reproduce a canonical ensemble since it's finite 'temperature' density matrix is projected to a artificial trial wave function. Our work on a canonical ensemble approach of QMC simulation at finite temperature is also briefly shown in this Chapter.

We will show several examples of non-Landau phase transition. Chapter. 3 includes two phase transitions: a Gross-Neveu critical point realized on Graphene system where its field theories necessarily involves fermions; and a deconfined quantum critical point [11], which can be captured by a bosonic field theory where the order parameter fails as an elementary object at the critical point. Chapter. 5 gives a numerical simulation of possible continuous field theory where the low energy cutoff is given by the landau level localization. Chapter. 4 introduces a doping induced insulator-

superconductor transition where the critical point is contrary to mean field behavior.

A famous example of Dirac fermions as emergent particles in 2D solid state system is Graphene[21]. Its non-interacting picture is based on free electron in p_z orbital hoping at a two dimensional Honeycomb lattice. Hence its ground state is neither an insulator or metallic state: low lying excitations has linear dispersion relation around the Dirac points. This state triggers two interesting questions. The first one is the correlation effects. At half filling, finite interaction may drive the ground state to an AFM, superconducting or charge density wave state.[22] (Here we ignore the difficultly of generating these phases in experimental approach.) All of these phases have gaped excitation of single electrons: they can be characterized by Dirac mass gaps where a certain symmetry is broken. If the interactions respect all the relevant symmetries, these examples of 'insulating' phase are spontaneous symmetry broken states.

The second one is the generation of topological band structure. Due to fermion statistics, there are complicated states of matter (i.e. topological insulator) beyond the notion of Landau order parameter even in the non-interacting case. Graphene gives the possibility of generating nontrivial topology without Landau quantization. Take the quantum spin hall system(QSH)[23] as an example, one needs to generate a Dirac mass which leads to a topological band structure. In any experimental approach of QSH insulator, finite spin-orbital coupling (SOC) is necessary to open the band gap: Dirac mass generation happens due to an explicit breaking of $SU(2)$ spin rotational symmetry. A toy model for understanding this behaviour is the Kane-Mele model, where terms of SOC are inserted to the Hamiltonian by hand. One is allowed to understand the notion of band topology by diagonalizing the single particle Hamiltonian and calculating the topological invariant by integrating over the Berry curvature in the bulk; or equivalently to understand the topological edge state by looking at a system with open boundaries.

In Chapter. 3 we show a new state of matter: topological Mott insulators[24]. It is basically a quantum spin hall insulator generated from a spontaneous broken of spin rotational symmetry. To approach this we used a spin rotational invariant interaction by combining spin current operators, such that at the mean field level a bosonic order parameter gaps the Dirac fermions and generate a Z_2 nontrivial QSH insulator. Hence from the symmetry point of view the phase transition from the Dirac semi-metal to QSH insulator is also described by Gross-Neveu Yukawa field theory. We will show numerical investigation of this Gross-Neveu Heisenberg transition, which belongs to the same universality class of the transition between semi metal and AFM driven by Coulomb interaction. Since the QSH state is generated from spontaneous symmetry breaking, it's excitation are characterised by Goldstone modes; moreover there are also skyrmions of the QSH order parameter. Remarkably a state with non-zero skyrimion number has nontrivial quantum number in the charge sector: a skyrimion of QSH order parameter carries charge number two. This brings interesting phenomena to two different critical points.

The aforementioned skyrimions are gaped objects in the QSH phase. Clearly one can destroy the QSH order by driving to another insulator state like charge density wave order, and in this transition the characteristic energy gap will be given by the fluctuation of spin current objects. On the other hand the notion of skyrimions will be useless in this case since they are always gaped. There are two ways to close this gap: either by tuning interaction (Chapter. 3) or doping (Chapter. 4). Specifically, the meaning of the 'gap' is the energy cost of a monopole insertion process: a monopole creates(annihilates) a skyrmion between different time slices. The fact that QSH skyrimions carries charge $2e$ gives a physical meaning for the skyrmion gap closing

process: a phase transition towards an s-wave superconducting state (SSC).

SSC is one kind of conventional superconductor which can be described by BCS theory[5]: singlet Cooper pairs which are time reversal invariant condenses at zero momentum. Our two routes to superconductivity (interaction or doping induced) are fundamentally different. The interaction induced QSH-SSC transition is one example of deconfined critical point (DQCP). The amazing numerical evidence of a direct and continuous phase transition between two ordered state can not be described by LGW picture when we only consider the spin current(transverse mode) or Cooper pair as elementary objects. One can view it from the opposite direction: the core of SSC vortex has nontrivial spin quantum number of $\frac{1}{2}$, which is also called 'spinons'. The gaped spinons in the superconducting state become gapless approaching the DQCP point, followed by their condensation into spin current objects in the QSH state. Hence the elementary objects at the critical point are not the $SO(3)$ and $U(1)$ order parameters(spin current and cooper pairs), but skyrimions and the spinons which are carried by the topological defects of order parameters. This is an analog of the DQCP proposed in AFM-VBS[11] transition, where AFM state breaks spin rotational symmetry and the VBS state breaks a Z_4 symmetry of the square lattice. The two critical points are very similar in the sense that, skyrimions of AFM order parameter carries the charge of VBS order parameter, and the VBS vortex carries spinons.

However there is a difference between the transition of AFM-VBS and the one of QSH-SSC. The VBS state necessarily breaks the lattice Z_4 symmetry: in the mean field level its ground state is always four fold degenerate. On the other hand its continuous field theory has a U(1) symmetry. As mentioned before, the $U(1)$ symmetry is recovered on the lattice in an emergent way, in the sense that the Z_4 symmetry breaking field is irrelevant at the critical point but relevant in the phase[17]. The dangerously irrelevant Z_4 symmetry breaking field introduced by the lattice quantization leads to the notorious 'two divergent length scales'. However in our case the SSC state can only spontaneously break the $U(1)$ charge conservation, which is an exact symmetry of our many body Hamiltonian. Generally, we do not even need to take care if we are working on the SSC state in a Honeycomb lattice or not. Hence in our case the lattice Hamiltonian describes the continuous field theory exactly. Either AFM-VBS or QSH-SSC transition can be described by bosonic field theory in the sense of finite gap of single fermions, hence one can start a field theory formulation by Dirac fermions. We can view AFM and QSH order parameters as O(3) order parameters coupled to fermions via Yukawa coupling in terms of Dirac mass terms, and one can build the VBS and SSC masses in a similar way. Then the notation of DQCP can be formulated by the competition of different masses, since the finite modulus of local order parameter corresponds to the gap of the Dirac fermions. Although their matrix structures are not the same, both two transitions are described by the competition between O(3) and $U(1)$ masses. Now we can see the subtlety of the fermionic formulation. A quantum spin model can be viewed as a 'gauge' theory in the sense that fermions have a $U(1)$ charge conservation locally. Now we lift the local $U(1)$ gauge redundancy by introducing hoping between fermions, such that when we formulate leading VBS component in the Dirac background, the action has an exact $U(1)$ symmetry. Note that it's only a trick of formulating field theories: for a fermionic lattice Hamiltonian, the VBS state in the Dirac background still breaks Z_4 symmetry. So can we reproduce the interaction induced QSH-SSC transition in a bosonic model? At a first glance, it is hard to exclude any lattice bosons in general. However, this could be explained by recent work[25]: the monopole free realization may necessarily requires gaped fermion degree's of freedom due to the 'emergent anomaly'

in our low energy field theory.

The second route to SSC generation via closing the gap of skyrmion excitation is by doping. This part will be shown in Chapter. 4. Unlike the aforementioned DQCP via interaction at half filled case, tuning the chemical potential breaks the particle-hole symmetry explicitly. Total particle number is still a good quantum number here, hence in many cases this kind of gap closing transition is 'trivial' when we are tuning the two parts of Hamiltonian which commute with each other. An example is the transition of Bose-Hubbard model[26] tuned by chemical potential: one know that the Mott insulator to superfluid transition is very nicely described by mean field theory in $2+2$ dimension. A superconductor is the same as a superfluid from the symmetry point of view, apart from the fact that the cooper pair is written as bounded object of two fermions. Hence a doping induced SSC state from a 'trivial' Mott insulator (say, a Kane-Mele model with attractive Hubbard interaction) should fall into the mean field category since we do not expect any intermediate metallic state.

As in the superfluid generation in the Boson-Hubbard model, the energy of exciting a cooper pair is a characteristic energy scale in the doping induced QSH-SSC transition. It decays linearly as a function of distance to the critical chemical potential. However it is only one part of the story. Recall that skyrmion defects of QSH order parameter carry charge 2. One can view the 'preformed pairs' by looking at excitation gaps at half filling in the QSH insulator: the excitation gap of a cooper pair is smaller than twice the gap of a single fermion. This is a close analog to the preformed pairs in high temperature superconductors. Hence the two order parameters are still locked in the doped case: the doped ground state with different particle numbers can be viewed as QSH insulators with different skyrimion numbers. (Of course the argument above only holds near half filling) We found by QMC study the transition is significantly different from the mean field expectation, in the sense that the critical chemical potential where SSC is generated is almost not distinguishable with the one where QSH ordering vanishes. The phase transition is either a continuous or a weakly first order one. Unlike the mean field transition in the Boson-Hubbard model, the dynamical exponent of the current critical point is significantly larger than 2. In this interesting example, we do not even know the nature of the field theory describing the critical point.

Now let's turn our attention back to the DQCP at half filling. The Dirac fermion formulation also gives a hint to a higher emergent symmetry group at the DQCP: an O(5) symmetry written by the euclidean rotation between five component order parameters (3 QSH and 2 SSC). Again this symmetry in the continuous field theory is exact only for the free Dirac action as well as the Yukawa coupling term due to the anti-commuting nature of the 5 Dirac masses: unless the interacting terms between bosonic order parameters are tuned in a specific way. This symmetry breaking term is important since we know that the higher symmetry is never respected by our lattice Hamiltonian. Crucially, there seems to be an emergent $O(5)$ symmetry right at the critical point shown by numerical simulations[27]. This means that the symmetry breaking term induced by the lattice might also be irrelevant: one can use an $O(5)$ invariant field theory to describe the critical point. Actually at this point one is allowed to write a clean field theory which is a sigma model at $2+1$D supplemented by a

topological Wess-Zumino-Witten (WZW)[28] term:

$$
\begin{aligned}
S &= \frac{1}{g}\int d^3x(\nabla\boldsymbol{\varphi})^2 + S_{\mathrm{WZW}} \\
S_{\mathrm{WZW}} &= \frac{2\pi i}{vol(S_4)}\int_0^1 d\mu \int d^2\boldsymbol{r} \int d\tau \epsilon_{abcde}\varphi_a\partial_x\varphi_b\partial_y\varphi_c\partial_\tau\varphi_d\partial_\mu\varphi_e
\end{aligned}
\tag{2}
$$

The aforementioned fact of charge $2e$ carried by QSH skyrimions, as well as the spin $1/2$ object carried by SSC vortices is encoded in this action. By the simplification based on assuming higher symmetry in the continuum limit, one see no difference between the AFM-VBS transition and QSH-SSC transition in this field theory. Without topological term, above theory has a Wilson-Fisher fixed point describing a $O(5)$ symmetry breaking phase transition in $3D$. When the WZW term is present, the large 'stiffness'$(1/g)$ limit of above theory still favors an ordered state, but the small stiffness region may favor a stable critical phase described by fractionalized object of order parameters.

How can we simulate the $O(5)$ invariant field theory mentioned above, since the high symmetry is not respected by any bosonic lattice model? Chapter. 5 shows a way which is followed by the picture of Dirac fermions: we can quench the fermions by magnetic field, and the UV regularization is given by the zeroth Dirac Landau level. Note that we are working in a continuum space instead of lattice Landau levels, such that the dimension of single particle Hilbert space is defined by the number of magnetic fluxes through the system. On the other hand, although the number of interaction operators is not bounded, its energy scale decays exponentially in the momentum space, such that a natural cutoff is obtained. On the other hand, the WZW topological term remains invariant under this approach of Landau Level quenching, since the interaction is still constructed by 5 anti-commuting Dirac masses.

When working on the interaction driven QSH-SSC transition on the lattice model, the notion of 'coupling' strength $1/g$ in sigma model is not very clear. One way to 'tune' it is to enlarge the range of spin current interactions, since it makes the fluctuation of spin current order parameters more energetically unfavorable. However we can not continuously tune the stiffness in this way. More generally, one could assume that our numerical evidence of a continuous phase transition between QSH and SSC is just an artifact of 'fine-tuning': two LGW-fixed point (a 3D O(2) and a 3D O(3)) just happened at the same point due to our detail designing of lattice interaction. The study of the sigma model based on LL projection in Chapter. 5 answers this question more generally. Here we do a have an interaction which does not change the symmetry of Hamilton: and tuning of this interaction continuously changes the stiffness of the sigma model. The important numerical result is that, we found numerically, the ground states in a finite range of coupling parameters is critical: this strongly suggests the absence of fine-tuning for DQCP.

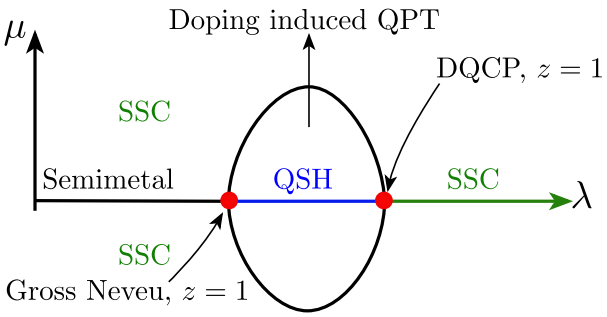

Figure 1: The ground-state phase diagram in Chapter. 3 and 4, as a function of interaction strength λ and chemical potential μ.

2 Methods

2.1 Auxiliary-field quantum Monte Carlo

2.1.1 General description

Generally, the starting point of quantum Monte Carlo is to write the partition function based on a many body Hamiltonian to a path integral formalism:

$$Z \equiv \mathrm{Tr}\, e^{-\beta H} = \int d\phi e^{-S(\phi)} \tag{3}$$

where $\phi \equiv \phi(\boldsymbol{i}, \tau)$ is a space and time dependent field. Specifically, we are interested in correlated fermions: the Hamiltonian H in the above formula is a function of creation (annihilation) operators in second quantized form. We can take the well known Hubbard model of spin $\frac{1}{2}$ fermions as an example:

$$\begin{aligned} &H = H_t + H_U \\ &H_t = -t \sum_{\boldsymbol{i},\boldsymbol{j},\sigma} c^\dagger_{\boldsymbol{i},\sigma} c_{\boldsymbol{j},\sigma} \qquad H_U = \frac{U}{2} \sum_{\boldsymbol{i}} (n_{\boldsymbol{i},\uparrow} + n_{\boldsymbol{i},\downarrow} - 1)^2 \end{aligned} \tag{4}$$

where the dimension of Hilbert space is 4^N for a N-site lattice. Working in the grand canonical ensemble, the definition of 'trace' for a second quantized operator is:

$$\begin{aligned} &TrO \equiv \sum_n \langle n|O|n\rangle \\ &|n\rangle \equiv (c^\dagger_{1\uparrow})^{n_{1\uparrow}} (c^\dagger_{1\downarrow})^{n_{1\downarrow}} ... (c^\dagger_{N\uparrow})^{n_{N\uparrow}} (c^\dagger_{N\downarrow})^{n_{N\downarrow}} |0\rangle \end{aligned} \tag{5}$$

As opposed to the stochastic series expansion (SSE) [29, 30] method, we perform a Trotter decomposition to Eq. 3:

$$\mathrm{Tr}\, e^{-\beta H} = \mathrm{Tr}\, (e^{-\Delta\tau H_t} e^{-\Delta\tau H_U})^{Ltrot} + \mathcal{O}(\Delta_\tau^2). \tag{6}$$

The leading correction of $\mathcal{O}(\Delta_\tau^2)$ holds in the case of Hubbard model, but we will show a general description in the following. For a general interaction written as the 'perfect square' of fermion bilinears we use an auxiliary field of four integers to perform Hubbard Stratonovitch (HS) decomposition:

$$e^{\Delta\tau A^2} = \sum_{l=\pm1,\pm2} \gamma(l) e^{\sqrt{\Delta\tau}\eta(l)A} + \mathcal{O}(\Delta_\tau^4). \tag{7}$$

where the explicit form of γ and η is shown in Ref. [31]. Here in the Hubbard model $A = i\sqrt{U/2}(n_{\boldsymbol{i},\uparrow} + n_{\boldsymbol{i},\downarrow} - 1)$. Hence for a given space time configuration $l(\boldsymbol{i}, \tau)$, we are dealing with a problem of free fermion propagation. The most important identity is:

$$Tr(e^{c^\dagger A_n c} ... e^{c^\dagger A_1 c}) = det(1 + e^{A_n} ... e^{A_1}) \tag{8}$$

Hence the fermion propagator after trace is simply a formula of matrices. We define the imaginary time propagator by a simplified notation $c^\dagger V(l_n) c \equiv \sqrt{\Delta\tau}\eta(l)A$ and $c^\dagger T c \equiv H_t$:

$$\begin{aligned} U_l(\tau_2, \tau_1) &= \prod_{n=n_1+1}^{n_2} e^{c^\dagger V(l_n) c} e^{-\Delta\tau c^\dagger T c} \\ B_l(\tau_2, \tau_1) &= \prod_{n=n_1+1}^{n_2} e^{V(l_n)} e^{-\Delta\tau T} \end{aligned} \tag{9}$$

Hence the weight of a given auxiliary field configuration can be written as a matrix form after tracing over the fermions:

$$Z = \sum_C A_C \,\mathrm{Tr}\,[U_l(\beta,0)] = \sum_C A_C \det[1 + B_l(\beta,0)] \tag{10}$$

where C denotes a certain distribution of l fields in space and time, and $A_C = \prod_{\tau=1}^{Ltrot}\prod_{i=1}^{N}\gamma(\boldsymbol{i},\tau)e^{i\eta(l)\alpha}$ (in the Hubbard example).

For a ground state study, we can also use the projector quantum Monte Carlo (PQMC) approach. We deal with the propagation problem from a given Slater determinant:

$$\begin{aligned} |\psi_T\rangle &= \prod_{y=1}^{N_p}(\boldsymbol{c}^\dagger P)_y|0\rangle \\ \langle\psi_T|e^{-2\Theta H}|\psi_T\rangle &= \sum_C A_C \det[P^\dagger B_l(2\Theta,0)P] \end{aligned} \tag{11}$$

Aim of quantum Monte Carlo is not to calculate partition function of Eq.3. We measure expectation values of operators. Take equal time quantities as example:

$$\begin{aligned} &\frac{\mathrm{Tr}\,[e^{-\beta H}O]}{\mathrm{Tr}\,[e^{-\beta H}]} && \text{FTQMC} \\ &\frac{\langle\psi_T|e^{-\Theta H}e^{-(\beta-\tau)H}Oe^{-\tau H}e^{-\Theta H}|\psi_T\rangle}{\langle\psi_T|e^{-(2\Theta+\beta)H}|\psi_T\rangle} && \text{PQMC} \end{aligned} \tag{12}$$

where O is a certain second quantized operator. When sampling over configuration space in a FTQMC simulation:

$$\begin{aligned} \frac{\mathrm{Tr}\,[e^{-\beta H}O]}{\mathrm{Tr}\,[e^{-\beta H}]} &= \sum_C P_C\langle\langle O\rangle\rangle_C \\ P_C &= \frac{A_C\det[1+B_C(\beta,0)]}{\sum_C A_C\det[1+B_C(\beta,0)]} \end{aligned} \tag{13}$$

The elementary measurement is the matrix of equal time single particle Green's function $O_{x,y} \equiv c_x^\dagger c_y$:

$$\langle\langle c_x^\dagger c_y\rangle\rangle_C = (1 + B_C(\tau,0)B_C(\beta,\tau))^{-1}_{x,y} \tag{14}$$

The corresponding equation for PQMC case can be found in Ref. [19]. Generally, to detect symmetry breaking based on particle-hole(particle-particle) order parameters, we need to measure multi-point correlation functions. They can be decoupled as products of single particle Green's functions for a given configuration. The details can be found in Ref. [31, 19].

Thanks to the ALF package [31], the finite temperature and projective version of AFQMC can be easily performed for a general class of lattice models. We can also work on quantum spin models with fermion QMC: one can impose the local particle number fluctuation exactly using onsite interactions.

2.1.2 Symmetry and sign problem

The AFQMC is sign problem free only under certain conditions. Specifically, the determinant ($\det[1 + B_l(\beta,0)]$) in Eq. 10 is not necessarily a real and positive number unless fermion propagators under any certain H-S field configuration respects certain

symmetry. To have a complete description, we write the canonical fermion degree's of freedom in a majorana representation:

$$c_i = \frac{1}{2}(\gamma_i^1 + i\gamma_i^2), \qquad c_i^\dagger = \frac{1}{2}(\gamma_i^1 - i\gamma_i^2). \tag{15}$$

All the fermion bilinears coupled to H-S fields can be written in the γ basis. In this basis, the tracing formula corresponding to Eq. 8 is now:

$$Tr(e^{i\gamma^T h_1 \gamma}...e^{i\gamma^T h_i \gamma}...e^{i\gamma^T h_L \gamma}) = \sqrt{\det(1 + e^{4ih_1}...e^{4ih_i}...e^{4ih_L})} \tag{16}$$

where h_i are always anti-symmetric ($h_i^T = -h_i$) matrices. Essentially one is dealing with diagonalization issue of a $2N \times 2N$ matrix. Two anti-unitary transformations which leaves all the h_i invariant are required to protect the above propagator to be positive-definite. We write them as $T_1 = U_1 K$ and $T_2 = U_2 K$. Here K denotes the complex conjugation, and $U_1(U_2)$ are real orthogonal matrices. The two transformations are required to anti-commute with each other : $\{T_1, T_2\} = 0$. General proof given in Ref. [32], shows that there are two classes of models which are free of negative sign problem:

Kramers class. In this case both two orthogonal matrices (U_1 and U_2) are anti-symmetric:

$$U^T = -U, \qquad T^2 = -1 \tag{17}$$

Defining an anti-symmetric unitary transformation $Q \equiv T_1 T_2$, one can define an exact $U(1)$ charge conservation since $[iQ, h_i] = 0$. Hence the positiveness of the determinant in Eq. 16 follows from the general proof of Kramers degeneracy: pairs of eigenstates with eigenvalues which are conjugate to each other.

Majorana class. Here one of two orthogonal matrices is symmetric:

$$U_1^T = -U_1 \;\; (T_1^2 = -1) \qquad U_2^T = U_2 \;\; (T_2^2 = 1) \tag{18}$$

A symmetric unitary transformation $P \equiv U_1 U_2$ can be defined, with the property of $P^2 = 1$. Since P commutes with h_i, one can diagonalize h_i matrix in the eigen-basis of P. It turns out that the $2N \times 2N$ matrix can be written into block diagonalized form and the two blocks are conjugate to each other.

The spinful time reversal symmetry which we apply in the model of QSH-SSC transition (as well as the doped case) is an example of Kramers class. Two anti-unitary transformation in this cases are:

$$\begin{aligned} &T_1 = Ki\sigma_y \otimes \tau_z \qquad T_2 = Ki\sigma_y \otimes \tau_x \\ &T_1^2 = -1 \qquad T_2^2 = -1 \qquad \{T_1, T_2\} = 0 \\ &Q \equiv \sigma_0 \otimes i\tau_y \end{aligned} \tag{19}$$

Here T_1 is simply the majorana version of Eq. 41 applying Eq. 15. Q is the generator of $U(1)$ charge transformation:

$$\begin{pmatrix} \gamma_i^1 \\ \gamma_i^2 \end{pmatrix} \longrightarrow \begin{pmatrix} \cos(\theta) & -\sin(\theta) \\ \sin(\theta) & \cos(\theta) \end{pmatrix} \begin{pmatrix} \gamma_i^1 \\ \gamma_i^2 \end{pmatrix} \tag{20}$$

This holds for all the system with spin$\frac{1}{2}$ time reversal symmetry and $U(1)$ charge conservation after H-S decomposition.

2.1.3 Reweighting process

We briefly shown the reweighting process when the QMC simulation encounters a sign problem. Generally the action for a given configuration is a complex number. Define the weight of certain configuration as $e^{-S(C)}$, we know that the partition function (in FTQMC) after summing up over the configurations is real:

$$Z = \sum_C e^{-S(C)} = \sum_C Re[e^{-S(C)}] \tag{21}$$

although the weight $e^{-S(C)}$ is complex in general. During the sampling we calculate the acceptance ratio based on the absolute value of the real part of weight:

$$\bar{P}(C) \equiv \frac{|Re[e^{-S(C)}]|}{\sum_C |Re[e^{-S(C)}]|} \tag{22}$$

which in general breaks the detail balance. In order to 'reweight' back to the unbiased measurement, we define the 'sign' for a given configuration as:

$$sign(C) \equiv \frac{Re[e^{-S(C)}]}{|Re[e^{-S(C)}]|} \tag{23}$$

and the average sign after sampling as:

$$\langle sign \rangle_P \equiv \frac{\sum_C Re[e^{-S(C)}]}{\sum_C |Re[e^{-S(C)}]|} = \frac{\sum_C |Re[e^{-S(C)}]| sign(C)}{\sum_C |Re[e^{-S(C)}]|} \tag{24}$$

Hence we can represent the unbiased expectation value by:

$$\begin{aligned} \langle O \rangle &\equiv \frac{\sum_C e^{-S(C)} \langle\langle O \rangle\rangle_C}{\sum_C e^{-S(C)}} \\ &= \frac{\{\sum_C |Re[e^{-S(C)}]| sign(C) \frac{e^{-S(C)}}{Re[e^{-S(C)}]} \langle\langle O \rangle\rangle_C\} / \sum_C |Re[e^{-S(C)}]|}{\{\sum_C |Re[e^{-S(C)}]| sign(C)\} / \sum_C |Re[e^{-S(C)}]|} \\ &= \frac{\langle sign \frac{e^{-S}}{Re[e^{-S}]} \langle\langle O \rangle\rangle \rangle_{\bar{P}}}{\langle sign \rangle_{\bar{P}}} \end{aligned} \tag{25}$$

For a measurement at certain QMC configuration we store $sign(C) \frac{e^{-S}}{Re[e^{-S}]} \langle\langle O \rangle\rangle_C$.

2.2 canonical ensemble simulation of interacting fermions

2.2.1 implementation

The FTQMC approach of Eq. 12 gives the thermal expectation value of certain operators in a grand canonical ensemble (GCE). On the other hand, the PQMC approach reproduces the ground state expectation value in a fixed particle number sector. However it is hard to justify the meaning of it's measurements at finite projection length Θ since it depends on the overlap between the trivial wave function and the eigenstates of Hamiltonian. A general interesting question would be, can we expand the QMC study to a canonical ensemble (CAN) ?

Specifically, the partition function of two ensembles read:

$$\begin{aligned} Z_{GCE} &\equiv \mathrm{Tr}\,[e^{-\beta \hat{H}}] \\ Z_{CAN} &\equiv \mathrm{Tr}\,[\delta_{\hat{N}_0,N} e^{-\beta \hat{H}}] \end{aligned} \tag{26}$$

where N is the desired particle number.

This means that we would like to constrain the particle number fluctuation (uniform charge susceptibility):

$$\chi_C \equiv \frac{\beta}{V}(\langle \hat{N}^2 \rangle - \langle \hat{N} \rangle^2) \tag{27}$$

at a finite temperature. μ here denotes the chemical potential. Our method is to work in the grand canonical ensemble combined with a long range interaction:

$$\begin{aligned} \hat{H}(\lambda) &= \hat{H} + \hat{H}_\lambda \\ \hat{H}_\lambda &\equiv \lambda(\hat{N} - N_0)^2 \end{aligned} \tag{28}$$

such that

$$Z_{can}(n) = \lim_{\lambda \to \infty} \mathrm{Tr}\left[e^{-\beta \hat{H}(\lambda)}\right]. \tag{29}$$

As discussed above, in Eqs. (28)-(29) the Hamiltonian $\hat{H}$ implicitly depends on the chemical potential μ, which needs to be tuned such that $\langle \hat{N} \rangle = n$. In practice, this is done by computing $\langle \hat{N} \rangle$ as a function of μ, for a suitable interval in μ, by means of auxiliary field QMC, and then fixing μ such that the equation $\langle \hat{N} \rangle = n$ is satisfied within the desired statistical accuracy; at half-filling one has exactly $\mu = 0$.

Since $\hat{H}$ conserves the particle number, one can foresee rapid convergence in λ because particle-number sectors with $\hat{N} = N \neq n$ have a weight suppressed by a factor $e^{-\lambda\beta(N-n)^2}$. The latter also shows that the relevant parameter for the convergence is $\beta\lambda$ rather than λ itself. The additional term is a perfect square term which is easily implemented within the ALF code [31]. Since $\left(\hat{N} - N\right)^2$ effectively corresponds to a long-ranged interaction, one may face the issue that the acceptance rate of a single HS flip becomes excessively small on large lattices. To circumvent this problem we have used the following decomposition:

$$e^{-\beta \hat{H}} = \prod_{\tau=1}^{L_\tau} \left[e^{-\Delta\tau \hat{T}} e^{-\Delta\tau \hat{V}} \underbrace{e^{-\frac{\Delta\tau}{n_\lambda}\hat{H}_\lambda} \cdots e^{-\frac{\Delta\tau}{n_\lambda}\hat{H}_\lambda}}_{n_\lambda\text{-times}} \right]. \tag{30}$$

Thereby, we need n_λ fields per time slice to impose the constraint. For each field, the coupling constant is effectively suppressed by a factor n_λ, thus allowing to control the acceptance of the QMC algorithm.

In order to test the efficiency of our QMC method in the canonical ensemble, we used the example of Hubbard model. We computed the uniform intensive charge susceptibility χ_c defined in Eq. 27. In Fig. 2 we show χ_c for the 1D Hubbard model as a function of $\beta\lambda$ and n_λ. As shown in Fig. 2(a), χ_c decays gradually from a finite value to zero upon increasing $\beta\lambda$. The threshold in λ for which χ_c converges to zero corresponds to the canonical ensemble. A comparison of the results for lattice sizes $L = 4, 8$ and 16 suggests that the charge fluctuations are easier to suppress for larger system sizes. The dependence of χ_c on n_λ defined in Eq. (30) is shown in Fig. 2(b), which indicates the increased Trotter error for larger values of $\beta\lambda$.

Fig. 3 shows the decay of charge susceptibility χ_c as a function of λ in the two dimensional Hubbard model, for $U = 4.0$, $L = 4$ and several increased temperatures $\beta = 0.5$,2.0 and 5.0. Inspection of Fig. 3 reveals that in the grand-canonical ensemble, the $\beta = 2.0$ case exhibits charge fluctuations larger than the $\beta = 0.5$ case, thereby requiring a larger value of $\beta\lambda$ to realize the canonical ensemble.

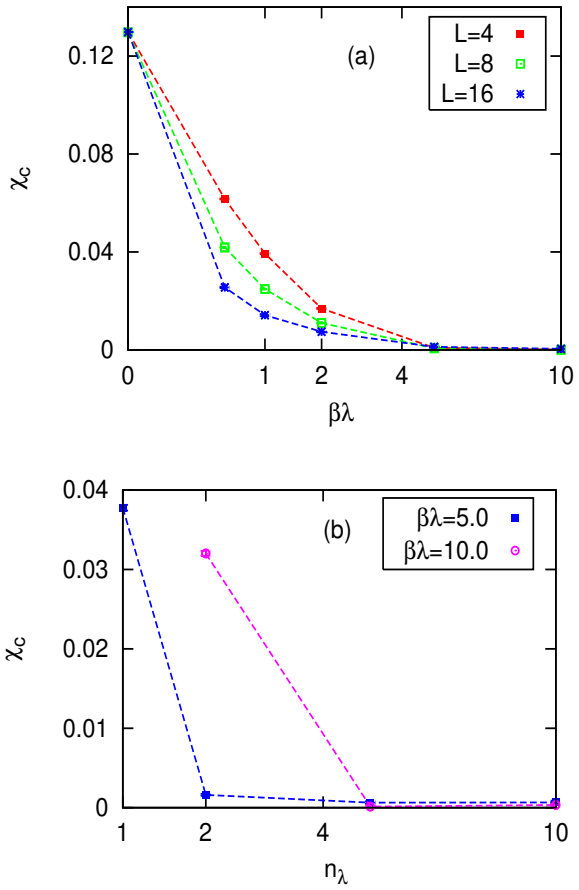

Figure 2: $\beta\lambda-$ and $n_\lambda-$dependence of χ_c for the $1D$ Hubbard model at $U = 4.0$ and $\beta = 0.5$. (a) χ_c as a function of $\beta\lambda$ for $L = 4$,8 and 16. For each $\beta\lambda$ we have taken the parameter n_λ large enough as to effectively suppress the discretization error in the decomposition of the constraint. (b) χ_c as a function of n_λ for $L = 8$ and two values of λ.

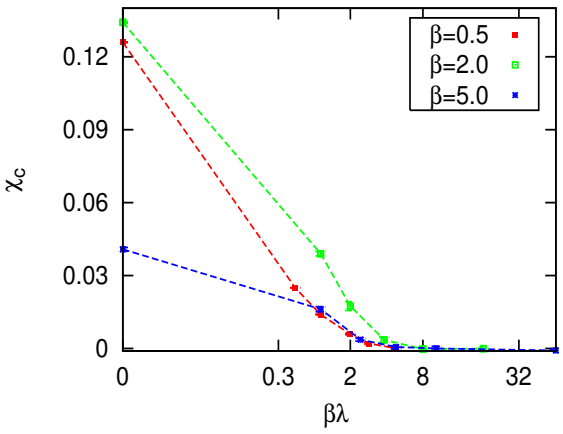

Figure 3: λ-dependence in the χ_c of $2D$ Hubbard model for $U = 4.0$, $L = 4$, and $\beta = 0.5$,2.0 and 5.0.

2.2.2 Finite size corrections of canonical ensemble

Ref. [33] shows that for a quantum model at finite volume V, a leading finite-size correction of the free energy in the canonical ensemble:

$$\begin{aligned} &F_{can}(n_0, V) - F_{gc}(V) \\ &\quad = \frac{1}{2V} \ln (2\pi V) + \frac{1}{2V} \ln \left(\frac{\chi_c}{\beta} \right) + O\left(\frac{1}{V^2} \right), \end{aligned} \tag{31}$$

where $F_{can}(n_0, V)$ and $F_{gc}(V)$ are the free energies per volume V and in units of $k_B T$ in the canonical and grand-canonical ensembles, respectively, and χ_c is the charge susceptibility (in the grand-canonical ensemble); the filling fraction n_0 in $F_{can}(n_0, V)$ is fixed to the corresponding expectation value in the grand-canonical ensemble. Eq. (31) provides the leading additional contribution to the free energy density due to the particle-number constraint. As discussed towards the end of this section, Eq. (31) allows also to determine the leading finite-size correction of observables in the canonical ensemble if, as expected, finite-size corrections in the grand-canonical ensemble decay faster than $1/V$.

We performed QMC simulation of the $SU(2)$ Hubbard model in both the grand-canonical and canonical ensemble. The Hamiltonian of the Hubbard model is defined as:

$$\begin{aligned} \hat{H} = &- t \sum_{<\boldsymbol{i},\boldsymbol{j}>,\sigma} \hat{c}^{\dagger}_{\boldsymbol{i},\alpha} \hat{c}_{\boldsymbol{j},\sigma} + U \sum_{\boldsymbol{i}} \left(\hat{n}_{\boldsymbol{i},\uparrow} - \frac{1}{2} \right) \left(\hat{n}_{\boldsymbol{i},\downarrow} - \frac{1}{2} \right) \\ &- \mu \sum_{\boldsymbol{i}} \left(\hat{n}_{\boldsymbol{i},\uparrow} + \hat{n}_{\boldsymbol{i},\downarrow} \right). \end{aligned} \tag{32}$$

The canonical ensemble is realized by adding the constraint shown in Eq. (28). For such a modified Hamiltonian, the total number of particles converges quickly to n upon increasing $\beta\lambda$.

Here we simulated both ensembles on a 1D lattice at finite temperature, which is known to be disordered. We mainly considered the models at half filling ($n = N/2$, with $N = 2L^d$) with zero chemical potential $\mu = 0$. Our basic MC observables are:

1. Energy density:
$$E = \frac{1}{L^d} \langle \hat{H} \rangle \tag{33}$$

2. Uniform spin susceptibility:
$$\chi_s = \frac{\beta}{L^d} \sum_{\boldsymbol{i},\boldsymbol{j}} \langle \hat{S}_{\boldsymbol{i}} \hat{S}_{\boldsymbol{j}} \rangle \tag{34}$$

The QMC simulations of the one-dimensional Hubbard model are performed in both the grand-canonical and canonical ensembles at inverse temperature $\beta = 0.5$, system sizes $L = 4$, 8, 12, 16, 20, 24, 28, 32, 40, 48, 64, 72, 80, and at half-filling. A comparison of the size effect for the Energy $E(L)$ and for the uniform spin susceptibility $\chi_s(L)$ in the two ensembles is shown in Fig. 4 and Fig. 5, respectively. We observe that in the grand-canonical ensemble both E and χ_s converge quickly to the thermodynamic limit for small system sizes. This indicates a small correlation length ξ at this temperature.

On the other hand, except for the smallest system sizes, in the canonical ensemble both observables exhibit a linear-like behavior as a function of $1/L$. A fit of energy

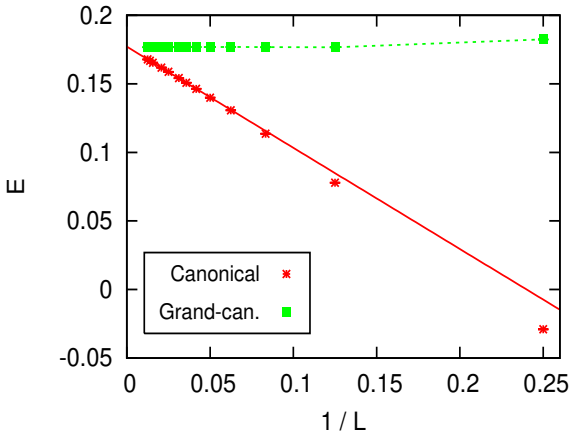

Figure 4: Finite-size data of the Energy density E for the 1D Hubbard model in the grand-canonical and canonical ensembles, at $\beta = 0.5$ and half-filling. The red line is a linear fit of the canonical ensemble data to $E_{can}(L) = E(L \to \infty) - a/L$, with $E(L \to \infty) = 0.1771(2)$ and $a = -0.738(4)$, where the minimum lattice size taken into account is $L_{min} = 16$; the dashed green line linking the grand-canonical data is a guide to the eye.

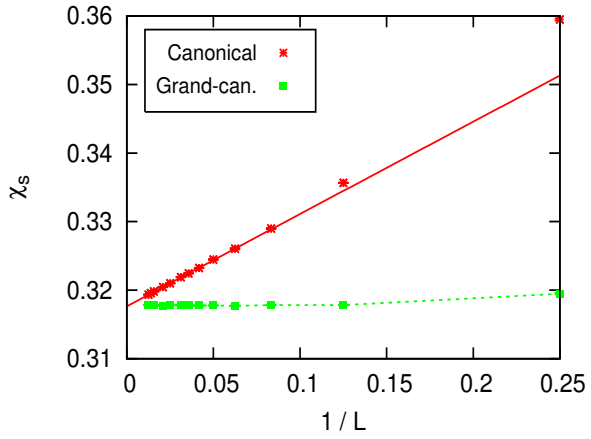

Figure 5: Same as Fig. 4 for the spin susceptibility χ_s. The red line is the linear fit of the canonical ensemble data to $\chi_{s,can}(L) = \chi_s(L \to \infty) + a/L$, with $\chi_s(L \to \infty) = 0.3177(1)$ and $a = -0.135(1)$, where the minimum lattice size taken into account is $L_{min} = 12$

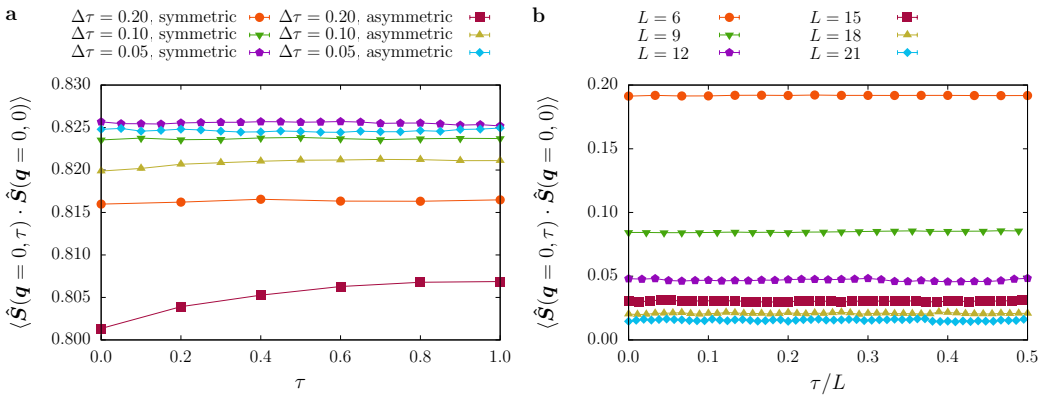

Figure 6: **(a)** Time-displaced spin correlation function at $\lambda = 0.04$, $\beta = 2$, and $L = 3$. The label 'symmetric' refers to the Trotter decomposition of equation (35), whereas 'asymmetric' refers to the alternative decomposition $Z = \mathrm{Tr}\left[e^{-\Delta\tau\hat{H}_t}\left(\prod_{i=1}^{N} e^{-\Delta\tau\hat{H}^x_\lambda(i)}e^{-\Delta\tau\hat{H}^y_\lambda(i)}e^{-\Delta\tau\hat{H}^z_\lambda(i)}\right)\right]$. **(b)** Time-displaced spin correlation function for the symmetric Trotter decomposition and $\lambda = 0.019$, $\beta = L$.

density in the canonical ensemble $E_{can}(L)$ to $E_{can}(L) = E(L\to\infty) + aL^{-1}$ exhibits a good χ^2/DOF (DOF denotes the number of degrees of freedom), when the data for the small sizes are discarded; the extrapolated value $E(L\to\infty)$ matches the grand-canonical result. Similar considerations hold for a fit of the spin susceptibility in the canonical ensemble $\chi_{s,can}(L)$ to $\chi_{s,can}(L) = \chi_s(L\to\infty) + aL^{-1}$.

Moreover, a fit of $E_{can}(L)$ to $E(L\to\infty) + aL^{-d}$, leaving d as a free parameter, gives $d = 1.05(2)$ when the smallest lattice size taken into account for the fit is $L_{min} = 16$. An equivalent fit for $\chi_s(L)$ gives $d = 1.04(2)$, when $L_{min} = 12$. This confirms that the finite-size corrections of observables in the canonical ensemble system are $\propto 1/L$.

Additional numerical results of 2D Hubbard model as well as the doped case $\mu \neq 0$ can be found in Ref. [33].

2.3 Trotter decomposition used for the QMC simulations

Generally the leading order of trotter error in Eq. 6 does not scale as $\mathcal{O}(\Delta\tau^2)$ if the propagator is not hermitian. We encountered this issue in the following projects of this thesis. Take the model of QSH-SSC transition (of Eq. 37) as an example for the discussion. For a direct trotter decomposition of Eq. 37, the exponential of a plaquette interaction does not commute with the one of it's nearest neighbours as well as the one of hopping matrix. To ensure hermiticity, the partition function is written as

$$Z = \mathrm{Tr}\left[e^{-\frac{\Delta\tau}{2}\hat{H}_t}\left(\prod_{i=1}^{N} e^{-\frac{\Delta\tau}{2}\hat{H}^x_\lambda(i)}e^{-\frac{\Delta\tau}{2}\hat{H}^y_\lambda(i)}e^{-\frac{\Delta\tau}{2}\hat{H}^z_\lambda(i)}\prod_{j=N}^{1} e^{-\frac{\Delta\tau}{2}\hat{H}^z_\lambda(j)}e^{-\frac{\Delta\tau}{2}\hat{H}^y_\lambda(j)}e^{-\frac{\Delta\tau}{2}\hat{H}^x_\lambda(j)}\right)e^{-\frac{\Delta\tau}{2}\hat{H}_t}\right]^{L_\tau} \tag{35}$$

where $\hat{H}_t$ is defined by equation (1) and the interaction (2) was partitioned into local operators $H^\alpha_\lambda(i)$ acting on spin component $\alpha = x, y, z$ and on hexagon i. The leading discretization error for the partition function then scales as $\Delta\tau^2$.

The Trotter decomposition in equation (35) breaks the global SU(2) spin rotation symmetry. For example, $[\hat{H}^x_\lambda(i), \hat{H}^y_\lambda(i)] \neq 0$, so that equation (35) will not be invariant under a global SU(2) rotation. Because SU(2) symmetry breaking is a relevant perturbation for both critical points considered, care has to be taken to ensure that its

effects, which scale as $\Delta\tau^2$, remain below the relevant energy scale. An explicit test involves the total spin operator and generator of global SU(2) rotations

$$\boldsymbol{S}_{\mathrm{tot}} = \frac{1}{L}\sum_{\boldsymbol{r},\boldsymbol{\delta}} \boldsymbol{S}_{\boldsymbol{r},\boldsymbol{\delta}} \,. \tag{36}$$

Here, $\boldsymbol{S}_{\boldsymbol{r},\boldsymbol{\delta}} = \hat{\boldsymbol{c}}^{\dagger}_{\boldsymbol{r}+\boldsymbol{\delta}}\boldsymbol{\sigma}\boldsymbol{c}_{\boldsymbol{r}+\boldsymbol{\delta}}$ and $\boldsymbol{\delta}$ runs over the positions of atoms in the unit cell at $\boldsymbol{r}$. Fig 6 shows the associated time-displaced spin-spin correlation function. A global SU(2) spin symmetry implies that this quantity is independent of imaginary time. The numerical results are essentially constant in imaginary time if the symmetric Trotter decomposition is used. Therefore, the latter was employed together with $\Delta\tau = 0.2$ for all results of of Section. 3.

3 Superconductivity from the Condensation of Topological Defects in a Quantum Spin-Hall Insulator

The discovery that spin-orbit coupling can generate a new state of matter in the form of quantum spin-Hall (QSH) insulators has brought topology to the forefront of condensed matter physics. While QSH states from spin-orbit coupling can be fully understood in terms of band theory, fascinating many-body effects are expected if the state instead results from interaction-generated symmetry breaking. In particular, topological defects of the corresponding order parameter provide a route to exotic quantum phase transitions. Here, we introduce a model in which the condensation of skyrmion defects in an interaction-generated QSH insulator produces a superconducting (SC) phase.

In this chapter, we will show a new studying of the deconfined quantum critical point (DQCP), which happens at the QSH-SC transition point where fermion particle number is pinned at half filling. This provide an improved model with only a single length scale that is accessible to large-scale quantum Monte Carlo simulations. This part is published in Ref. [1].

3.1 Implementation of model

The Hamiltonian is setup based on spinfull fermions in the 2D Honeycomb lattice:

$$\hat{H} = \hat{H}_t + \hat{H}_\lambda. \tag{37}$$

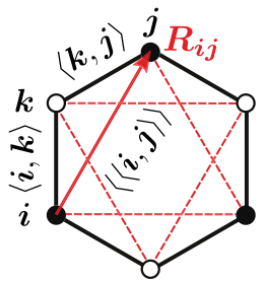

Figure 7: Illustration of the nearest- and next-nearest neighbours and the vector $\boldsymbol{R}_{ij}$ on a plaquette of the honeycomb lattice.

The first part above is the well-known tight-binding model of Dirac fermions in the form of electrons on the honeycomb lattice with nearest-neighbour hopping (see Fig. 7b) , as described by

$$\hat{H}_t = -t \sum_{\langle \boldsymbol{i},\boldsymbol{j} \rangle} (\hat{\boldsymbol{c}}_{\boldsymbol{i}}^\dagger \hat{\boldsymbol{c}}_{\boldsymbol{j}} + \text{H.c.}). \tag{38}$$

The spinor $\hat{\boldsymbol{c}}_{\boldsymbol{i}}^\dagger = \left(\hat{c}_{\boldsymbol{i},\uparrow}^\dagger, \hat{c}_{\boldsymbol{i},\downarrow}^\dagger\right)$, where $\hat{c}_{\boldsymbol{i},\sigma}^\dagger(\hat{c}_{\boldsymbol{i},\sigma})$ creates(annihilates) an electron at lattice site $\boldsymbol{i}$ with spin σ. Equation (38) yields the familiar graphene band structure with gapless, linear excitations at the two Dirac points.[34] The second part of Eq.37 denotes the interaction:

$$\hat{H}_\lambda = -\lambda \sum_{\hexagon} \left(\sum_{\langle\langle \boldsymbol{ij} \rangle\rangle \in \hexagon} \hat{J}_{\boldsymbol{i},\boldsymbol{j}} \right)^2, \qquad \hat{J}_{\boldsymbol{i},\boldsymbol{j}} = i\nu_{\boldsymbol{ij}} \hat{\boldsymbol{c}}_{\boldsymbol{i}}^\dagger \boldsymbol{\sigma} \hat{\boldsymbol{c}}_{\boldsymbol{j}} + H.c. \tag{39}$$

The first sum is over all the hexagons of a honeycomb lattice with $L \times L$ units cells and periodic boundary conditions. The second sum is over all pairs of next-nearest-neighbour sites of a hexagon, see Fig. 7. The quantity $\nu_{ij} = \pm 1$ is identical to the Kane-Mele model;[23] for a path from site $\boldsymbol{i}$ to site $\boldsymbol{j}$ (connected by $\boldsymbol{R_{ij}}$, see Fig. 7b) via site $\boldsymbol{k}$, $\nu_{ij} = \hat{\boldsymbol{e}}_z \cdot (\boldsymbol{R_{ik}} \times \boldsymbol{R_{kj}})/|\hat{\boldsymbol{e}}_z \cdot (\boldsymbol{R_{ik}} \times \boldsymbol{R_{kj}})|$ with $\hat{\boldsymbol{e}}_z$ a unit vector perpendicular to the honeycomb plane. Finally, $\boldsymbol{\sigma} = (\sigma^x, \sigma^y, \sigma^z)$ with the Pauli spin matrices σ^α. For $\lambda > 0$, the model defined by $\hat{H} = \hat{H}_t + \hat{H}_\lambda$ can be simulated without a sign problem by auxiliary-field quantum Monte Carlo methods.[35, 36, 19] In the following, we set $t = 1$ and consider a half-filled band with one electron per site.

Without the square, and taking just one of the three Pauli matrices (say σ^z), above Hamiltonian reduces to the Kane-Mele model:[23]

$$\hat{H} = \hat{H}_t - \lambda \left(\sum_{\langle\langle \boldsymbol{ij} \rangle\rangle} i\nu_{\boldsymbol{ij}} \hat{\boldsymbol{c}}_{\boldsymbol{i}}^\dagger \sigma^z \hat{\boldsymbol{c}}_{\boldsymbol{j}} + H.c. \right) \tag{40}$$

where the $SU(2)$ spin rotational symmetry is broken explicitly. Once $\lambda \neq 0$, the spin orbital coupling above introduce a small Dirac mass which generate a quantum spin hall (QSH) insulator. A spin 1/2 time reversal symmetry:

$$T\alpha \hat{\boldsymbol{c}}_i T^{-1} \equiv \bar{\alpha} i \sigma_y \hat{\boldsymbol{c}}_i \tag{41}$$

relate two counter propagating edge states of different spin channel. This way of coupling Chern bands with opposite Chern number give a vanishing total Chern number, but a nontrivial Z_2 topological index. The above time reversal symmetry is the one which will protect our QMC simulation to be sign problem free.

In contrast, the spin $SU(2)$ symmetry is not broken by the interacting model of Eq.37. However, one could expect a QSH state to be generated at low temperature due to a spontaneous symmetry breaking. This guess is not surprising if one directly use a polarized order parameter in the $SU(2)$ space to decouple the perfect square terms of Eq. 39 in the mean field approach.

3.2 Theoretical expectations

3.2.1 Charged skyrimions and superconductivity

A dynamically generated topological insulator has been proposed in Ref.[24], with a mean field calculation on an extended Hubbard model, supporting a QAH or QSH phase in the ground state. On the other hand, a DQMC simulation of this model would suffer from sign problem. Our Hamiltonian is built to be sign problem free, although it seems to be far from a real material.

The Z_2 QSH insulator due to spontaneous spin rotational symmetry breaking adiabatically connects to the ground state of Eq. 40. However there would be significant differences compare to the band insulator: low lying Goldstone modes; topological defects, e.g. skyrimion configurations of the $O(3)$ order parameter. Especially the second point is important for our discussion here: it's proposed via Ref. [37] that the skyrimion defects of QSH order parameter carry charge $2e$.

We retell the ideas in Ref. [37]. An action in terms of Dirac fermions coupled to fluctuating $O(3)$ QSH order parameter

$$S = \int d^2\boldsymbol{x} d\tau \psi^\dagger(\boldsymbol{x}, \tau)[\gamma_0 \gamma_\mu (-i\partial_\mu) + im\vec{N}(\boldsymbol{x}, \tau) \cdot \gamma_0 \gamma_3 \gamma_5 \otimes \vec{\sigma}]\psi(\boldsymbol{x}, \tau) \tag{42}$$

where $\vec{N}(\boldsymbol{x},\tau)$ is defined as a continuous and normalized vector field in space and time, and γ_μ denotes the Dirac Gamma matrices which is written in the Appendix. The number of 'skyrimions' is counted by the Pontryagin index which is a integration over $2D$ space on a certain time slice:

$$Q \equiv \int d^2\boldsymbol{x} \frac{1}{8\pi} \epsilon^{0\nu\lambda} \vec{N} \cdot \partial_\nu \vec{N} \times \partial_\lambda \vec{N} \tag{43}$$

under a imaginary time and spacial dependent local gauge transformation:

$$\begin{aligned} &\psi(\boldsymbol{x},\tau) \to e^{-i\frac{\beta}{2}\vec{e}\cdot\vec{\sigma}}\psi(\boldsymbol{x},\tau) \\ &\vec{e} \equiv \frac{(-N_2, N_1, 0)}{\sqrt{(N_1^2+N_2^2)^2}} \qquad \cos(\beta) = N_3 \end{aligned} \tag{44}$$

Thus Eq. 42 is identical to a 'polarized' QSH where the Dirac fermion is in a background of a 'spin' gauge field:

$$\begin{aligned} S = &\int d^2\boldsymbol{x} d\tau \psi^\dagger [\gamma_0\gamma_\mu(-i\partial_\mu + \frac{\sigma_z}{2}A^s_\mu) + im\gamma_0\gamma_3\gamma_5\sigma_z]\psi \\ &\frac{\sigma_z}{2}A^s_\mu = ie^{i\frac{\beta}{2}\vec{e}\cdot\vec{\sigma}}\frac{\partial}{\partial_\mu}e^{-i\frac{\beta}{2}\vec{e}\cdot\vec{\sigma}} \end{aligned} \tag{45}$$

Take Eq. 44 to Eq. 45, with a direct expansion, one can see a direct mapping between the magnetic field and curvature of O(3) order parameter:

$$\epsilon^{0\mu\nu}\partial_\mu A^s_\nu = \frac{1}{2}\epsilon^{0\nu\lambda}\vec{N}\cdot\partial_\nu\vec{N}\times\partial_\lambda\vec{N} \tag{46}$$

which holds locally at certain space time $\tau, \boldsymbol{x}$. Integrating over 2D space on a certain time slice gives:

$$\int d^2\boldsymbol{x}\epsilon^{0\mu\nu}\partial_\mu A^s_\nu = 4\pi Q \tag{47}$$

Hence we know that a 'insertion' of skyrmion configuration from imaginary time $\tau = 0$ to $\tau = t_1$ exactly maps to a insertion of total (spin) magnetic flux of 4π. In another word, a magnetic monopole of quantized flux 4π exist between $\tau = 0$ and $\tau = \tau_1$.

Recall that the electric charge current as a response to the spin gauge field: $j^c_\mu = \frac{1}{2\pi}\epsilon^{\mu\nu\lambda}\partial_\nu A^s_\lambda$. Hence the charge response in terms of a gradually inserting a single skyrimion into the system from imaginary time $t = 0$ to t_1 is:

$$\begin{aligned} Q_e = &\int_0^{t_1} d\tau \oint j^c_{\boldsymbol{r}} r d\theta \\ = &\int_0^{t_1} d\tau \oint \frac{1}{2\pi}\frac{\partial A^s_\theta}{\partial\tau} r d\theta \\ = &\oint \frac{1}{2\pi}(A^s_\theta(t_1) - A^s_\theta(t_0)) r d\theta \\ = &2 \end{aligned} \tag{48}$$

Thus we know that a skyrimion of QSH vector order parameter carries electricity charge 2.

Now we turn to an explicit calculation for a lattice model on Graphene, to show the relation between electricity charge and Pontryagin index:

$$Q_{\mathrm{e}} = 2\mathrm{e}Q \tag{49}$$

Our starting point is the Hamiltonian

$$\hat{H} = -t\sum_{\langle ij\rangle}\left(\hat{\boldsymbol{c}}_{\boldsymbol{i}}^{\dagger}\hat{\boldsymbol{c}}_{\boldsymbol{j}} + \text{H.c.}\right) + \lambda\sum_{\hexagon}\boldsymbol{N}(\boldsymbol{x})\cdot\left(\sum_{\langle\langle \boldsymbol{i},\boldsymbol{j}\rangle\rangle\in\hexagon}\underbrace{\mathrm{i}\nu_{\boldsymbol{ij}}\hat{\boldsymbol{c}}_{\boldsymbol{i}}^{\dagger}\boldsymbol{\sigma}\hat{\boldsymbol{c}}_{\boldsymbol{j}} + \text{H.c.}}_{\equiv\hat{\boldsymbol{J}}_{\boldsymbol{ij}}}\right), \tag{50}$$

where $\boldsymbol{N}(\boldsymbol{x}) = (N^x(\boldsymbol{x}), N^y(\boldsymbol{x}), N^z(\boldsymbol{x}))$ is a unit vector at position $\boldsymbol{x}$ corresponding to the centre of a hexagon. Since $\hat{H}$ is invariant under time reversal symmetry, $\hat{T}^{-1}\alpha\binom{\hat{c}_{i,\uparrow}}{\hat{c}_{i,\downarrow}}\hat{T} = \overline{\alpha}\binom{\hat{c}_{i,\downarrow}}{-\hat{c}_{i,\uparrow}}$, Kramers' theorem holds and stipulates that all eigenstates are doubly degenerate.

On the honeycomb lattice, the Pontryagin index is defined as

$$Q = \frac{1}{8\pi}\sum_{\boldsymbol{x}}\boldsymbol{N}(\boldsymbol{x})\cdot(\boldsymbol{N}(\boldsymbol{x}+\boldsymbol{a}_1)-\boldsymbol{N}(\boldsymbol{x}))\times[(\boldsymbol{N}(\boldsymbol{x})-\boldsymbol{N}(\boldsymbol{x}+\boldsymbol{a}_2))+(\boldsymbol{N}(\boldsymbol{x})-\boldsymbol{N}(\boldsymbol{x}-\boldsymbol{a}_1+\boldsymbol{a}_2))] \tag{51}$$

with unit vectors $\boldsymbol{a}_1 = (1,0)$ and $\boldsymbol{a}_2 = (\frac{1}{2}, \frac{\sqrt{3}}{2})$.

For an arbitrary vector field $\boldsymbol{N}(\boldsymbol{x})$, Hamiltonian (50) does not preserve particle-hole (P-H) symmetry. For example, defining the P-H transformation as

$$\hat{P}_z^{-1}\alpha\begin{pmatrix}\hat{c}_{\boldsymbol{i},\uparrow}^{\dagger}\\ \hat{c}_{\boldsymbol{i},\downarrow}^{\dagger}\end{pmatrix}\hat{P}_z = \eta_i\overline{\alpha}\begin{pmatrix}\hat{c}_{\boldsymbol{i},\uparrow}\\ -\hat{c}_{\boldsymbol{i},\downarrow}\end{pmatrix}, \tag{52}$$

where $\eta_i = 1\,(-1)$ for $i \in \mathrm{A}\,(\mathrm{B})$, we have

$$\begin{aligned}\hat{P}_z^{-1}\hat{J}_{\boldsymbol{i},\boldsymbol{j}}^{x}\hat{P}_z &= \hat{J}_{\boldsymbol{i},\boldsymbol{j}}^{x}\,,\\ \hat{P}_z^{-1}\hat{J}_{\boldsymbol{i},\boldsymbol{j}}^{y}\hat{P}_z &= \hat{J}_{\boldsymbol{i},\boldsymbol{j}}^{y}\,,\\ \hat{P}_z^{-1}\hat{J}_{\boldsymbol{i},\boldsymbol{j}}^{z}\hat{P}_z &= -\hat{J}_{\boldsymbol{i},\boldsymbol{j}}^{z}\,.\end{aligned} \tag{53}$$

A general P-H transformation can be written as

$$\hat{P}(\theta,\phi) = \hat{U}^{-1}(\theta,\phi)\hat{P}_z\hat{U}(\theta,\phi) \tag{54}$$

where

$$\hat{U}^{-1}(\theta,\phi)\begin{pmatrix}\hat{c}_{i,\uparrow}\\ \hat{c}_{i,\downarrow}\end{pmatrix}\hat{U}(\theta,\phi) = \begin{pmatrix}\cos(\theta/2) & -\sin(\theta/2)e^{-i\phi}\\ \sin(\theta/2)e^{i\phi} & \cos(\theta/2)\end{pmatrix}\begin{pmatrix}\hat{c}_{\boldsymbol{i},\uparrow}\\ \hat{c}_{\boldsymbol{i},\downarrow}\end{pmatrix}. \tag{55}$$

For Hamiltonian (50), it yields

$$\hat{P}^{-1}(\theta,\phi)\hat{H}(\boldsymbol{N})\hat{P}(\theta,\phi) = H(\boldsymbol{N}') \tag{56}$$

where

$$\boldsymbol{N}'(\boldsymbol{x}) = R^{-1}(\theta,\phi)\begin{pmatrix}1&0&0\\0&1&0\\0&0&-1\end{pmatrix}R(\theta,\phi)\boldsymbol{N}(\boldsymbol{x}) \tag{57}$$

and

$$R(\theta,\phi) = \begin{pmatrix}\cos^2(\theta/2)-\sin^2(\theta/2)\cos(2\phi) & -\sin^2(\theta/2)\sin(2\phi) & -\sin(\theta)\cos(\phi)\\ -\sin^2(\theta/2)\sin(2\phi) & \cos^2(\theta/2)+\sin^2(\theta/2)\cos(2\phi) & -\sin(\theta)\sin(\phi)\\ \sin(\theta)\cos(\phi) & \sin(\theta)\sin(\phi) & \cos(\theta)\end{pmatrix}. \tag{58}$$

Thus, there is no generic P-H transformation that leaves this Hamiltonian invariant, unless $\boldsymbol{N}(\boldsymbol{x})$ is varied in an R^2 space (θ and ϕ can be defined such that $\sin\theta\cos\phi N_x +$

$\sin\theta \sin\phi N_y + \cos\theta N_z = 0$). Since the transformation has a determinant of -1, the generic P-H transformation gives

$$Q(\boldsymbol{N}'(\boldsymbol{x})) = -Q(\boldsymbol{N}(\boldsymbol{x})). \tag{59}$$

The 'electric charge' refers to the number of occupied states at zero temperature, relative to half filling. The sign change of the Pontryagin index under a P-H transformation provides a natural way of understanding equation (49). Note that in contrast to a skyrmion, a 2D topological defect (such as vortex) has a vanishing Pontryagin index and carries no charge.

The argument of charged skyrmions fails when other Dirac mass terms are considered. For example, a system with fluctuations of a three component vector field Yukawa-coupled to the three antiferromagnetic mass terms does not break P-H symmetry. In this case, a skyrmion configuration with nonzero Pontryagin index does not carry electric charge.

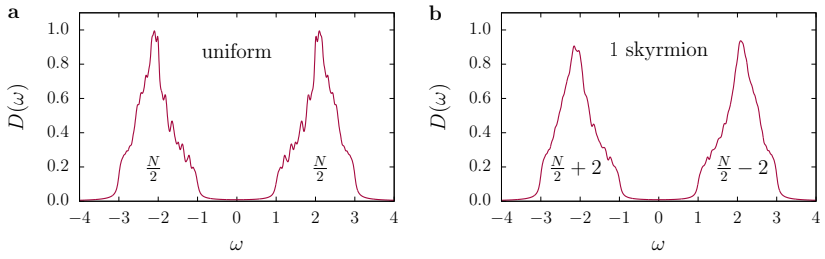

Figure 8: Density of states $N(\omega)$ of Hamiltonian (50) for (a) uniform polarisation, (b) a 'single skyrmion' configuration with $Q \approx -0.989$. We have included an artificial broadening by using the form $D(\omega) = -\pi^{-1} \sum_n \mathrm{Im}\,(\omega - \varepsilon_n + \mathrm{i}\delta)^{-1}$, where ε_n are the eigenvalues and $\delta = 0.05$. Here, $L = 36$, $\lambda = 0.5$.

We diagonalised Hamiltonian (50) on a honeycomb lattice with $L = 36$, setting $t = 1$ and $\lambda = 0.5$. Supplementary Fig 8 compares the density of states for a uniform field $\boldsymbol{N}(\boldsymbol{x})$ and for a 'hedgehog' configuration corresponding to a single skyrmion. On the lattice, the Pontryagin index is not quantized and we obtain $Q \approx -0.989$. The system remains gaped when one skyrmion is inserted, see Fig. 8b. The breaking of P-H symmetry is also apparent from $D(\omega) \neq D(-\omega)$. Simple number counting shows that

$$\int_{-\infty}^{0} D(\omega)d\omega = N/2 + 2\,, \quad \int_{0}^{\infty} D(\omega)d\omega = N/2 - 2. \tag{60}$$

Compared to the case of uniform polarisation in Fig. 8a, an additional charge 2e is generated.

On a system with open boundary conditions, the Pontryagin index is not necessarily quantized and we can investigate how charge is transferred during the *insertion* of a skyrmion by varying the Pontryagin index from zero to one. Fig 9 shows that the total charge is 'pumped' from 0 to 2e and we observe a step function at a non-integer value of Q. This is a consequence of the aforementioned Kramers theorem. As shown in Fig. 10, the bulk remains gaped during this process, while the edge stays gapless. Thus, the charge 2e is pumped through the edge under insertion of a skyrmion.

Note that the charge 2e skyrimions suggest a way to another correlated state: the superconductor. Normally a conventional superconducting state is one kind of Bose–Einstein condensate while the condensed bosonic particle is written as the bounded

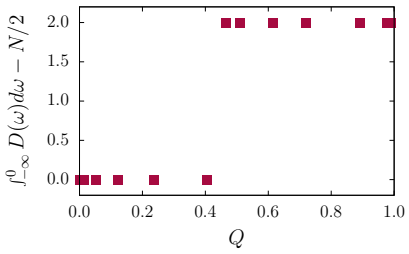

Figure 9: Integrated density of states as a function of Q for open boundary conditions and $L = 36$.

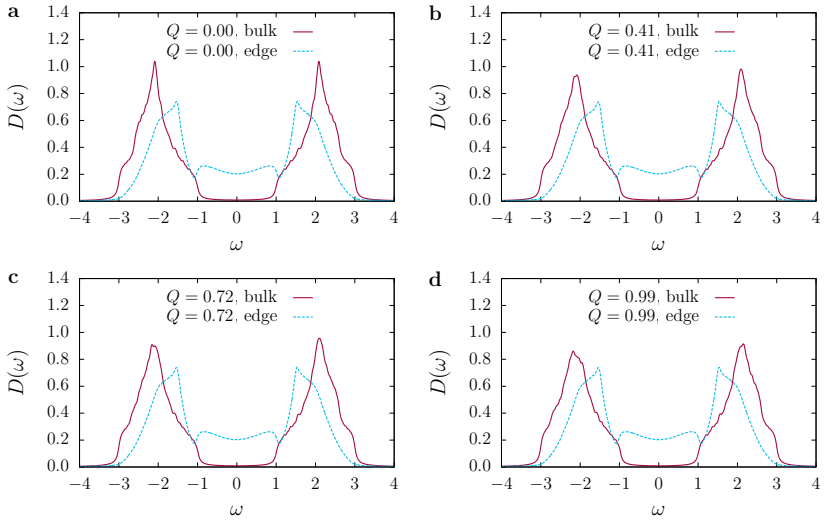

Figure 10: Edge and bulk density of states for different $\boldsymbol{N}(\boldsymbol{x})$, corresponding to (a) $Q = 0$, (b) $Q = 0.41$, (c) $Q = 0.72$ and (d) $Q = 0.99$. Here, $L = 36$, and $D(\omega)$ was broadened as explained in Fig. 8.

state of pairs of electrons. In the well-known BCS theory, the so called 'cooper pair' is written as a coherent state of electrons with opposite spin and momentum. Usually the pairing comes from the effective attractive interaction mediated by the electron phonon coupling. Our model introduces a new way towards pairing : condensation of skyrimions of QSH vector field. The numeric investigation of this effect will be shown in the following.

In fact the QSH-SSC transition at zero temperature is one kind of 'deconfined quantum critical point'(DQCP): a single bosonic quantum critical point between two different symmetry broken state. It certainly breaks the Landau-Ginzburg-Wilson (LGW) framework. Take an example of coupled LGW theory of two different order parameters:

$$\begin{aligned} S =& S_A + S_B + S_{Int} \\ S_A =& \int d^2\boldsymbol{x} d\tau [\frac{1}{2}((\partial_{x_1}\vec{\phi})^2 + (\partial_{x_2}\vec{\phi})^2 + {c_A}^2(\partial_\tau\vec{\phi})^2 + r_A|\vec{\phi}|^2) + \frac{u_A}{24}|\vec{\phi}|^4] \\ S_B =& \int d^2\boldsymbol{x} d\tau [\frac{1}{2}((\partial_{x_1}\vec{\Psi})^2 + (\partial_{x_2}\vec{\Psi})^2 + {c_B}^2(\partial_\tau\vec{\Psi})^2 + r_B|\vec{\Psi}|^2) + \frac{u_B}{24}|\vec{\Psi}|^4] \\ S_{Int} =& v|\vec{\phi}|^2|\vec{\Psi}|^2 \end{aligned} \tag{61}$$

The LGW transition points corresponds to the points where $|\phi|$ (or $|\Psi|$) acquire nonzero value. Since the required coarse gaining step from lattice to field theory parameters (r_A, r_B and v) depends on non-universal feature, two order parameters in terms of different symmetry breaking does not need to condense at the same point, without certain fine tuning process.

3.2.2 Deconfined quantum critical point

We briefly introduce the idea of 'deconfined quantum critical point' (DQCP) in this section as well as it's relation to our study. It follows from the ideas of Ref.[38],[39] and [11]. Within in the framework of LGW theory two different symmetry broken states are connected by intermediate phases or first order phase transitions. However, there is interesting argument of the possibility of continuous phase transitions which belong to the category of so called 'deconfined quantum critical points'(DQCP). The key point for the continuity of the transition relies on 'deconfined' fractionalized degrees of freedom. The original idea of DQCP was proposed for transitions in quantum spin systems [38] [11]: more specifically for a transition between an anti-ferro magnetic (AFM) ordered state and a valence band solid (VBS) state in the 2 dimensional case. The AFM state breaks spin rotational symmetry in $SU(2)$ space, while the VBS breaks a discrete $Z4$ symmetry. The latter symmetry broken process necessarily requires a Hamiltonian on a square lattice.

As an example describing LGW transition, the so called 'coupled dimer' model [40] reads:

$$H_d = J \sum_{\langle ij\rangle \in A} \boldsymbol{S}_i \cdot \boldsymbol{S}_j + \frac{1}{g} J \sum_{\langle ij\rangle \in B} \boldsymbol{S}_i \cdot \boldsymbol{S}_j \tag{62}$$

Where $\boldsymbol{S}_i$ is the spin 1/2 moment on site i. On the square lattice, nearest neighbour links of A alternately covers half of the bonds on the x direction, while the B set denotes the rest of the links. We only consider the case $g \geq 1$ and $J > 0$. It is clear that the above Hamiltonian explicitly breaks the $Z4$ symmetry of the square lattice. At zero temperature, an AFM state exists when g is close to 1 while a paramagnetic ground state in terms of decoupled dimerlized singlet wave function happens in the large g limit. It is known that at $1/g_c = 0.52337(3)$[41] a continues phase transition

between AFM and paramagnetic state which belongs to the field theory of $O(n)$ rotor model happens.[6]

The elementary excitation in above AFM state is the two branch of goldstone modes around momentum $Q = (\pi, \pi)$ of square lattice. These gapless modes has 'elementary' spin quantum number of 1. In the decoupled dimerlized state all the excitations are gaped, but the lowest one among them are still the spin 1 excitations which corresponds to a process of breaking any certain local singlet into triplet states. In both two phases as well as the transition point, delocalized spin 1/2 'spinon' excitations does not appear (more specifically, they have much higher energies). The characteristic length scale which diverges at this LGW transition point is the defined by the correlation of $O(3)$ order parameter, while the 'confinement length scale' in terms of the distance for pairs of spinons stays finite crossing the transition.

A simple example of quantum spin model which does not break Z_4 symmetry of 2D square lattice is the so called ' $J-Q$ ' model[17]:

$$H_{JQ} = J \sum_{\langle ij \rangle} \boldsymbol{S}_i \cdot \boldsymbol{S}_j + Q \sum_{\langle ijkl \rangle} (\boldsymbol{S}_i \cdot \boldsymbol{S}_j - \frac{1}{4})(\boldsymbol{S}_k \cdot \boldsymbol{S}_l - \frac{1}{4}) \tag{63}$$

where the Heisenberg interaction between nearest neighbour sites (i, j) is same as Eq.62. The second part of above Hamiltonian denotes the 4 site 'ring exchange' interaction, where $\langle ijkl \rangle$ are four sites on the corners for a certain plaquette of square lattice. At zero temperature, although the AFM state in the small Q limit is adiabatically connected to the one in coupled dimer model, the paramagnetic ordered state in the large Q limit has a fundamental difference compare to the one of Eq.62 in large g limit. This paramagnetic state, which is also called valence bond solid (VBS) state, spontaneously broke the lattice Z_4 symmetry. Hence the present VBS ground state has a significant difference compared to the one in coupled dimer model due to its four fold degeneracy. To link the AFM and VBS state at zero temperature, there are several possibilities: a finite intermediate region where both two order parameters co-exists; an intermediate paramagnetic state which has no broken symmetry between the two ordered state; a direct first order transition; or a deconfined quantum critical point. Remarkably it is found that within numerical reachable system size of Monte Carlo [17][42], the last scenario is favored.

The four fold degeneracy of VBS ground state has an important consequence for describing the field theory of AFM-VBS transition. One can introduce a path integral using spin coherent state. Consider the AFM phase close to the critical point. In this case the low-energy fluctuations of the Neel order parameter are described by the O(3) nonlinear sigma model with a Berry phase term:

$$S = \frac{1}{2g} \int d\tau \int d^2 r [(\partial_\tau \vec{N})^2 + (\nabla_r \vec{N})^2] + iS \sum_r (-1)^r \mathcal{A}_r \tag{64}$$

where the three component vector field $\vec{N}$ is the eigenvalue of spin coherent state in the spin $\frac{1}{2}$ case. $\mathcal{A}_r$ is the oriented area enclosed by trajectory of spin configuration along imaginary axis at site r on the unit sphere. The last term of berry phase actually described the monopole tunneling effects, which measures the creation or annihilation of skyrmion configurations of $O(3)$ order parameters:

$$Q \equiv \int d^2 \boldsymbol{x} \frac{1}{8\pi} \epsilon^{0\nu\lambda} \vec{N} \cdot \partial_\nu \vec{N} \times \partial_\lambda \vec{N} \tag{65}$$

The monopoles, described by the summation over $\mathcal{A}_r$ term, are not relevant unless process of changing the number Q happens along imaginary time. Note that many configurations of monopoles does not contribute to the action of Eq. 64 after summing up over the configurations. A specific calculation given by Haldane[10], shows that the lowest skyrmion changing process on the square lattice with nonzero fugacity comes with changing Q by ± 4. It is actually related to the four fold degeneracy of VBS wave function. Indeed the VBS phase comes from the condensation of skyrimion number changing operator.

A necessary condition of DQCP is the emergence of skyrmion number conservation at the critical point. In another words, the monopoles which correspond to the skyrmion number changing operator has to be absent. Actually it is not so obvious to show: Senthil. et. al [38] argue that the single monopoles fugacity goes to zero after averaging over the oscillations, while the quadruple ones renormalizes to zero only at the critical point.

There is another way to look at DQCP from 'opposite' direction: a transition from VBS to AFM phase. The VBS phase is a Z_4 symmetry breaking state, but one can not simply interpret it's transition toward AFM state as the one of $3D$ clock model. The topological defects of the Z_4 clock order parameter is actually the Z_4 vortices [43]: An unpaired 'spinon' with spin quantum number 1/2 is always left at the center of a vortex.

Recall the example of aforementioned 'coupled dimer' model, in the paramagnetic (dimerized) state two unpaired spin 1/2 object would cost high excitation energy which depends 'linearly' on the distance between them. Crucially it not only holds inside dimerized state: even at $O(3)$ critical point there are no free spin 1/2 excitations. Now for J-Q model, although the 'linear law' still holds inside VBS phase, unpaired spinons can proliferate approaching the DQCP. Finally, the spinons condense and form the AFM order parameter across the transition point.

A field theory to describe the second order phase transition between AFM and VBS is to rewrite the spin order parameter as a composite of spinon fields:

$$\vec{N} = z^{\dagger}\vec{\sigma}z \tag{66}$$

where z is the two component spin 1/2 complex spinor, and $\vec{\sigma}$ denote the three component Pauli matrices. The description of DQCP is then:

$$\begin{aligned} Z_{deconfined} &= \int Dz_a Da_\mu e^{-\int d^2\boldsymbol{x}d\tau L_z} \\ L_z &= \sum_{a=1}^{2} |(\partial_\mu - ia_\mu)z_a|^2 + s|z|^2 + u(|z|^2)^2 + \frac{1}{2e^2}(\epsilon_{\mu\nu\kappa}\partial_\nu a_\kappa)^2 \end{aligned} \tag{67}$$

A $U(1)$ gauge field a_μ is introduced due to the $U(1)$ local redundancy of z field in Eq. 66. Note that field a_μ is defined as a compact $U(1)$ field here. To tune the parameter Q/J in Eq. 63 is effectively to tune s here. The key point now is to argue that when approaching the critical point as function of s, the field a_μ has to become effectively non-compact. This is a necessary condition for the skyrimion conservation at the critical point, since the skyrimion number can also be described as :

$$\frac{1}{2\pi}\int d^2\boldsymbol{x}\epsilon^{0\mu\nu}\partial_\mu a_\nu = Q \tag{68}$$

if the U(1) gauge field is compact, then monopoles which can change the number of skyrimions ($\Delta Q = \pm 1$) on different time slices are allowed. Hence we require the field to be non-compact approaching the critical point.

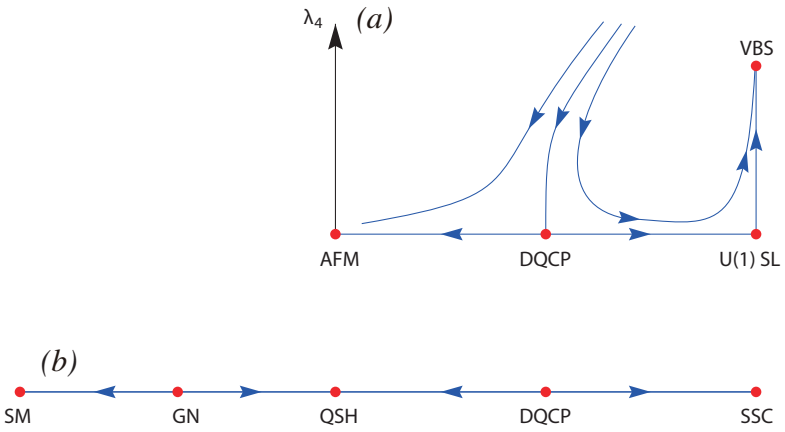

Figure 11: (a). Renormalization group flows of the DQCP in terms of AFM-VBS transition on the square lattice proposed by Ref.[11]. Here the critical point of 'DQCP' flows to fixed point corresponding to the AFM state or a $U(1)$ spin liquid. λ_4 is the strength of Z_4 symmetry breaking field which is only irrelevant only at the DQCP. (b) The corresponding RG diagram of our model. Here a Gross-Neveu Heisenberg critical point happens between the DSM and QSH phase, while a DQCP flows to either QSH or SSC fixed points. Our interaction strength works as the only tuning parameter, and there is no additional dangerous irrelevant symmetry breaking field.

Although the monopoles are irrelevant around the DQCP, they are relevant at the 'deconfined' phase of photons. As shown before, the Z_4 symmetry breaking field introduced by the four fold VBS degeneracy is relevant and break the conservation law of skyrimions. A schematic flow draw in Ref. [11] is shown in fig. 11. One could simply take the line with zero values of λ_4 as the one of a pure U(1) gauge theory : the right part of $\lambda_4 = 0$ line favor the phase of deconfined photon field A_μ. On the other hand any nonzero values of λ_4 field is driven the Z_4 symmetry breaking phase under RG, where the spinons are confined. This necessarily leads to the argument of two divergent length scale: a 'spinon' correlation length as well as the VBS correlation length. The latter one is captured by the correlation of Z_4 order parameter.

Now we turn back to our model of QSH-SSC transition. There is a significant difference compared to the AFM-VBS transition: the SSC phase breaks only the U(1) charge conservation of fermions:

$$[\hat{N}, \hat{H}] = 0 \tag{69}$$

where $\hat{N}$ is the summation of particle number operator. This is not involved with any lattice point group (say, Z_4) symmetry breaking field. Thus, the skyrimion number conservation law is exact not only at the deconfined critical point. Deep inside the SSC phase, the excitation gap of a skyrmion, which is basically the gap of a cooper pair, is much smaller that the finite fermionic single particle gap. Hence the absence of monopoles is an exact statement: there is only one characteristic length scale ξ_{SSC}, which is the one of U(1) order parameter.

The key point of our fermionic approach is that both $SU(2)$ and $U(1)$ symmetries are onsite. Very recently, Thorngren et. al.[25] give an understanding of why the monopole

free DQCP is not able to be realized in bosonic models: emergent anomaly. Here we briefly recall their ideas. Our $SU(2)$ and $U(1)$ transformation also contain a (global)Z_2 degree of freedom in the spin 1/2 representation, which is the fermion parity for $\theta = \pi$ transformation of $e^{i\vec{e}\cdot\vec{\sigma}\theta}$(along any axis $\vec{e}$). Note that this transformation acts trivially on spin model due to the exactly constraint on charge fluctuation. In our case the Z_2 transformation is charged although always gaped. The crucial point is that the low energy effective field theory is after gaping out the fermion charge degrees of freedom is anomalous: it can not be gauged trivially on open boundary conditions.

3.2.3 DQCP from Dirac fermions

The above discussion of DQCP based on quantum spin system has no local charge fluctuation : one can view the J-Q like models as fermionic systems with local $U(1)$ gauge redundancy, such that there is effective reduction of Hilbert space.

One could also study bosonic quantum phase transition with fermionic models where the local gauge redundancy is broken. For example, the critical point of $2+1D$ $O(2)$ quantum rotor model can be either realized on quantum spin or fermionic models. An example of the second case is the QSH-AFM transition in Kane-Mele Hubbard model[44]. Due to the finite fermionic single particle gap introduced by spin orbital coupling, the low energy effective theory is described by the bosonic degrees of freedom. To investigate the universality class by large scale numerical simulation, this example of fermionic model is very inefficient.

However, the fermionic approach in our study introduces new possibilities of tackling the DQCP. Specifically, we take Dirac fermions from the low energy effective theories of lattice Hamiltonian : e.g. honeycomb lattice or π flux square lattice. As mentioned before current work of QSH-SSC transition is based on the honeycomb lattice. Bosonic order parameters are naturally coupled to fermion bilinears, which has matrix structure depending on the corresponding broken symmetry of the order parameter. We are interested in the case where the coupling not only breaks a symmetry but also introduces a gap to single fermionic excitation : Dirac masses.

One can write an effective low energy theory based on the approximation around two dirac cones of the Honeycomb lattice. We take the Nambu notation of $\Psi(\boldsymbol{x},\tau) \equiv \begin{pmatrix}\psi(\boldsymbol{x},\tau) & \psi^\dagger(\boldsymbol{x},\tau)\end{pmatrix}$, such that the Hilbert space read: $\mathbb{R}^2 \otimes \mathbb{C}^2_{valley} \otimes \mathbb{C}^2_{orbital} \otimes \mathbb{C}^2_{spin} \otimes \mathbb{C}^2_{BdG}$. We need the Nambu basis since to describe superconducting mass, particle-particle (hole-hole) bilinears is necessarily involved.

Generally the action reads:

$$S = S_{\text{Dirac}} + S_{\text{Boson}}. \tag{70}$$

where S_{Dirac} denotes the free dirac action as will as the the Yukawa coupling term between bosonic order parameters and dirac fermions:

$$\begin{aligned} S_{Dirac} = &\int d\tau \int d\boldsymbol{k}\{\Psi^\dagger(\boldsymbol{k},\tau)(\frac{\partial}{\partial\tau} + iv_F\gamma_0\gamma_1 \otimes \tau_0 k_x + iv_F\gamma_0\gamma_2 \otimes \tau_z k_y)\Psi(\boldsymbol{k},\tau) \\ &+ m\int d\boldsymbol{q}[\vec{N}_A(\boldsymbol{q},\tau)\cdot\Psi^\dagger(\boldsymbol{k}+\boldsymbol{q},\tau)\vec{M}_A\Psi(\boldsymbol{k},\tau) + \vec{N}_B(\boldsymbol{q},\tau)\cdot\Psi^\dagger(\boldsymbol{k}+\boldsymbol{q},\tau)\vec{M}_B\Psi(\boldsymbol{k},\tau)]\} \end{aligned} \tag{71}$$

where v_F is the fermion velocity. Note that we've take the approximations around the two Dirac points, hence v_F is proportional to the hoping pre-factor t in Eq. 38. $\vec{N}_A$ and $\vec{N}_B$ are the 3 and 2 component vector order parameters. In the case of

$$\{M^\alpha_{A(B)}, \gamma_0\gamma_1 \otimes \tau_0\} = 0 \qquad \{M^\alpha_{A(B)}, \gamma_0\gamma_2 \otimes \tau_z\} = 0 \tag{72}$$

finite value of $|\vec{N}_{A(B)}|$ introduces Dirac mass gap.

We took the bosonic order parameters $\vec{N}_A$ and $\vec{N}_B$ as 'soft' vectors in the sense they don't have a unit module. Then we assume the bosonic part of the action to be:

$$S_{Boson} = \int d^2\boldsymbol{x} d\tau (r_A|\vec{N}_A|^2 + u|\vec{N}_A|^4 + r_B|\vec{N}_B|^2 + u|\vec{N}_B|^4 + g|\vec{N}_A|^2|\vec{N}_B|^2) \tag{73}$$

The crucial point of understanding the DQCP from the point of view of competing dirac mass is that we require all the 16×16 matrices in the space of $\mathbb{C}^2_{valley} \otimes \mathbb{C}^2_{orbital} \otimes \mathbb{C}^2_{spin} \otimes \mathbb{C}^2_{BdG}$ to anti-commute with each other :

$$\begin{aligned} \{M_A^\alpha, M_A^\beta\} &= 2\delta_{\alpha,\beta}\mathbb{1}_{16} \\ \{M_A^\alpha, M_B^\beta\} &= 0 \end{aligned} \tag{74}$$

Hence at the Dirac point, the mass gap opens as:

$$\Delta_{sp} \propto m\sqrt{|\vec{N}_A|^2 + |\vec{N}_B|^2} \tag{75}$$

The fermion part of action has an exact SO(5) symmetry due to the anti-commuting nature of 5 matrices. This symmetry is broken by S_{Boson} unless:

$$r_A = r_B, \qquad \Delta \equiv g - 2u = 0 \tag{76}$$

A calculation by Abanov and Wiegmann (AW)[45] shows that after integrating out the fermionic degrees of freedom, S_{Dirac} will host an O(5) non-linear sigma model in $2+1$ dimension:

$$S_{\text{nlsm}} = \frac{1}{g}\int d^2x d\tau [(\partial_\mu \vec{n}_A)^2 + (\partial_\mu \vec{n}_B)^2] \tag{77}$$

where

$$\vec{n}_A \equiv \frac{\vec{N}_A}{\sqrt{|\vec{N}_A|^2 + |\vec{N}_B|^2}} \qquad \vec{n}_B \equiv \frac{\vec{N}_B}{\sqrt{|\vec{N}_A|^2 + |\vec{N}_B|^2}} \tag{78}$$

and the 'stiffness' scales as:

$$\frac{1}{g} \propto m\sqrt{|\vec{N}_A|^2 + |\vec{N}_B|^2} \tag{79}$$

Note that we normalized S_{Dirac} as $\vec{N}_{A(B)} \to \vec{n}_{A(B)}$ and $m \to m\sqrt{|\vec{N}_A|^2 + |\vec{N}_B|^2}$ before performing the AW integration, since the later calculation was performed for vectors of unit module.

Crucially, the anti-commuting nature allows us to get a geometrical WZW term [37] of level 1 in $2+1D$:

$$\begin{aligned} S_{\text{WZW}} =& \frac{2\pi i}{vol(S_4)} \int d\tau d^2\boldsymbol{x} \int_0^1 du \epsilon^{abcde} n^a \partial_x n^b \partial_y n^c \partial_\tau n^d \partial_u n^e \\ =& \frac{3i}{4\pi} \int d\tau d^2\boldsymbol{x} \int_0^1 du \epsilon^{abcde} n^a \partial_x n^b \partial_y n^c \partial_\tau n^d \partial_u n^e \end{aligned} \tag{80}$$

where we could label the 5 component vector n^a as:

$$n^1 \equiv n^1_A,\ n^2 \equiv n^2_A,\ n^3 \equiv n^3_A,\ n^4 \equiv n^1_B,\ n^5 \equiv n^2_B \tag{81}$$

If the above labeling is performed carelessly, there is only a sign ambiguity in front of Eq. 80. One the other hand, above integration process does not require the action

S_{Boson} to be SO(5) invariant: even in the case of $\Delta \neq 0$, the topological contribution from WZW term still exist.

The WZW term in $2+1D$ play a crucial role, in the sense that a critical point as a function of $r_A(r_B)$ might be stable in this case, in a finite region of $1/g$. This breaks the role of Landau-Ginsberg transition: one can also perform of reduction from the action of Eq. 80 and extract the charge $2e$ response of QSH skyrimions or the spin $1/2$ object from the SSC vortices.

Assume that by varying $r_A(r_B)$ a deconfined quantum critical point happened at $r_A = r_B$. It is natural that the anisotropy $r_A - r_B$ is a relevant perturbation to the critical point: renormalzation from the parameter range $|r_A - r_B| \neq 0$ flows to either the SO(3) broken phase or the $U(1)$ broken one. Right at the critical point ($|r_A - r_B| = 0$), there will be an emergent O(5) symmetry if

$$\Delta \equiv g - 2u \tag{82}$$

is irrelevant. This condition is actually not necessary for the continuous nature of transition. Numerical investigators would like to avoid this possibility since an additional bound of the continuous nature for DQCP comes from the conformal bootstrap study : $\eta_A(\eta_B)$ has to be larger than 0.52 when Δ is irrelevant.

On the other hand, one can impose the constraint of $\Delta = 0$ and try to perform a study of O(5) non-linear sigma model with WZW term. In Section. 5 we will introduce the numerical study of sigma model with exact O(5) symmetry by project interacting fermions to the zeroth Landau Level of Graphene.

Amazingly, there seems to be relation between fermion statistics and the absence of Z_4 symmetry breaking field. However, this question is very hard to be answered rigorously. We would just briefly discuss the idea of recent work in Ref. [25]. The condensation of two SSC mass:

$$M^x_{SSC} = i\gamma_0\gamma_2\gamma_3 \otimes \sigma_y \otimes \tau_x \qquad M^y_{SSC} = i\gamma_0\gamma_2\gamma_3 \otimes \sigma_y \otimes \tau_y \tag{83}$$

spontaneously breaks the global U(1) charge conservation of fermions:

$$\begin{pmatrix} \psi^\dagger \\ \psi \end{pmatrix} \longrightarrow \begin{pmatrix} e^{i\theta} & 0 \\ 0 & e^{-i\theta} \end{pmatrix} \begin{pmatrix} \psi^\dagger \\ \psi \end{pmatrix} \tag{84}$$

which is not directly coupled to the lattice degrees of freedom. On the other hand, the dynamical generation of two VBS mass, say:

$$M^x_{VBS} = i\gamma_0\gamma_3 \otimes \sigma_0 \otimes \tau_0 \qquad M^y_{VBS} = i\gamma_0\gamma_5 \otimes \sigma_0 \otimes \tau_0 \tag{85}$$

breaks a U(1) symmetry

$$\begin{pmatrix} \psi^\dagger \\ \psi \end{pmatrix} \longrightarrow \begin{pmatrix} e^{i\theta\gamma_3\gamma_5} & 0 \\ 0 & e^{-i\theta\gamma_3\gamma_5} \end{pmatrix} \begin{pmatrix} \psi^\dagger \\ \psi \end{pmatrix} \tag{86}$$

which is not an exact symmetry of the lattice Hamiltonian: the unitary transformation is not within internal degree's of freedom when we transform the operators back to lattice. A general understanding is formulated in the following way.

QSH and AFM order parameters break exactly the same SO(3) rotational symmetry which is a subgroup of the $SU(2)$ unitary group:

$$SO(3) = SU(2)/Z_2 \tag{87}$$

for any canonical operator on a lattice, a $SU(2)$ transformation is formulated as

$$\hat{c}_i \longrightarrow e^{i\theta\vec{e}\cdot\vec{\sigma}}\hat{c}_i \tag{88}$$

where $\vec{\sigma}$ are the three Pauli matrices. Clearly for $\theta = \pi$:

$$\hat{c}_i \longrightarrow -\hat{c}_i \qquad \hat{c}_i^\dagger \longrightarrow -\hat{c}_i^\dagger \tag{89}$$

both our spin current operator (order parameter of QSH) and the spin operator (order parameter of SSC) are invariant. Note that here the operations above are performed for all i globally. After this two-to-one mapping both two order parameters live in the SO(3) space. On the other hand, the Z_2 symmetry group are gaped at both symmetry breaking phase and critical point:[2] the single fermion excitation have finite gap.

Crucially, the Z_2 group is also a subgroup of the $U(1)$ transformation in Eq. 84. It again leaves the SO(2) order parameters invariant since the cooper pairs are particle-particle(hole-hole) operators.

Theories given by Ref. [25] gives a clear argument: to get rid to the lattice induced symmetry breaking field, a 'gaped symmetry'(in our case, the Z_2 symmetry) which is the subgroup of both symmetries which are breaking at two sides of the critical points is necessarily required. In this sense, the seemingly 'redundant' fermionic degrees of freedom is important. For example, a superfluid state is very similar to our superconducting state from symmetry point of view and the symmetry breaking is also internal. However, it lacks the gaped Z_2 degrees of freedom that we mentioned before.

3.3 Numerical results

3.3.1 Ground state phase diagram and observables

We show our numerical results of the model $\hat{H} = \hat{H}_t + \hat{H}_\lambda$ mentioned before. As mentioned before, the auxiliary field QMC simulation is sign problem free due to a spin $\frac{1}{2}$ time reversal symmetry at $\lambda > 0$, which is also the physical region that we are interested in.

As shown in Fig. 12, we found three phases as well as two phase transitions as a function of interacting strength λ: A Dirac semimetal (DSM) state at weak interaction ($\lambda < \lambda_{c1}$) case; a dynamically generated QSH state at intermediate interaction range ($\lambda_{c1} < \lambda < \lambda_{c2}$) ; a S-wave superconducting (SSC) state at strong interaction limit ($\lambda > \lambda_{c2}$). The fermionic phase transition (λ_{c1}) corresponds to a Gross-Neveu Heisenberg critical point while the bosonic one is surprisingly a deconfined quantum critical point.

[2] A symmetry group is gaped explicitly means that all the operators which are charged under this transformation are gaped.

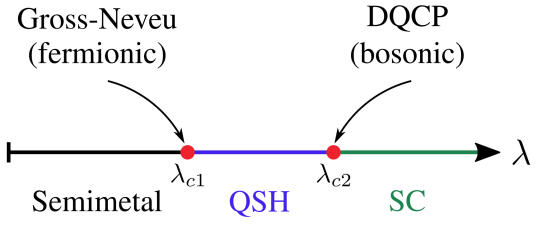

Figure 12: Schematic ground-state phase diagram with semimetallic, QSH, and SC phases.

To detect the two symmetry broken state, we measure the corresponding order parameters: the one for QSH ordering which corresponds to the spin-orbit coupling operators

$$\hat{\boldsymbol{O}}^{\mathrm{QSH}}_{\boldsymbol{r},n} = \hat{J}_{\boldsymbol{r}+\boldsymbol{\delta}_n,\boldsymbol{r}+\boldsymbol{\eta}_n} \tag{90}$$

Here, $\boldsymbol{r}$ denotes a unit cell and n runs over the six next-nearest neighbor bonds of the corresponding hexagon with legs $\boldsymbol{r}+\boldsymbol{\delta}_n$ and $\boldsymbol{r}+\boldsymbol{\eta}_n$.

To detect SC order, we used the order parameter

$$\hat{O}^{\mathrm{SC}}_{\boldsymbol{r},\tilde{\boldsymbol{\delta}}} = \frac{1}{2}\left(\hat{c}^{\dagger}_{\boldsymbol{r}+\tilde{\boldsymbol{\delta}},\uparrow}\hat{c}^{\dagger}_{\boldsymbol{r}+\tilde{\boldsymbol{\delta}},\downarrow} + \mathrm{H.c.}\right) \tag{91}$$

where $\boldsymbol{r}+\tilde{\boldsymbol{\delta}}$ runs over the two orbitals of unit cell $\boldsymbol{r}$.

To study the phase transition, we computed the associated susceptibility

$$\chi^{O}_{\boldsymbol{\delta},\boldsymbol{\delta}'}(\boldsymbol{q}) = \frac{1}{L^2}\sum_{\boldsymbol{r},\boldsymbol{r}'}\int_0^{\beta} \mathrm{d}\tau e^{\mathrm{i}\boldsymbol{q}\cdot(\boldsymbol{r}-\boldsymbol{r}')}\langle\hat{\boldsymbol{O}}_{\boldsymbol{r},\boldsymbol{\delta}}(\tau)\hat{\boldsymbol{O}}_{\boldsymbol{r}',\boldsymbol{\delta}'}(0)\rangle. \tag{92}$$

Here, $\langle\hat{\boldsymbol{O}}_{\boldsymbol{r},\boldsymbol{\delta}}(\tau)\rangle = 0$ by symmetry for finite L and we concentrate on the largest eigenvalue of $\chi^{O}_{\boldsymbol{\delta},\boldsymbol{\delta}'}(\boldsymbol{q})$ (see Section. 3.3.2), henceforth denoted as $\chi^{O}(\boldsymbol{q})$. To detect the transition, we consider the renormalization-group invariant correlation ratio

$$1 - \frac{\chi^{O}(\boldsymbol{Q}+\Delta\boldsymbol{q})}{\chi^{O}(\boldsymbol{Q})} = R^{O}_{\chi}\left(L^{1/\nu}\left(\lambda-\lambda^{O}_{c}\right), L^{-w}\right) \tag{93}$$

with $|\Delta\boldsymbol{q}| = \frac{4\pi}{\sqrt{3}L}$, the ordering wavevector $\boldsymbol{Q}=0$, the correlation length exponent ν, and the leading corrections-to-scaling exponent ω. Here we use susceptibilities rather than equal-time correlators to suppresses background contributions to the critical fluctuations.

Although the aim of our study is the ground state phase diagram an transitions, we used the finite temperature version of QMC and set the inverse temperature $\beta = L$ in our simulations. It's due to our assumption of a dynamical critical exponent $z=1$ for both the SM-QSH and the QSH-SC transition. This is motivated by the Lorentz invariance of the corresponding field theories [39, 8].

3.3.2 Advantage of susceptibilities

Generally to study a phase transition, one can take the equal time correlation functions of the symmetry breaking operators instead of the susceptibilities based on the imaginary time correlation function. Thus why do we need to compute the susceptibility ? The key point is the scaling correction due to the non-singular part of the free energy.

Symmetry-broken states are characterised by a local order parameter $\hat{\boldsymbol{O}}_{\boldsymbol{r},\boldsymbol{\delta}}$, where $\boldsymbol{r}$ denotes a unit cell and $\boldsymbol{\delta}$ an orbital within the unit cell. The associated time-displaced correlation functions read

$$S^{O}_{\boldsymbol{\delta},\boldsymbol{\delta}'}(\boldsymbol{q},\tau) = \frac{1}{L^2}\sum_{\boldsymbol{r},\boldsymbol{r}'}\langle\hat{\boldsymbol{O}}_{\boldsymbol{r},\boldsymbol{\delta}}(\tau)\cdot\hat{\boldsymbol{O}}_{\boldsymbol{r}',\boldsymbol{\delta}'}(0)\rangle e^{i\boldsymbol{q}\cdot(\boldsymbol{r}-\boldsymbol{r}')}\ . \tag{94}$$

For the finite-size scaling analysis, one could consider the order parameter

$$m^{O} = \sqrt{\frac{\Lambda_1(S^{O}_{\boldsymbol{\delta},\boldsymbol{\delta}'}(\boldsymbol{0},0))}{L^2}}\,, \tag{95}$$

and the equal-time correlation ratios

$$R^O = 1 - \frac{\Lambda_1(S^O_{\boldsymbol{\delta},\boldsymbol{\delta'}}(\Delta\boldsymbol{q},0))}{\Lambda_1(S^O_{\boldsymbol{\delta},\boldsymbol{\delta'}}(\boldsymbol{0},0))}\,, \tag{96}$$

with $|\Delta\boldsymbol{q}| = \frac{4\pi}{\sqrt{3}L}$, the susceptibilities

$$\chi^O = \Lambda_1\left(\int_0^\beta d\tau S^O_{\boldsymbol{\delta},\boldsymbol{\delta'}}(\boldsymbol{0},\tau)\right)\,, \tag{97}$$

and the corresponding correlation ratios

$$R^O_\chi = 1 - \frac{\Lambda_1\left(\int_0^\beta d\tau S_{\boldsymbol{\delta},\boldsymbol{\delta'}}(\Delta\boldsymbol{q},\tau)\right)}{\Lambda_1\left(\int_0^\beta d\tau S^O_{\boldsymbol{\delta},\boldsymbol{\delta}}(\boldsymbol{0},\tau)\right)}\,. \tag{98}$$

Here, $\Lambda_1()$ indicates the largest eigenvalue of the corresponding matrix in orbital space (6×6 for spin currents, 2×2 for pairing) and the ordering wave vector is at the Γ point.

These quantities exhibit the following finite-size scaling behaviour near the critical point:

$$\begin{aligned}
m^O(L,\lambda) &= L^{(2-d-z-\eta)/2} f_1(L^z/\beta, (\lambda-\lambda_c)L^{1/\nu}, L^{-\omega_1})\,,\\
R^O(L,\lambda) &= f_2(L^z/\beta, (\lambda-\lambda_c)L^{1/\nu}, L^{-\omega_2})\,,\\
\chi^O(L,\lambda) &= L^{2-\eta} f_3(L^z/\beta, (\lambda-\lambda_c)L^{1/\nu}, L^{-\omega_3})\,,\\
R^O_\chi(L,\lambda) &= f_4(L^z/\beta, (\lambda-\lambda_c)L^{1/\nu}, L^{-\omega_4})\,.
\end{aligned} \tag{99}$$

Here, λ_c, ν, η, and z are the critical coupling, the correlation length exponent, the anomalous dimension, and the dynamical critical exponent, respectively.

The correlation ratios R^O and R^O_χ are both renormalization group (RG) invariant quantities at the critical point and hence provide a simple way to estimate λ_c and ν without any knowledge about η. However, the generic corrections-to-scaling exponent ω is not necessarily the same for all four quantities in equation (99). Such corrections generally arise from irrelevant operators of the fixed point and the analytic part of the free energy. If the absolute value of the negative RG dimension is relatively large, the main contribution to ω will come from the background term of the free energy [46]. In this case,

$$\omega_1 = \omega_2 = 2 - z - \eta, \quad \omega_3 = \omega_4 = 2 - \eta\,. \tag{100}$$

This suggests that the susceptibility χ and the corresponding correlation ratio R_χ will have smaller scaling corrections than the corresponding equal-time quantities if the effect of the negative RG dimension is small at λ_c.

3.3.3 Gross-Neveu Heisenberg criticality

The semimetal-QSH transition involves the breaking of spin rotation symmetry and is expected to be in the O(3) Gross-Neveu universality class for $N = 8$ Dirac fermions (two sublattices, two Dirac points, $\sigma = \uparrow, \downarrow$).

The results for the semimetal-QSH transition are shown in Fig. 13. The finite-size estimate of the critical value, $\lambda_{c1}^{\mathrm{QSH}}(L)$, corresponds to the crossing point of R_χ^{QSH} for L and $L+6$. Extrapolation to the thermodynamic limit (inset of Fig. 13a) yields $\lambda_{c1}^{\mathrm{QSH}} = 0.0187(2)$. The correlation length exponent was estimated from [42]

$$\frac{1}{\nu^O(L)} = \frac{1}{\log r}\log\left(\frac{\frac{d}{d\lambda}R^O_\chi(\lambda, rL)}{\frac{d}{d\lambda}R^O_\chi(\lambda, L)}\right)\Bigg|_{\lambda=\lambda_c^O(L)} \tag{101}$$

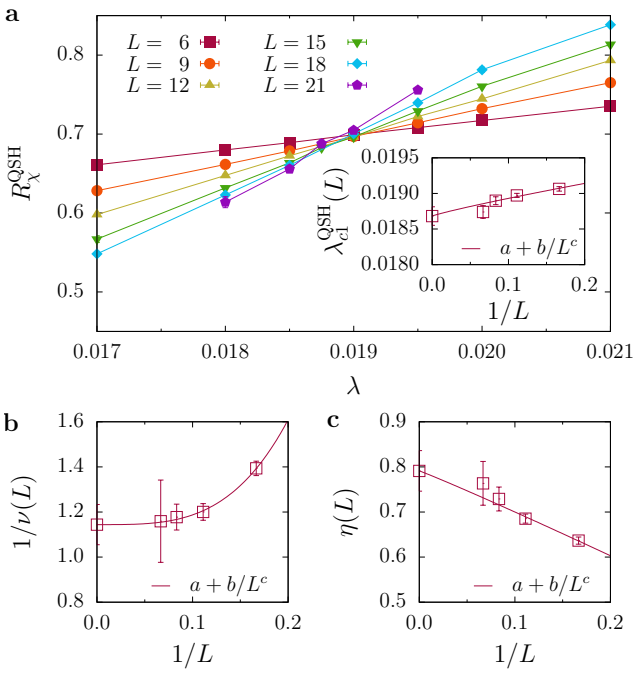

Figure 13: **Gross-Neveu semimetal-QSH transition.** **(a)** Correlation ratio R_χ^{QSH} [equation (93)] for different system sizes L. The extrapolation of the crossing points of R_χ^{QSH} for L and $L+6$ in the inset gives the critical value $\lambda_{\mathrm{c1}} = 0.0187(2)$. **(b)** Finite-size scaling based on equation (101) gives an inverse correlation length exponent $1/\nu = 1.14(9)$. **(c)** Estimation of the anomalous dimension $\eta = 0.79(5)$.

with $r = \frac{L+6}{L}$. Similarly the anomalous dimension η can be fit via

$$\eta^O(L) = 2 - \frac{1}{\log r} \log \left(\frac{\chi^O(\lambda, rL)}{\chi^O(\lambda, L)} \right) \Bigg|_{\lambda=\lambda_c^O(L)} , \tag{102}$$

Aside from a polynomial interpolation of the data as a function of λ for each L, this analysis does not require any further fitting and, by definition, converges to the correct exponents in the thermodynamic limit with rate $L^{-\omega}$. While previous estimates of the critical exponents vary,[46, 47, 48] the values $1/\nu = 1.14(9)$ and $\eta = 0.79(5)$ from Fig. 13 are consistent with $\nu = 1.02(1)$ and $\eta = 0.76(2)$ from previous work.[47] This suggest that the semimetal-QSH transition is in the same universality class as the semimetal-AFM transition [49, 46, 47].

In addition to the 'two-size crossing' with sizes L and $L+6$, we provide a cross check based on crossings of L and $L+3$. Fig 14**a**, **b** and **c** show the crossing values of λ, $1/\nu$ and η at the semimetal-QSH transition in the case of $r = 3$.

As an independent consistency check on such a 'two crossing' method, we also consider a collective fitting of multiple system sizes.

The collective fitting of λ_c and ν is based on a polynomial expansion of the scaling function of $R_\chi^O(L, \lambda)$ in equation (99). Taking $\beta = L$, we have

$$R_\chi^O(L, \lambda) \approx \sum_{p=0}^{n} a_p (\lambda - \lambda_c)^p L^{p/\nu} + L^{-\omega} \sum_{q=0}^{m} b_q (\lambda - \lambda_c)^q L^{q/\nu} . \tag{103}$$

Here, n and m are the expansion orders for the dimensionless and the scaling correction part of the universal function, respectively.

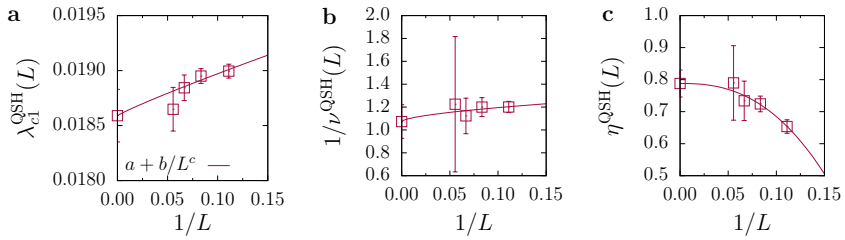

Figure 14: $L, L+3$ **extrapolation of Gross-Neveu semimetal-QSH transition.** (a) Extrapolation of the crossing points of R_χ^{QSH} for L and $L+3$ gives the critical value $\lambda_{c1}^{\mathrm{QSH}} = 0.0186(3)$. (b) The inverse correlation length exponent $1/\nu^{\mathrm{QSH}} = 1.1(2)$. (c) Estimation of the anomalous dimension $\eta^{\mathrm{QSH}} = 0.79(5)$. Reported errors and error bars correspond to standard errors.

Gross-Neveu – QSH					
$L_{\min}$	λ_c	$R_\chi^{\mathrm{QSH}}(\lambda_c)$	$1/\nu$	ω	χ^2/DOF
6	0.01898(2)	0.6970(6)	1.26(2)	n/a	94.6/34
9	0.01891(2)	0.693(1)	1.17(3)	n/a	34.8/27
12	0.01882(4)	0.687(2)	1.17(5)	n/a	18.6/20
15	0.01870(7)	0.678(5)	1.14(11)	n/a	9.22/13
18	0.0186(2)	0.67(2)	1.3(4)	n/a	1.90/6

Gross-Neveu – QSH		
$L_{\min}$	η	χ^2/DOF
6	0.666(7)	210/33
9	0.70(1)	111/26
12	0.76(2)	28.6/18
15	0.78(2)	4.4/12
18	0.81(6)	1.9/6

Table 1: Collective fitting for the Gross-Neveu transition. Here $n = 2$, while scaling corrections are ignored. Reported errors correspond to standard errors.

To reduce the number of degrees of freedom in the fit of the anomalous dimension η, a substitution in terms of the scaling form for χ^O and R_χ^O in equation (99) is performed, using the expansion (we ignore the correction-to-scaling term)

$$\chi^O(L, R) = L^{2-\eta} f(R) \approx L^{2-\eta} \sum_{p=0}^{n} a_p R^p \,. \tag{104}$$

A collective fit is shown in table 1. Here we gradually toss small system sizes instead of taking the scaling correction term into consideration. As can be seen, a good χ^2/DOF is obtained once the $L = 6$ data set is neglected, and fits for $L_{min} = 9, 12, 15$ or 18 produce consistent results. Taking $\lambda_{c1} = 0.01891(2)$ and $1/\nu = 1.17(3)$ from $L_{\min} = 9$, the results match those of the analysis from two size crossing method.

Results for the anomalous dimension at the Gross-Neveu critical point are also listed in table 1. The fits yield acceptable χ^2 values for $L_{\min} \geq 12$. The exponent $\eta = 0.76(1)$ from $L_{\min} = 12$ also matches previous analysis.

3.3.4 Deconfined quantum criticality

As shown in Fig. 16, the QSH state induced by spin rotational symmetry breaking gives way to the SC state at strong enough interaction, in the sense that the correlation ratio of SC order parameter grows toward 1 in the large size limit at $\lambda > \lambda_{c2}$. What is surprising is the direct and continues transition between the two different broken symmetry phase within our numerical precision. Fig 16 shows that, within the very small error bars, the critical value for SC order $\lambda_{c2}^{\mathrm{SC}} = 0.0332(2)$ and the critical value for the disappearance of long-range QSH order $\lambda_{c2}^{\mathrm{QSH}} = 0.03322(3)$ are identical, suggesting a direct QSH-SC transition.

If the QSH-SSC transition at $T = 0$ corresponds to a deconfined quantum critical point, two necessary conditions are needed. First, the elementary excitations along the transition point have to be bosonic and the ground state remains an insulator. Second, the transition has to be direct and continues. The conventional Landau-Ginzburg-Wilson framework is certainly violated when the above two conditions are satisfied: without any fine tuning, two order parameters with different symmetries do not need to condense at the same point.

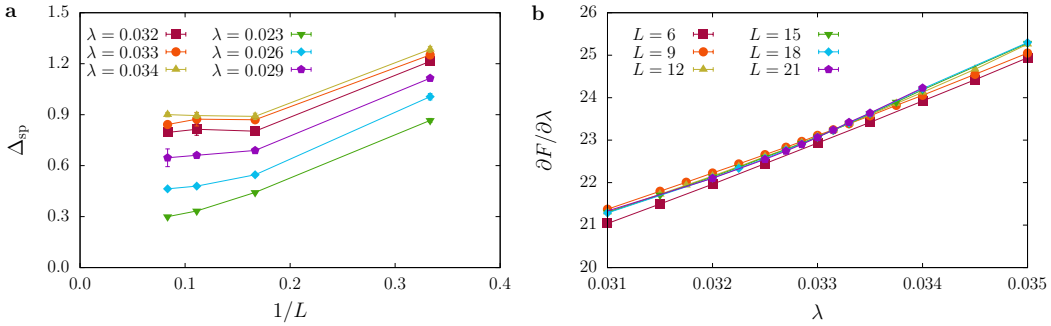

Figure 15: (a) Fermionic single-particle gap and (b) free-energy derivative $\partial F/\partial\lambda$ across the QSH-SC transition at $\lambda_{c2}^{\mathrm{SC}} = 0.0331(3)$. Reported errors and error bars correspond to standard errors.

The single-particle gap Δ_{sp} is obtained from the single-particle Green function

$$G(\boldsymbol{k}, \tau) = \frac{1}{L^2} \sum_{\boldsymbol{r},\boldsymbol{r'},\boldsymbol{\delta},\sigma} \langle \hat{c}^{\dagger}_{\boldsymbol{r}+\boldsymbol{\delta},\sigma}(\tau) \hat{c}_{\boldsymbol{r}+\boldsymbol{\delta},\sigma}(0) \rangle e^{\mathrm{i}\boldsymbol{k}\cdot(\boldsymbol{r}-\boldsymbol{r'})} \tag{105}$$

where $\boldsymbol{r} + \boldsymbol{\delta}$ runs over the two orbitals of the unit cell located at $\boldsymbol{r}$. The single-particle gap is minimal at the Dirac point $\mathrm{K} = (\frac{4\pi}{3}, 0)$ and is extracted by noting that asymptotically

$$G(\mathrm{K}, \tau) \propto e^{-\Delta_{\mathrm{sp}}\tau} . \tag{106}$$

Here, we used $\beta = 36$. Fig 15a demonstrates that Δ_{sp} remains nonzero across the QSH-SC transition at $\lambda_{c2} \approx 0.033$.

In order to clarify the continuity of the QSH-SC transition, we also calculated the first partial derivative of the free energy density with respect to the coupling λ

$$\frac{\partial F}{\partial \lambda} = -\frac{1}{L^2} \sum_{\hexagon} \left\langle \left(\sum_{\langle\langle \boldsymbol{i},\boldsymbol{j} \rangle\rangle \in \hexagon} \mathrm{i}\nu_{\boldsymbol{ij}} \hat{\boldsymbol{c}}^{\dagger}_{\boldsymbol{i}} \boldsymbol{\sigma} \hat{\boldsymbol{c}}_{\boldsymbol{j}} + \mathrm{H.c.} \right)^2 \right\rangle . \tag{107}$$

Fig 15b shows $\partial F/\partial\lambda$ for $\beta = L$ in the vicinity of $\lambda_{c2} \approx 0.033$. As expected for a continuous transition, we observe no sign of a jump.

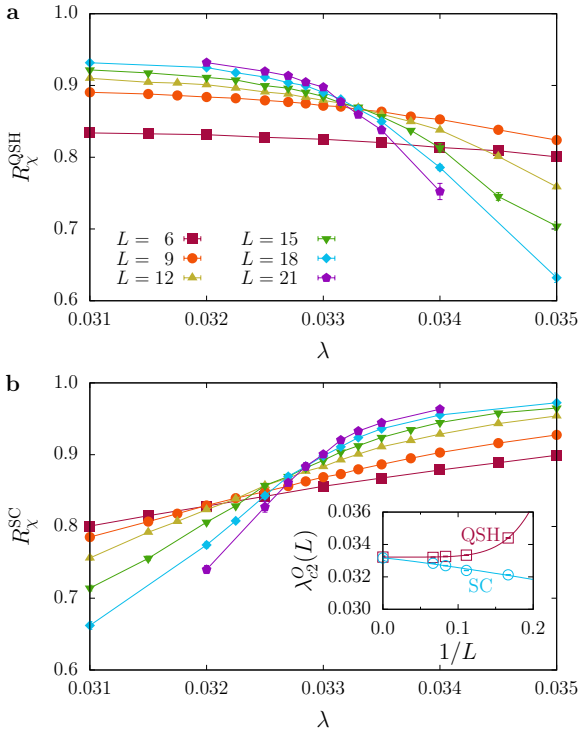

Figure 16: **Deconfined QSH-SC transition.** (a) Correlation ratio $R_\chi^{\rm QSH}$ and (b) correlation ratio $R_\chi^{\rm SC}$ for different system sizes L. The extrapolation of the crossing points for L and $L+6$ using the form $a+b/L^c$ (see inset of (b)) gives $\lambda_{c2}^{\rm QSH} = 0.03322(3)$ and $\lambda_{c2}^{\rm SC} = 0.0332(2)$.

Fig 17 shows a finite-size analysis for the correlation length exponent and the anomalous dimension, as obtained either from the QSH or the SC correlation ratio. The resulting estimates $\eta^{\rm QSH} = 0.21(5)$ and $\eta^{\rm SC} = 0.22(6)$ are compatible with those from loop models [50] where $\eta^{\rm AFM} = 0.259(6)$ and $\eta^{\rm VBS} = 0.25(3)$. Given the very similar anomalous dimensions $\eta^{\rm QSH}$ and $\eta^{\rm SC}$ of QSH and SC fluctuations, the ratio of the QSH and SC susceptibilities is expected to be a renormalization group invariant, as confirmed by Fig. 17c.

The equivalence of two anomalous dimensions is a necessary but not sufficient condition for an emergent SO(5) symmetry at the DQCP. For a SO(5) invariant field theory, 10 generators of the SO(5) group, which can also be written as second quantized operators, are conserved quantities. In our lattice model one can measure the imaginary time correlation function of them, in order to see the emergence of conservation in the low energy limit.

On the other hand, we would like to avoid the possibility of high symmetry here. The reason is that, a continuous transition with emergent SO(5) symmetry can be essentially excluded in the light of the condition $\eta > 0.52$ from the conformal bootstrap method.[51] Hence, as a way out, one can always argue that our numerical equivalence of $\eta^{\rm QSH}$ and $\eta^{\rm SSC}$ is an approximate effect due to the finite error bars.

The correlation length exponent at the DQCP is also shown in Fig. 17, with $1/\nu^{\rm SC} = 1.8(2)$ and $1/\nu^{\rm QSH} = 1.7(4)$. This number does not violate the bootstrap bound of $1/\nu < 1.957$ for a unitary conformal field theory with only one tuning parameter [52]. However, this might be from the large error bar of our calculation. Note that in the JQ model, a value $1/\nu = 2.24(4)$ quoted in Ref. [42] violate the bootstrap bound.

When considering the L and $L+6$ crossings the estimation of $\lambda_{c2}^{\rm SC}$, we are obliged

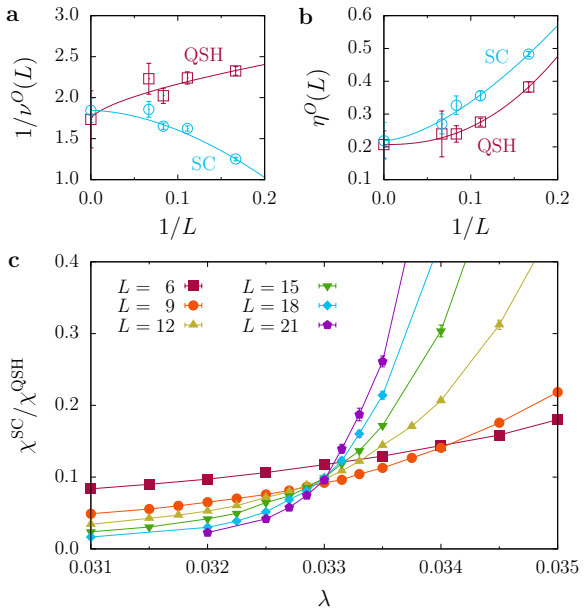

Figure 17: **Critical exponents for the QSH-SC transition.** (a), (b) Critical exponents $1/\nu^{\mathrm{SC}} = 1.8(2)$, $1/\nu^{\mathrm{QSH}} = 1.7(4)$, $\eta^{\mathrm{SC}} = 0.22(6)$, and $\eta^{\mathrm{QSH}} = 0.21(5)$ from finite-size scaling of the crossing points for L and $L+6$. (c) Ratio of the QSH and SC susceptibilities for different system sizes L.

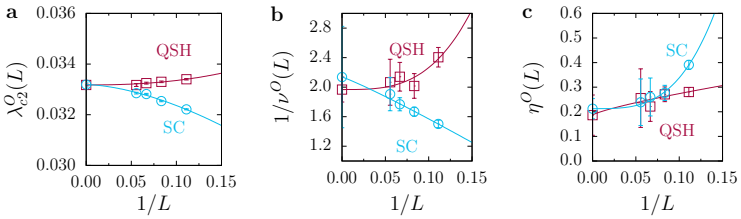

Figure 18: $L, L+3$ **extrapolation of deconfined QSH-SC transition.** **a** Estimation of the critical values $\lambda_{c2}^{\mathrm{QSH}} = 0.03317(4)$ and $\lambda_{c2}^{\mathrm{SC}} = 0.0332(1)$. **b** , **c** Critical exponents $1/\nu^{\mathrm{SC}} = 2.1(7)$, $1/\nu^{\mathrm{QSH}} = 2.0(2)$, $\eta^{\mathrm{SC}} = 0.21(5)$, and $\eta^{\mathrm{QSH}} = 0.19(9)$ from finite-size scaling of the crossing points of L and $L+3$. Reported errors and error bars correspond to standard errors.

to take into account the $L = 6$ data. Upon inspection, the fit turns out to be rather bad since $\chi^2/\mathrm{DOF} = 66.9$. On the other hand, if we consider the L and $L+3$ crossing points, we can omit the $L = 6$ data and get a more acceptable $\chi^2/\mathrm{DOF} = 6.8$. As apparent from Fig. 18, the extrapolated value of $\lambda_{c2}^{\mathrm{SC}}$ based on the crossing points of L and $L+3$ compares favourably with the $L, L+6$ analysis mentioned before.

As in the Gross-Neveu transition, we also performed a collective fit using the expansion form of Eq. 103 and Eq. 104. Table 2 reports the results of fits for the two order parameters at the DQCP, including the case with $m = 1$, as well as the case without considering any scaling correction. We set $n = 2$ for all the fits. For $m = 1$, the fitting of the QSH correlation ratio is satisfactory in terms of χ^2/DOF for $L_{\min} \geq 9$, and the results are consistent with each other for $L_{\min} = 9, 12, 15$. Taking $\lambda_{c2} = 0.03314(5)$ and $1/\nu = 1.55(9)$ from the fit with $L_{\min} = 9$, we get consistency with $\lambda_{c2}^{\mathrm{QSH}} = 0.03322(3)$ and $1/\nu^{\mathrm{QSH}} = 1.7(4)$ from the 'two-size crossing' analysis . The results of a fit with a smaller data window are shown in the last three rows of table 2, revealing that the results are stable upon variation of the number of degrees of freedom. A fit using R_χ^{SC}

DQCP – QSH					
$L_{\min}$	λ_c	$R_\chi^{\mathrm{QSH}}(\lambda_c)$	$1/\nu$	ω	χ^2/DOF
9	0.03332(1)	0.8665(4)	2.22(5)	n/a	139/44
12	0.03326(2)	0.8702(8)	2.21(7)	n/a	58.9/32
15	0.03326(3)	0.870(2)	2.3(2)	n/a	33.4/22
18	0.03321(5)	0.875(5)	2.4(3)	n/a	13.9/12
9	0.3314(5)	0.89(2)	1.55(9)	0.9(3)	29.1/41
12	0.331(2)	0.92(9)	1.5(2)	0.4(9)	24.7/29
15	0.331(2)	0.89(2)	1.6(3)	4(3)	15.1/19
9	0.3315(5)	0.89(2)	1.5(2)	0.9(4)	28.2/36
12	0.331(2)	0.91(8)	1.5(2)	0.5(9)	23.8/26
15	0.331(2)	0.89(3)	1.7(3)	3(3)	13.9/16
DQCP – SC					
$L_{\min}$	λ_c	$R_\chi^{\mathrm{SC}}(\lambda_c)$	$1/\nu$	ω	χ^2/DOF
9	0.032675(4)	0.8592(4)	1.32(3)	n/a	1239/40
12	0.032791(5)	0.8742(5)	1.60(4)	n/a	123/29
15	0.032843(8)	0.882(1)	1.83(6)	n/a	15.9/18
18	0.03286(3)	0.884(4)	1.9(2)	n/a	2.23/9
9	0.03296(5)	0.907(9)	2.1(2)	1.7(3)	53.8/37
12	0.03287(2)	0.887(2)	2.3(2)	4.4(8)	26.0/26
15	0.0329(2)	0.89(3)	2.0(4)	3(13)	15.1/15
9	0.0331(2)	0.94(4)	1.9(2)	1.1(5)	42.5/33
12	0.03285(3)	0.884(5)	2.0(3)	8(6)	20.6/22
15	0.0329(2)	0.89(3)	1.7(5)	4(16)	14.4/13

Table 2: Collective fitting at the DQCP for λ_c, $1/\nu$, and $R_\chi^O(\lambda_c)$ based on the correlation ratios $R_\chi^O(L,\lambda)$ and equation (103). We compare the case without taking into account scaling corrections (data rows 1–4) to the case with $m = 1$ (rows 5–7 correspond to a larger data window, rows 8–10 to a smaller one); in both cases, $n = 2$. Reported errors correspond to standard errors.

also produces acceptable values of χ^2/DOF for $L_{\min} = 9$, 12 and 15 and compares favourably with the results from the crossing analysis.

As shown in table 3, the collective fitting for both order parameters is acceptable for $L_{\min} \geq 12$. The corresponding values $\eta^{\mathrm{QSH}} = 0.194(9)$ and $\eta^{\mathrm{SC}} = 0.279(9)$ agree well with the values 0.21(5) and 0.22(6) obtained with the 'two-size crossing' approach mentioned before.

3.4 Discussion

Our model provides a realisation of a QSH insulator emerging from spontaneous symmetry breaking. The corresponding SO(3) order parameter permits both long-wavelength Goldstone modes and topological skyrmion defects. By means of a single parameter λ, we can trigger continuous quantum phase transitions to either a semimetal or an s-wave SC state. For the semimetal-QSH transition, the critical exponents are consistent with Gross-Neveu universality [46, 47]. The QSH-SC transition is of particular interest since it provides a monopole-free, improved model of deconfined quantum crit-

DQCP – QSH		
$L_{\min}$	η	χ^2/DOF
6	0.30(2)	990/68
9	0.24(1)	249/57
12	0.19(2)	92.0/40
15	0.24(3)	49.8/25
18	0.18(6)	12.0/12

DQCP – SC		
$L_{\min}$	η	χ^2/DOF
6	0.344(8)	525/45
9	0.308(7)	128/36
12	0.28(2)	65.6/26
15	0.23(2)	24.2/17
18	0.19(9)	7.47/8

Table 3: Same analysis as in table 2 but for the exponent η using equation (104). Here $n = 2$, while scaling corrections are ignored. Reported errors correspond to standard errors.

icality with only one length scale. The mechanism for SC order from the QSH state is the condensation of skyrmion defects of the QSH order parameter with charge 2e. For the QSH-SC transition, our values of the anomalous dimension match those of previous work on the AFM-VBS transition,[17, 50] which are inconsistent with results from conformal bootstrap studies if an SO(5) symmetry emerges at the critical point (as is supported by numerical and analytical studies). One possible resolution is the scenario of 'pseudo-criticality' or 'walking coupling constant' [53, 50, 54, 55]. In contrast, our estimate of $1/\nu$ is still within the conformal bootstrap bound,[52] although a bound-violating result is not completely ruled out given the numerical uncertainty. Consequently, it is of considerable interest to exploit the full potential of quantum Monte Carlo methods in order to access even larger lattices.

Other promising approaches that can shed further light on DQCPs make use of a lattice discretisation scheme based on projection onto a Landau level that does not break continuum symmetries.[56][3] This approach makes the assumption of exact SO(5) symmetry at the critical point. Our numerical progress on this topic will be shown in the following section.

A monopole-free realisation of DQCPs is impossible in traditional settings because of an anomaly[54] associated with the SO(3)×U(1) symmetry. In the standard realisation, this anomaly is matched by the non-onsite nature of lattice rotation symmetries[57], but since lattice rotations are discrete, monopoles can never be completely suppressed. Alternatively, the anomaly can be eliminated by properly enlarging the SO(3)×U(1) symmetry, essentially allowing microscopic degrees of freedom that carry 'fractional' symmetry quantum numbers. This is what is being done in this work, where the fermions carry half-spin and half-charge (in terms of Cooper pair charges). An even simpler extension of the symmetry that eliminates the anomaly is SU(2)×U(1), meaning that microscopically there are charged spinless bosons, together with both charged and neutral spin-1/2 bosons. A challenge for future studies is to find a reasonably simple Hamiltonian that realises a DQCP and is amenable to sign-free bosonic QMC simulations in, e.g., the stochastic series expansion representation.[58]

On the other hand, the concept of 'emergent anomaly'[25] gives us a new possibility of understanding the critical point. Hence the low energy degrees of freedom written as an $SO(3) \otimes U(1)$ action after gaping out the fermions is anomalous, it would be interesting to look at the edge physics based on single fermion propagation in an open boundary system. This is beyond the simple understanding based on topological insulators since our DQCP is not a symmetry broken phase, in the sense that the QSH order parameter is not long range ordered.

The SC phase generated from skyrmion defects motivates further investigations. Its vortex excitations carry a spin-1/2 degree of freedom,[37] so that in the quantum critical fan thermal melting will yield a spin liquid [59]. It is also possible to add an independent attractive Hubbard interaction to explore a semimetal-QSH-SC tricritical point (as opposed to the recently discovered semimetal-AFM-VBS tricritical point[60]) with predicted SO(5) Gross-Neveu criticality.[61] The vector form of $\hat{H}_\lambda$ makes it straight forward to reduce the SO(3) QSH symmetry to U(1) and thereby investigate easy-plane realisation of DQCPs with a U(1)×U(1) symmetry on the lattice. On the other hand, a direct investigation of the fractionalization of QSH and SSC order parameters based on measuring the dynamical properties of the operators is in progress.

4 Doping-induced quantum spin Hall insulator to superconductor transition

In this Chapter, we consider aforementioned model which describes a dynamically generated QSH insulator and investigate a new path toward superconductivity: doping. Within the model considered in last Chapter, we observe, upon varying the chemical potential, two transitions: An s-wave superconducting order parameter develops at a critical chemical potential μ_{c1}, corresponding to the excitation gap of pairs of fermions, and at μ_{c2} the SO(3) order parameter of the quantum spin Hall state vanishes. Using negative-sign-free, large-scale quantum Monte Carlo simulations, we show that $\mu_{c1} = \mu_{c2}$ within our accuracy—we can resolve dopings away from half filling down to $\delta = 0.0017$. The length scale associated with the fluctuations of the quantum spin Hall order parameter grows down to our lowest doping, suggesting either a continuous or a weakly first-order transition. Contrary to mean-field expectations, the doping versus chemical potential curve is not linear, indicating a dynamical critical exponent $z > 2$ if the transition is continuous. This work has been published in Ref. [2].

4.1 Motivation

Here we generalize the Hamiltonian of Eq. 37 in Chapter. 3 including a chemical potential:

$$\hat{H} = \hat{H}_t + \hat{H}_\lambda + \mu \sum_{\boldsymbol{i}} n_{\boldsymbol{i}} \tag{108}$$

where $\hat{n}_i \equiv \hat{c}^\dagger_{\boldsymbol{i},\alpha}\hat{c}_{\boldsymbol{i},\alpha}$ denotes the particle number operator on site i. The ($SU(2)$ invariant) particle hole (P-H) symmetry defined by transformation:

$$\hat{P}^{-1}\alpha\begin{pmatrix}\hat{c}^\dagger_{\boldsymbol{i},\uparrow}\\ \hat{c}^\dagger_{\boldsymbol{i},\downarrow}\end{pmatrix}\hat{P} \equiv \eta_i\overline{\alpha}\begin{pmatrix}\hat{c}_{\boldsymbol{i},\uparrow}\\ \hat{c}_{\boldsymbol{i},\downarrow}\end{pmatrix} \tag{109}$$

is broken by finite chemical potential. $\eta_{\boldsymbol{i}}$ is defined as $1(-1)$ for $\boldsymbol{i} \in A(B)$ sublattice. We are interested in the effect of doping from the aforementioned QSH insulator in last Chapter.

Recall the half-filed case, the P-H transformation is the generator of Z_2 subgroup of $O(3)$ ($Z_2 \otimes SO(3)$) symmetry of spin current operators: it leaves the many body Hamiltonian $\hat{H}_t + \hat{H}_\lambda$ invariant but flips the sign of the determinant in the $O(3)$ transformation of 3 component spin current. This was crucial to our discussion about 'charged skyrimions' at half filling: the Pontryagin index of spin current order parameter is odd under under P-H transformation, (which is a symmetry of our many body Hamiltonian) such that the number of skyrmions has to be identical to the number of anti-skyrmions. In another words, zero value of Pontryagin index is pinned at any imaginary time. However in the doped case, the P-H symmetry is broken explicitly, which necessarily implies a finite 'fugacity' of skyrimions.

What can happen in the doped case? The first guess would be a SSC ground state, which was found in our model at half filling in the strong interaction count. As long as finite doping exists, the pairing instability of Fermi surfaces to 'attractive' interactions within the Bardeen-Cooper-Schrieffer (BCS) theory should be favored. This can be checked in a mean field approach introduced in next section. We propose the ground state phase diagram as a function of λ and μ in Fig. 19. The phase diagram at half

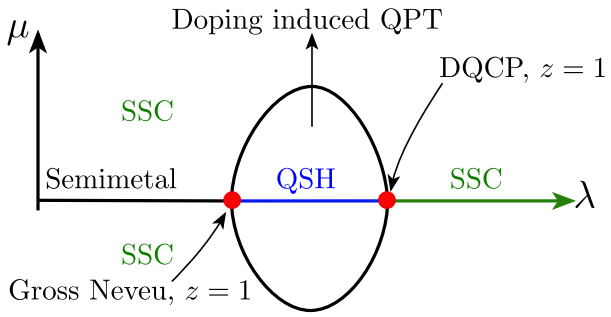

Figure 19: The proposed ground-state phase diagram as a function of interaction strength λ and chemical potential μ.

filing is known by QMC simulation in Chapter. 3. The ground state is symmetric under flipping sign of μ due to the P-H symmetry defined by the transformation of Eq. 109.

On the other hand, we can not forget that the QSH is a symmetry broken state. The charge 2 skyrmions of spin current order parameter would necessarily lead to the preformed pairs in QSH state. We can gain intuition by looking at the dispersion relation of two order parameters in the half filled case. Let's consider $t = 1$ and $\lambda = 0.026$, which places us in the center of the QSH phase at half-filling.

At this filling, we show in Fig. 20 the momentum dependence of the spin-orbit coupling gap $\Delta_{\mathrm{QSH}}(\boldsymbol{q})$ and the SSC gap $\Delta_\eta(\boldsymbol{q})$. To obtain these data, we measured the imaginary-time displaced correlation functions of the spin-orbit coupling operators $\hat{\boldsymbol{O}}^{\mathrm{QSH}}_{\boldsymbol{r},n} = \hat{J}_{\boldsymbol{r}+\boldsymbol{\delta}_n,\boldsymbol{r}+\boldsymbol{\eta}_n}$. Here, $\boldsymbol{r}$ denotes a unit cell and n runs over the six next-nearest neighbor bonds of the corresponding hexagon with legs $\boldsymbol{r}+\boldsymbol{\delta}_n$ and $\boldsymbol{r}+\boldsymbol{\eta}_n$. We also consider the s-wave pairing operators $\hat{\eta}^+_{\boldsymbol{r},\tilde{\boldsymbol{\delta}}} = \hat{c}^\dagger_{\boldsymbol{r}+\tilde{\boldsymbol{\delta}},\uparrow}\hat{c}^\dagger_{\boldsymbol{r}+\tilde{\boldsymbol{\delta}},\downarrow}$, where $\tilde{\delta}$ runs over the two orbitals in unit cell $\boldsymbol{r}$. The gaps were obtained from

$$\begin{aligned} S^{\mathrm{QSH}}(\boldsymbol{q},\tau) &= \sum_n \langle \hat{\boldsymbol{O}}^{\mathrm{QSH}}_{\boldsymbol{q},n}(\tau)\hat{\boldsymbol{O}}^{\mathrm{QSH}}_{-\boldsymbol{q},n}(0)\rangle \propto e^{-\Delta_{\mathrm{QSH}}(\boldsymbol{q})\tau} \\ S^{\mathrm{SSC}}(\boldsymbol{q},\tau) &= \sum_{\tilde{\boldsymbol{\delta}}} \langle \hat{\eta}^+_{\boldsymbol{q},\tilde{\boldsymbol{\delta}}}(\tau)\hat{\eta}^-_{\boldsymbol{q},\tilde{\boldsymbol{\delta}}}(0) + \hat{\eta}^-_{\boldsymbol{q},\tilde{\boldsymbol{\delta}}}(\tau)\hat{\eta}^+_{\boldsymbol{q},\tilde{\boldsymbol{\delta}}}(0)\rangle \\ &\propto e^{-\Delta_\eta(\boldsymbol{q})\tau}, \end{aligned} \tag{110}$$

in the limit of large imaginary time τ. As expected for a Goldstone mode, $\Delta_{\mathrm{QSH}}(\boldsymbol{q})$ in Fig. 20(b) exhibits a gapless, linear dispersion around the ordering wave vector $\boldsymbol{q} = \Gamma$. On the other hand, $\Delta_\eta(\boldsymbol{q})$ remains clearly nonzero with quadratic dispersion (see Fig. 20(a)).

It is important to note that an s-wave pair has a smaller excitation energy than twice the single-particle gap, as shown in the inset of Fig. 20(a). This indicates an effective attractive interaction between the electrons. Thus, pairing is present and we can foresee that these preformed pairs would condense and form a superconducting state upon doping. This is a significant difference as compared to a trivial insulator. We know that the pairing gap is exactly twice the single electron gap in a band insulator without interaction. This is generalized to the interacting case in some numerical works. Take a Kane-Mele model with attractive Hubbard interaction[62][3], when U is not large

[3]Here we consider a partial particle-hole transformation to only spin up(down) channel in the S_z basis. Under this transformation the kinetic part of Hamiltonian defined in Ref. [62] is invariant but the Hubbard term change the sign. Simultaneously the $\hat{S}_+$($\hat{S_-}$) operator is transformed to be the real(imaginary) part of the cooper pair operator.

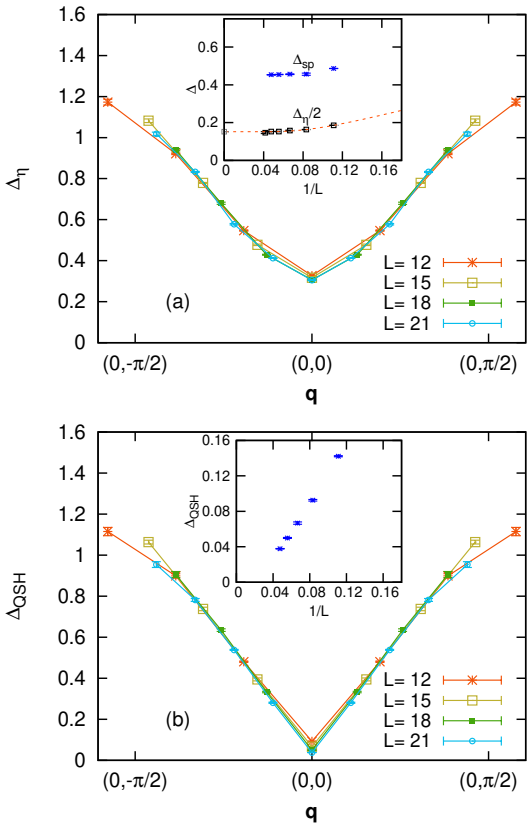

Figure 20: Momentum dependence of (a) the pairing gap and (b) the QSH gap for the half-filled case, in the vicinity of Γ point along the direction towards the M point in the Brillouin zone of the honeycomb lattice. The inset of (a) shows the $1/L$ dependence of the single-particle gap $\Delta_{\rm sp}$ and half of the s-wave pairing gap $\Delta_\eta/2$. The inset of (b) shows the $1/L$ dependence of the QSH gap $\Delta_{\rm QSH}$.

enough, the ground state is in a QSH state where the spin rotational symmetry is explicitly broken. In this case, the pairing gap is smaller than twice single particle gap at finite system sizes, but their difference $2\Delta_{sp}-\Delta_{\eta}$ scales to zero in the thermodynamic limit[62].

Focusing on the gaped dispersion relation of pairing at Fig. 20, we may naively think that doping will induce a pairing condensation which follows the field theory of Bose-Hubbard model (BHM)[26]:

$$\mathcal{L} = K_1\Psi^*\frac{\partial\Psi}{\partial\tau} + K_2|\frac{\partial\Psi}{\partial\tau}|^2 + K_3|\nabla\Psi|^2 + r|\Psi|^2 + u|\Psi|^4 \tag{111}$$

for $K_1 \neq 0$. It will be a transition with a dynamical exponent $z = 2$, and one can also consider the doped particle number (which is the density operator of boson in BHM) as an order parameter. This assumption is simply based on viewing the pairing operator as the creation and annihilation operators of single boson, and we know it's valid from the symmetry point of view. However the QSH order parameter does not exist in above theory.

Finite chemical potential explicitly broke the Z_2 part of the $O(3)$ symmetry of QSH order parameter. Hence one may formulate a field theory based on a $O(3)$ nonlinear sigma model with an additional term of μQ, where Q is the Pontryagin index. It's a theory which violate Lorenz invariance since Q is not spacial-time symmetric. Note that the $U(1)$ charge conservation is not broken by chemical potential: Q is still conserved along imaginary propagation.

We don't write down this assumed theory without rigorous argument here, and especially we don't know how to extract the order parameter of cooper pairs from the $SO(3)$ order parameter. Nevertheless, the evidence of preformed pairs from the our numerical observation of $\Delta_{\eta} < 2\Delta_{sp}$ at half filing is generally related to topology, and it may bring exotic phases or phase transitions upon doping. It's highly related to the concept of high-temperature superconductivity in doped two-dimensional antiferomagnets. As documented experimentally [63], the spin dynamics is well described by spin-wave theory that captures the Goldstone modes of the broken global SO(3) symmetry. Upon doping, these modes can act as a glue providing the pairing for the superconducting state [64]. Alternatively, due to the small spin quantum number and low dimensionality, the quantum antiferromagnet could be *close* to a resonating valence bond state [65, 66]. This leads to the notion of preformed pairs that are present in the insulating phase and become charged upon doping.

4.2 Mean field

Before discussing our QMC results, it is instructive to carry out a mean-field approximation. When expanding the square in Eq. (109), diagonal terms, $\hat{J}^2_{\boldsymbol{i},\boldsymbol{j}}$, contain, among other interactions, s-wave pair hopping terms that allow us to introduce an SSC order

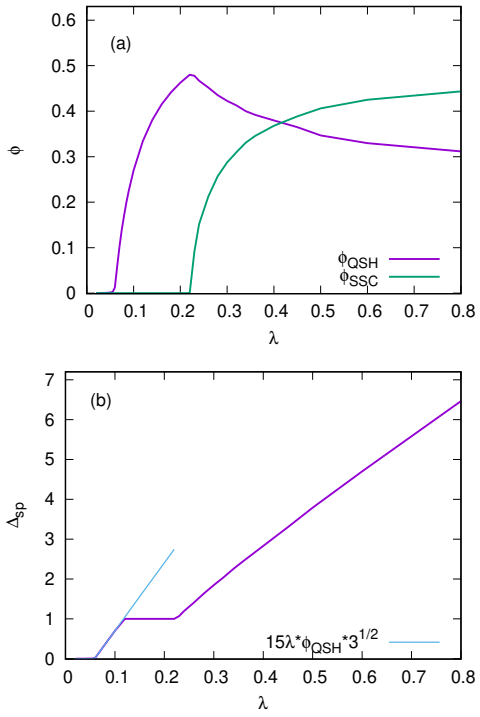

Figure 21: Mean-field solution as a function of λ at half-filling. (a) QSH and SSC order parameters. (b) Fermionic single-particle gap. Blue line in (b) denotes the gap at Dirac point.

parameter:

$$\begin{aligned} H_V =& -\lambda \sum_{\hexagon} \left(\sum_{\langle\langle \boldsymbol{ij} \rangle\rangle} i\nu_{\boldsymbol{ij}} \hat{c}_{\boldsymbol{i}}^{\dagger} \boldsymbol{\sigma} \hat{c}_{\boldsymbol{j}} + H.c. \right)^2 \\ =& -\lambda \sum_{\hexagon} \sum_{\langle\langle \boldsymbol{ij} \rangle\rangle} \sum_{\langle\langle \boldsymbol{i'j'} \rangle\rangle \neq \langle\langle \boldsymbol{ij} \rangle\rangle} \hat{\boldsymbol{J}}_{\langle\langle i,j \rangle\rangle} \cdot \hat{\boldsymbol{J}}_{\langle\langle i',j' \rangle\rangle} \\ & -\lambda \sum_{\hexagon} \sum_{\langle\langle \boldsymbol{ij} \rangle\rangle} [+6\hat{\eta}_{\boldsymbol{i}}^{\dagger} \hat{\eta}_{\boldsymbol{j}} + h.c - 4\hat{\boldsymbol{S}}_{\boldsymbol{i}} \cdot \hat{\boldsymbol{S}}_{\boldsymbol{j}} \\ & - 5\hat{n}_{\boldsymbol{i}} \hat{n}_{\boldsymbol{j}} + 5(\hat{n}_{\boldsymbol{i}} + \hat{n}_{\boldsymbol{j}})] \end{aligned} \tag{112}$$

where

$$\begin{aligned} & \hat{\boldsymbol{J}}_{\langle\langle i,j \rangle\rangle} \equiv i\nu_{\boldsymbol{ij}} \hat{c}_{\boldsymbol{i}}^{\dagger} \boldsymbol{\sigma} \hat{c}_{\boldsymbol{j}} + H.c., \\ & \hat{\eta}_{\boldsymbol{i}} \equiv \hat{c}_{\boldsymbol{i}\downarrow} \hat{c}_{\boldsymbol{i}\uparrow}, \quad \hat{\eta}_{\boldsymbol{i}}^{\dagger} \equiv \hat{c}_{\boldsymbol{i}\uparrow}^{\dagger} \hat{c}_{\boldsymbol{i}\downarrow}^{\dagger}, \\ & \hat{\boldsymbol{S}}_{\boldsymbol{i}} \equiv \frac{1}{2} \hat{c}_{\boldsymbol{i}}^{\dagger} \boldsymbol{\sigma} \hat{c}_{\boldsymbol{i}}. \end{aligned} \tag{113}$$

The self-consistent calculation is based on selecting a polarization direction for the three (two) components of the QSH (SSC) order parameter. This is valid since the pairing operator is invariant under the $SU(2)$ spin rotational transformation; while the spin current operators are invariant under $U(1)$ charge transformation.

The calculation is done by numerically minimizing the free energy in the space of the two order parameters

$$f(\beta)_{\phi} = \frac{-1}{\beta V} \ln \mathrm{Tr}\, e^{-\beta(H_T + H_V) - 15\beta V \lambda {\phi_{\mathrm{QSH}}}^2 - 36\beta V \lambda {\phi_{\mathrm{SSC}}}^2} \tag{114}$$

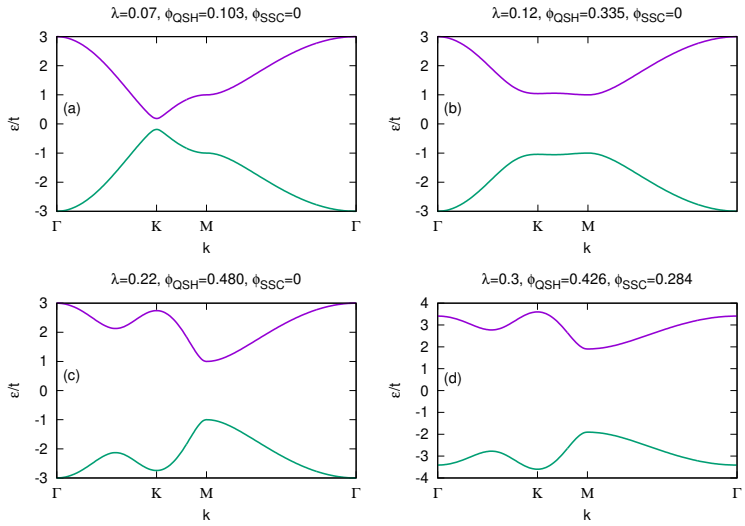

Figure 22: Mean field band structure at half filed case: (a) $\lambda = 0.07$, (b) $\lambda = 0.12$, (c) $\lambda = 0.22$ and (d) $\lambda = 0.3$(coexisting region).

where

$$\begin{aligned} H_T =& -t \sum_{\langle \boldsymbol{i},\boldsymbol{j}\rangle} (\hat{\boldsymbol{c}}_{\boldsymbol{i}}^\dagger \hat{\boldsymbol{c}}_{\boldsymbol{j}} + H.c.) + \mu \sum_{\boldsymbol{i}} \hat{\boldsymbol{c}}_{\boldsymbol{i}}^\dagger \hat{\boldsymbol{c}}_{\boldsymbol{i}} \\ H_V =& -5\lambda \sum_{\hexagon} \sum_{\langle\langle \boldsymbol{ij}\rangle\rangle} \phi_{\text{QSH}} \cdot \hat{J}^z{}_{\langle\langle i,j\rangle\rangle} \\ & -36\lambda \sum_{\boldsymbol{i}} \phi_{\text{SSC}} \hat{\eta}_{\boldsymbol{i}}^x. \end{aligned} \tag{115}$$

We consider a paramagnetic saddle point with $\langle \hat{\boldsymbol{S}}_{\boldsymbol{i}} \rangle = 0$ and $\langle \hat{n}_{\boldsymbol{i}} \rangle = 1 - \delta$. Thus, for any local minimum of Eq. (114) with $\frac{\partial f}{\partial \phi_{\text{QSH}}} = 0$ and $\frac{\partial f}{\partial \phi_{\text{SSC}}} = 0$,

$$\begin{aligned} \phi_{\text{QSH}} &= \frac{1}{6} \sum_{\langle\langle \boldsymbol{ij}\rangle\rangle} \langle \hat{J}^z{}_{\langle\langle i,j\rangle\rangle} \rangle \\ \phi_{\text{SSC}} &= \frac{1}{2} \langle \hat{\eta}_{\boldsymbol{i},A}^x + \hat{\eta}_{\boldsymbol{i},B}^x \rangle \end{aligned} \tag{116}$$

which holds locally due to translational symmetry. We numerically integrated over the Brillouin zone of an $L = 120$ lattice and took the zero-temperature limit $\beta \to \infty$.

The two order parameters as a function of λ in the half-filled case are shown in Fig. 21(a). We observe a semimetal ($\phi_{\text{QSH}} = \phi_{\text{SSC}} = 0$), a pure QSH state ($\phi_{\text{QSH}} \neq 0, \phi_{\text{SSC}} = 0$) as well as a coexistence (QSH+SSC) state ($\phi_{\text{QSH}} \neq 0, \phi_{\text{SSC}} \neq 0$). Since charge conservation is a protecting symmetry of the QSH insulator, the transition between the QSH and QSH+SSC states can be continuous without a closing of the single-particle gap (see Fig. 21(b)).

On the other hand, it might be interesting to mention the single particle band structure at half filling. In a pure QSH state, the single particle gap at K (Dirac) point opens proportionally to the amplitude of QSH order parameter ϕ_{QSH}; while the gap at M point is invariant as a function of ϕ_{QSH}. Hence in Fig. 22, we can see that the momentum of minimal gap 'shifts' from K point to M point as λ grows. It's interesting to see that even in the coexisting (QSH+SSC) phase, gap at M point is still the smallest. We can also see this effect in Fig. 21(b): the plateau of gap in the intermediate region of λ happens in the pure QSH state when $\Delta_M < \Delta_K$.

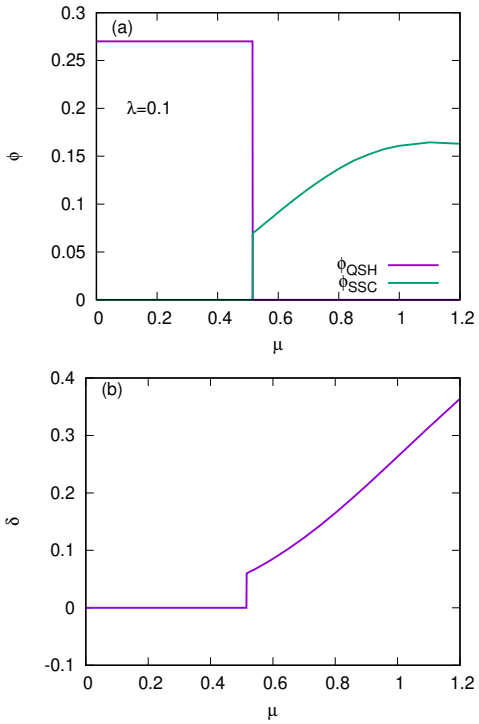

Figure 23: Mean-field solution as a function of chemical potential μ at $\lambda = 0.1$. (a) QSH and SSC order parameters. (b) Doping factor δ.

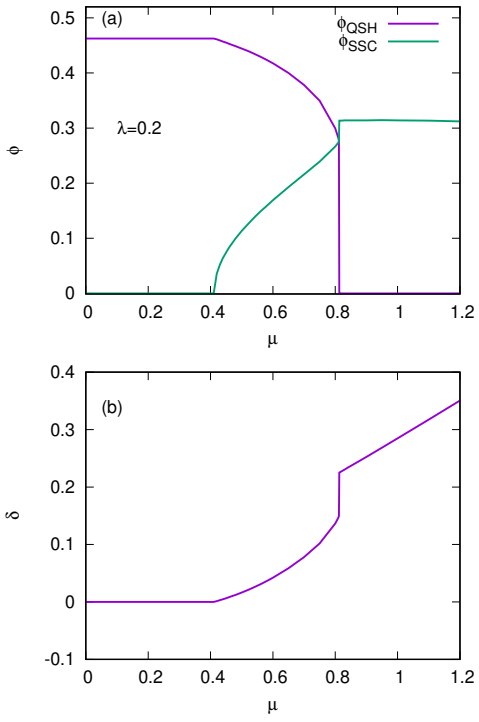

Figure 24: Mean-field solution as a function of chemical potential μ at $\lambda = 0.2$. (a) QSH and SSC order parameters. (b) Doping factor δ.

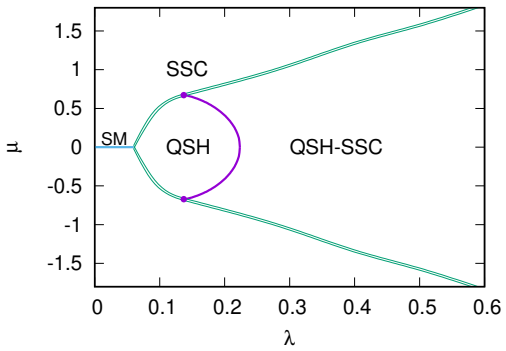

Figure 25: Mean-field ground-state phase diagram. The blue and purple (green) lines correspond to continuous (first-order) transitions.

Then we turn our attention to the doped case. Upon doping the pure QSH state, the phase diagram exhibits two distinct mean-field scenarios. Two representative examples at $\lambda = 0.1$ and $\lambda = 0.2$ are shown in Figs. 23 and 24, respectively. In the case of $\lambda = 0.1$ (Fig. 23), which is close to the Gross-Neveu transition, a clear first-order transition between the QSH and SSC phases is observed. Doping at $\lambda = 0.2$ (Fig. 24) leads to two phase transitions: (i) a $z = 2$ transition from the pure QSH state to the coexistence state at $\mu \approx 0.4$, characterized by a linear growth of δ and (ii) a first-order phase transition to an SSC state at $\mu \approx 0.8$. Such first-order transitions are characterized by a level crossing corresponding to two local minimum in the free-energy density in Eq. (114).

Here we summarize the MF result in the 2D plane of λ and μ. As shown Fig. 25, doping the semimetal produces the SSC. This reflects the pairing instability of Fermi surfaces to attractive interactions within Bardeen-Cooper-Schrieffer (BCS) theory. The protecting symmetries of the QSH state are related to time reversal and global charge conservation. Hence, the coexistence region (QSH+SSC) is topologically trivial. Furthermore, the transition at half-filling from the QSH to QSH+SSC is continuous and does not require the closing of the single-particle gap. Upon doping, the mean-field approximation generically supports two scenarios: (i) a continuous transition with dynamical exponent $z = 2$ from the QSH to QSH+SSC, (ii) a first-order transition from the QSH to SSC [4]. Our mean-field approximation provides examples of both scenarios. As expected, it fails to capture the DQCP between the QSH and SSC phases at half-filling [1].

4.3 Numerical results

4.3.1 Projective QMC approach

A natural way of achieving finite doping would be to use the FTQMC and to tune the chemical potential μ. However it is very inefficient from the numerical point of view. First, it is not possible to take the zero temperature limit before taking infinite system size limit: 'infinite' inverse temperature β is needed once two ground state in different particle number sectors are tuned to be nearly degenerate at a certain chemical potential. On the other hand, a $\beta \propto L^z$ calculation is required once if we assume the dynamical exponent z. However it's hard to detect z without numerics: as we will shown latter it seems that we have a transition with $z > 2$.

[4] An intermediate metallic state would be unstable to pairing and we have excluded fine-tuning

Hence we use the PQMC method, and view the partition function of the grand canonical ensemble as:

$$\begin{aligned} Z_{GCE}(\beta \longrightarrow \infty) &= \sum_{n-N=0,\pm1,\pm2,\pm3,\ldots} e^{-\beta(E_0(n)-\mu n)} \\ &= \sum_{n-N=0,\pm2,\ldots} e^{-\beta(E_0(n)-\mu n)} \end{aligned} \tag{117}$$

where n is the particle number (which is a good quantum number), and $N = 2L^2$. $E_0(n)$ denotes the ground state energy in the sector of particle number n. The first identity is based on ignoring the 'excited' state in all the particle number sectors in the zero temperature limit. The second identity is based on the assumption that singlet many body ground state have lowest energy. We are not able to prove this point analytically; but we will show numerical benchmarks latter on.

We used the projective QMC algorithm of the ALF-library [31]. This canonical algorithm filters out the ground state, $|\psi_0\rangle$, from a trial wave function, $|\psi_T\rangle$, that is required to be non-orthogonal to the ground state:

$$\frac{\langle\psi_0|\hat{O}|\psi_0\rangle}{\langle\psi_0|\psi_0\rangle} = \lim_{\Theta\to\infty} \frac{\langle\psi_T|e^{-\Theta\hat{H}}\hat{O}e^{-\Theta\hat{H}}|\psi_T\rangle}{\langle\psi_T|e^{-2\Theta\hat{H}}|\psi_T\rangle}. \tag{118}$$

The trial wave function $|\psi_T\rangle$ is chosen to be a Slater determinant with N_p particles ($\hat{N}|\psi_T\rangle = N_\mathrm{p}|\psi_T\rangle$). In particular,

$$|\psi_T\rangle = |\psi_T^\uparrow\rangle \otimes |\psi_T^\downarrow\rangle \tag{119}$$

with

$$|\psi_T^\sigma\rangle \equiv \prod_{n=1}^{N_\mathrm{p}/2} \left(\sum_{\boldsymbol{i}} \hat{c}^\dagger_{\boldsymbol{i},\sigma} U_{\boldsymbol{i},n} \right) |0\rangle. \tag{120}$$

$U_{\boldsymbol{i},n}$ is the n^{th} single-particle eigenstate, ordered in ascending energy eigenvalues, of the spinless fermion Hamiltonian

$$\hat{H} = -t \sum_{\langle \boldsymbol{i},\boldsymbol{j}\rangle} (\hat{c}^\dagger_{\boldsymbol{i}} \hat{c}_{\boldsymbol{j}} + H.c.) + \sum_{\langle \boldsymbol{i},\boldsymbol{j}\rangle} \xi_{\boldsymbol{i},\boldsymbol{j}} (\hat{c}^\dagger_{\boldsymbol{i}} \hat{c}_{\boldsymbol{j}} + H.c.). \tag{121}$$

The first term corresponds to the tight-binding Hamiltonian on the honeycomb lattice. We require the perturbing hopping matrix elements $|\xi_{\boldsymbol{i},\boldsymbol{j}}| \ll t$ and $Im\xi_{\boldsymbol{i},\boldsymbol{j}} = 0$. The sign and modulus of $\xi_{\boldsymbol{i},\boldsymbol{j}}$ are chosen randomly so that all energy eigenvalues of the spinless Hamiltonian are non-degenerate. Our trial wave function hence breaks lattice and point group symmetries. Crucially, however, time-reversal symmetry is present. Since $\lambda > 0$ (see Eq. (108)), we can decouple the interaction with a real Hubbard-Stratonovich transformation such that both the imaginary time propagation and the trial wave function are invariant under time reversal:

$$T\alpha \begin{pmatrix} \hat{c}_{\boldsymbol{i},\uparrow} \\ \hat{c}_{\boldsymbol{i},\downarrow} \end{pmatrix} T^{-1} = \bar{\alpha} \begin{pmatrix} \hat{c}_{\boldsymbol{i},\downarrow} \\ -\hat{c}_{\boldsymbol{i},\uparrow} \end{pmatrix}. \tag{122}$$

Hence, the eigenvalues of the fermion matrix come in complex conjugate pairs and no negative sign problem occurs.

A projection length $\Theta = L$ was found to be sufficient to converge to the finite-size ground state for all of our system sizes. We have used an imaginary time step $\Delta_\tau = 0.2$ and a symmetric Trotter decomposition to guarantee the Hermiticity of the imaginary time propagator.

4.3.2 Single particle spectrum at finite doping

Why do we ignore the states in odd particle number sectors of Eq. 117? Here we show numerically that the single electron excitations are gaped from even particle number sector. This also indicates that the low energy physics of doping is described by a bosonic field theory which has only particle-hole and particle-particle excitations.

Consider the single-particle spectral function at finite doping. Away from half-filling, particle-hole symmetry is broken and we have to separately calculate the spectra for electron addition and removal,

$$\begin{aligned} A(\boldsymbol{k},\omega) = & \frac{1}{Z}\sum_n (|\langle n|c_{\boldsymbol{k}}|0\rangle|^2 \delta(E_n - E_0 - \omega)) \\ & + \frac{1}{Z}\sum_m (|\langle m|c^\dagger_{\boldsymbol{k}}|0\rangle|^2 \delta(E_m - E_0 + \omega)) \end{aligned} \tag{123}$$

via the independent analytical continuations

$$\begin{aligned} \langle c_{\boldsymbol{k}}(\tau) c^\dagger_{\boldsymbol{k},\alpha}(0)\rangle &= \int d\omega e^{-\tau\omega} A_+(\omega) \\ \langle c^\dagger_{\boldsymbol{k}}(\tau) c_{\boldsymbol{k},\alpha}(0)\rangle &= \int d\omega e^{-\tau\omega} A_-(\omega) \end{aligned} \tag{124}$$

with $A(\omega) = A_+(\omega) + A_-(-\omega)$. Here, $|0\rangle$ in Eq. (123) is the ground state at finite doping and $\langle n|$ is an eigenstate of the Hamiltonian with energy E_n and an additional particle (hole) relative to the ground state. In Fig. 26, we plot the spectral functions for $L = 21$ and $\delta = 0, \frac{1}{441}, \frac{3}{441}$ and $\frac{4}{441}$ ($2L^2 - N_{\rm p} = 0, 2, 6$ and 8). We see that the single particle spectrum is gaped at finite doping.

On the other hand, the dominant feature follows the mean-field BCS form $E(\boldsymbol{k}) = \pm\sqrt{(\epsilon(\boldsymbol{k}) - \mu)^2 + |\Delta|^2}$, where $\pm\epsilon(k)$ denotes the Dirac dispersion of the honeycomb lattice. This result shows that the Goldstone modes do not strongly couple to single-particle excitations.

In fact, the Green's function at the Γ point has a special property, due to a commutation rule between the fermion operator and the interaction term of Hamiltonian (we use the notation $\boldsymbol{c}^\dagger_{\boldsymbol{i}} = (\hat{c}^\dagger_{\boldsymbol{i},\uparrow}, \hat{c}^\dagger_{\boldsymbol{i},\downarrow})$)

$$\left[\sum_{\boldsymbol{i}} \hat{c}_{\boldsymbol{i},\alpha}, \sum_{\hexagon} \left(\sum_{\langle\langle \boldsymbol{ij}\rangle\rangle \in \hexagon} i\nu_{\boldsymbol{ij}} \hat{\boldsymbol{c}}^\dagger_{\boldsymbol{i}} \boldsymbol{\sigma} \hat{\boldsymbol{c}}_{\boldsymbol{j}} + H.c. \right)^2 \right] = 0. \tag{125}$$

The above relation follows directly from

$$\left[\sum_{\boldsymbol{i}} \hat{c}_{\boldsymbol{i},\alpha}, \sum_{\langle\langle \boldsymbol{ij}\rangle\rangle \in \hexagon} i\nu_{\boldsymbol{ij}} \hat{\boldsymbol{c}}^\dagger_{\boldsymbol{i}} \boldsymbol{\sigma} \hat{\boldsymbol{c}}_{\boldsymbol{j}} + H.c. \right] = 0 \tag{126}$$

which holds for the summation of spin-orbit operators inside each hexagon and for any vector $\boldsymbol{\sigma}$ in the space of Pauli matrices σ_x, σ_y, σ_z. Hence, the Green's function $\langle \hat{\boldsymbol{c}}^\dagger_{\boldsymbol{k}}(\tau) \hat{\boldsymbol{c}}_{\boldsymbol{k}}(0)\rangle$ at the $\boldsymbol{k} = \Gamma$ point is identical to that of the non-interacting Hamiltonian.

4.3.3 Phase diagram

We turn to the ground state phase diagram by PQMC study. We focus on a line as function of doped particle number at $t = 1$ and $\lambda = 0.026$ (which is the same parameter

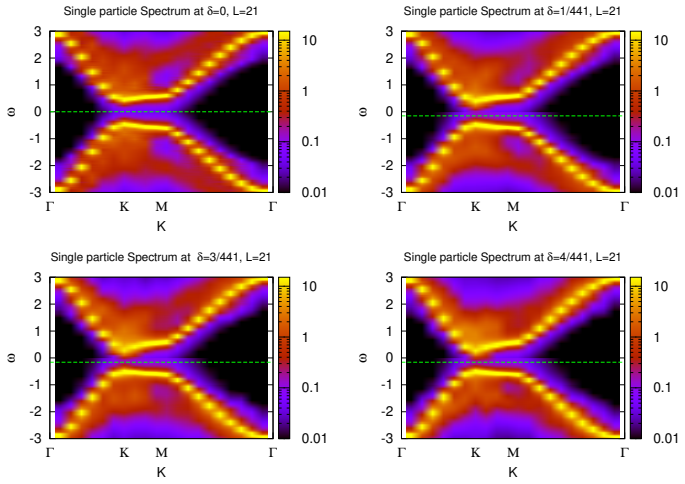

Figure 26: Single-particle spectrum at dopings (a) $\delta = 0$, (b) $\frac{1}{441}$, (c) $\frac{3}{441}$, and (d) $\frac{4}{441}$. The green dotted line is the chemical potential μ evaluated from $\mu \equiv \frac{E(N_\mathrm{p})-E(N_\mathrm{p}-2)}{2} = \frac{\Delta_{\eta^-}(N_\mathrm{p})}{2}$ which will be shown latter.

as the one for Fig. 20 shown before). For the aforementioned trial wave function, we observed that a projection parameter set by the linear length of the lattice is sufficient to reach the ground state. We fist focus on the equal-time correlation functions of the spin current and s-wave paring operators in momentum space, $S_{QSH}(\mathbf{q})$ and $S_{SSC}(\mathbf{q})$.

In Fig. 27, we show the momentum dependence of the equal-time QSH and SSC structure factors at $\delta = 0$ and at $\delta = 1/36$. Upon doping, the QSH structure factor does not develop incommensurate features. At $\delta = 1/36$, the QSH data (Fig. 27(b)) are consistent with the absence of long-range order, whereas the SSC structure factor (Fig. 27(d)) shows a marked increase as a function of system size.

Another important question to answer is if the onset of superconductivity is tied to the vanishing of the QSH order parameter. To this end, we consider the renormalization-group invariant correlation ratios ($\alpha = QSH, SSC$)

$$R_\alpha \equiv 1 - \frac{S^\alpha(\boldsymbol{q}_0 + \delta\boldsymbol{q})}{S^\alpha(\boldsymbol{q}_0)} \tag{127}$$

Here, $\boldsymbol{q}_0 = (0, 0)$ is the ordering wave vector and $\boldsymbol{q}_0 + \delta\boldsymbol{q}$ a neighboring wave vector. By definition, $R_\alpha \to 1$ ($\to 0$) in the ordered (disordered) state for $L \to \infty$. At a critical point, R_α is scale invariant and for sufficiently large L, one should observe a crossing in R_α for different system sizes. Figures 28(a) and (b) show results for R_{SSC} and R_{QSH} as a function of δ. Due to the observed binding of electrons in the insulating state, we expect superconductivity for any $\delta > 0$. This is confirmed by Fig. 28(a). The drift in the crossings due to corrections to scaling is consistent with $\delta_c^{SSC} \to 0$ in the thermodynamic limit. The same quantity is plotted for the QSH correlation ratio in Fig. 28(b). The data show that the QSH order parameter vanishes very rapidly as a function of doping. Again, the drift of the crossing point as a function of system size scales to smaller values of δ. Given the data, we can provide an upper bound $\delta_c^{QSH} < 0.0017$ which corresponds to our resolution [5]. On our finite systems, neither of the correlation ratios show a discontinuity, consistent with a continuous transition.

[5]Since we are working in the canonical ensemble, the smallest doping is set by $2/(2L^2)$.

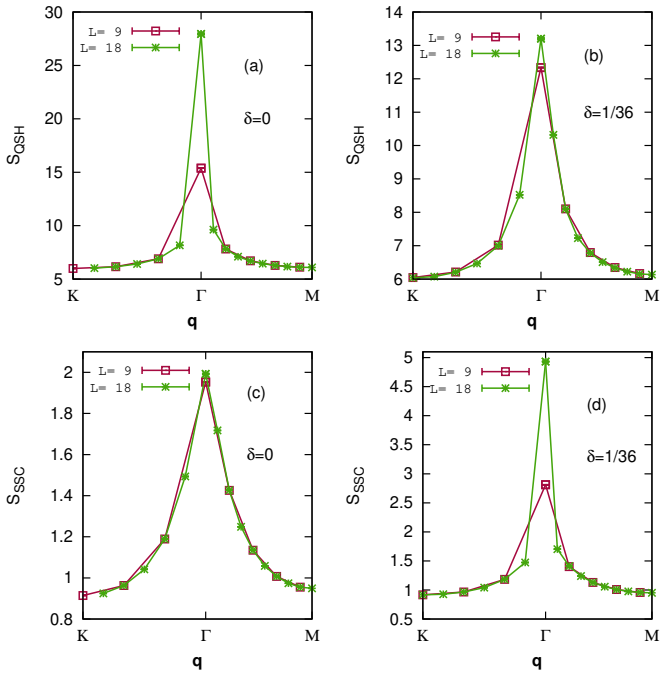

Figure 27: Momentum dependence of the equal-time structure factor for ((a),(b)) QSH and ((c),(d)) SSC operators for ((a),(c)) $\delta = 0$ and and ((b),(d)) $\delta = \frac{1}{36}$.

As a crosscheck, we consider the second-moment, finite-size correlation length [67]:

$$\xi_\alpha^2 \equiv \frac{\sum_{\boldsymbol{r}} |\boldsymbol{r}|^2 S^\alpha(\boldsymbol{r})}{\sum_{\boldsymbol{r}} S^\alpha(\boldsymbol{r})} \tag{128}$$

obtained from the real-space, equal-time correlation functions [6]. The inset of Fig. 28(b) reveals the absence of saturation of the QSH correlation length at any finite doping $\delta > 0.0017$. Saturation would be expected for a first-order transition.

The onset of long-range order as well as a measure for the correlation length can be obtained by considering $1/S(\boldsymbol{Q} = 0)$ as function of δ (see Fig. 29). The SSC ordering appears immediately at $\delta > 0$, characterized by the quick decay of $1/S_{\mathrm{SSC}}$ as function of system size. In particular, $1/S_{\mathrm{SSC}}$ shows no saturation as a function of system size. On the other hand, $1/S_{\mathrm{QSH}}$ shows a clear saturation at *large* doping. For a given doping, the lattice size at which this quantity converges is a measure of the correlation length. Upon inspection, one will see that larger lattice sizes are required to achieve convergence upon approaching half-filling. In particular, following the envelope of these curves again suggests that the correlation length of the QSH fluctuations grows continuously and diverges as $\delta \to 0$. This is consistent with the data of correlation ratio.

4.3.4 Nature of transition

A key quantity to understand the nature of the metal or superconductor to insulator transition is the behavior of the chemical potential upon doping away from half-filling [68, 69, 26]. For first-order transitions, μ shows a jump. For continuous transitions, and with the assumption of a single length scale, the singular part of the free energy scales as

[6] The fact that there is no additional phase factor in the above summations comes from the known ordering wave vector $\boldsymbol{k} = \Gamma$.

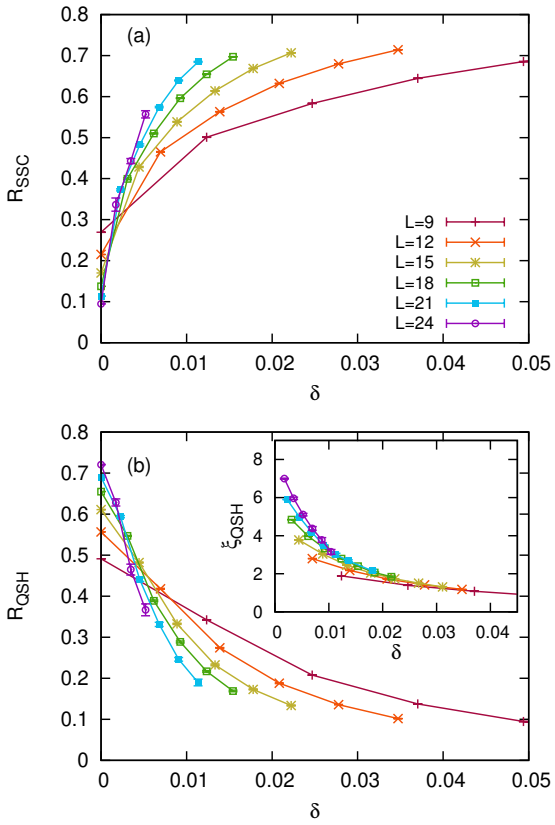

Figure 28: Correlation ratios for (a) SSC and (b) QSH orders as a function of doping δ. The system sizes are $L = 9$, 12, 15, 18, 21, and 24. The inset of (b) shows the δ-dependence of the finite-size correlation length for the QSH order parameter.

$f \propto |\mu - \mu_c|^{\nu(d+z)}$ with d the dimensionality and ν (z) the correlation length (dynamical) exponent. Since the doping $\delta \propto \partial f/\partial\mu$ and the compressibility is associated with twisting boundaries in the imaginary-time direction, one can show that for transitions driven via the chemical potential the hyper scaling relation $\nu z = 1$ holds. Thereby,

$$\delta \propto |\mu - \mu_c|^{\nu d} . \tag{129}$$

Doping a band insulator satisfies the hyper-scaling assumption. For a quadratic band, $z = 2$ so that $\delta \propto |\mu - \mu_c|^{d/2}$. This scaling behavior is satisfied upon doping a bosonic Mott insulator [26].

With the PQMC, we can compute the ground-state energy for a given, even particle number $N_{\rm p}$ and then derive the chemical potential. However, we found it more efficient to extract μ from an estimate of $\Delta_{\eta^-}(N_{\rm p})$ by analyzing the long imaginary time behavior of the pair correlation function $\sum_{\tilde{\boldsymbol{\delta}}} \langle \hat{\eta}^+_{\boldsymbol{q},\tilde{\boldsymbol{\delta}}}(\tau) \hat{\eta}^-_{\boldsymbol{q},\tilde{\boldsymbol{\delta}}}(0) \rangle \sim e^{-\Delta_{\eta^-}\tau}$, where $\boldsymbol{q} = \Gamma$. In particular,

$$\mu \equiv \frac{E(N_{\rm p}) - E(N_{\rm p}-2)}{2} = \frac{\Delta_{\eta^-}(N_{\rm p})}{2} . \tag{130}$$

With the doping relative to half-filling defined as $\delta \equiv 1 - \frac{N_{\rm p}-1}{2L^2}$ [7], we obtain the data shown in Fig. 30. Alternative ways of computing μ will be shown latter.

[7] Here, $N_{\rm p} - 1$ is the thermal average of particle numbers, with the $N_{\rm p}$ and the $N_{\rm p} - 2$ sector tuned to have the same ground-state energy at the chemical potential defined in Eq. (130).

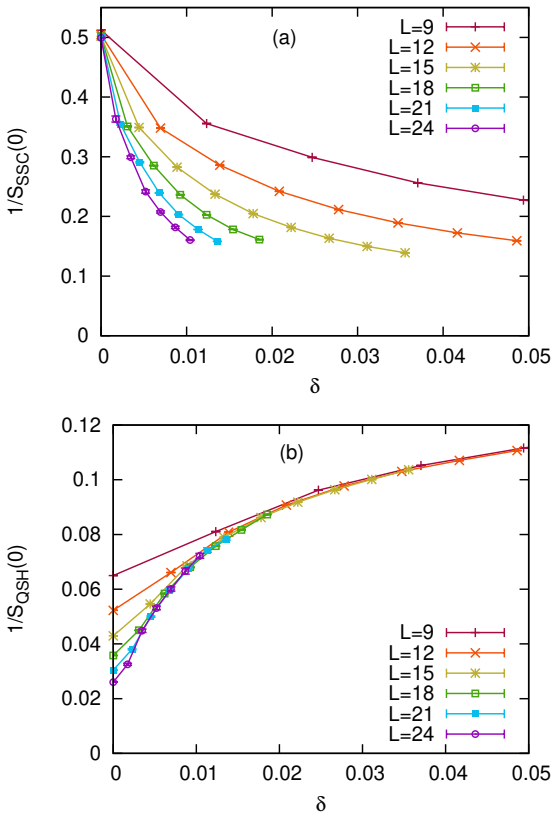

Figure 29: δ dependence of $1/S(\boldsymbol{Q}=0)$ for SSC (a) and QSH (b), as a function of δ, for $L = 9$, 12, 15, 18, 21 and 24

Figure 30 plots δ as a function of μ. The vertical dash-dotted line corresponds to the critical chemical potential. The data support a linear behavior for $\mu > 0.16$, but this form would overshoot the critical chemical potential. In a narrow window of dopings, $\delta < 0.01$, we observe a downturn in the functional form. Within our precision, we can offer two interpretations: a weakly first-order transition or a continuous transition with dynamical exponent $z > 2$. We note that continuous metal-insulator transitions with $z > 2$ have been put forward in the context of doped quantum antiferromagnets [68, 70].

As we mentioned before, the FTQMC algorithm formulated in the grand-canonical ensemble is quite inefficient in this case. Nevertheless we still shown the results as a crosscheck here. Hence, for a given chemical potential μ in Eq. (108) of the main text, we can compute the doping from

$$\delta \equiv \frac{\langle \sum_{\boldsymbol{i}} \hat{n}_{\boldsymbol{i}} \rangle}{2L^2} - 1. \tag{131}$$

Figure 31 shows the corresponding result for the case where the inverse temperature β and the system size L scale as $\beta = L^2/3$. This implicitly makes the assumption that $z = 2$. Overall, our limited data are consistent with the more efficient PQMC calculation. At large values of δ, results for $L = 12$ and $L = 15$ are consistent with a linear dependence of δ on μ that overshoots the critical chemical potential and suggest $z > 2$.

From the numerical point of view, the FTQMC is not as efficient as the PQMC. The numerical cost to reach the low-temperature limit scales as $V^3\beta^z$. We have also

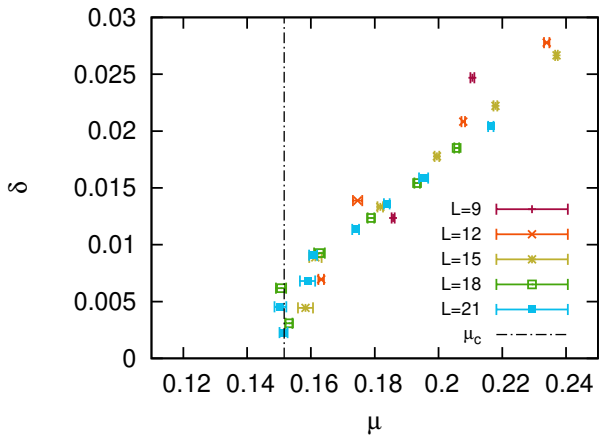

Figure 30: Doping factor δ as a function of chemical potential $\mu \equiv \frac{\Delta_{\eta^-}}{2}$ for sizes $L = 9$, 12, 15, 18, and 21. The red dashed line is the critical chemical potential from the extrapolated pairing gap $\Delta_\eta/2$ shown in Fig. 20.

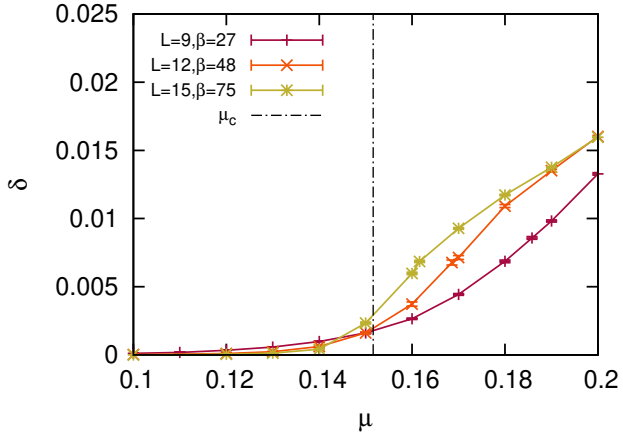

Figure 31: Doping factor δ as a function of chemical potential μ from FTQMC simulations, with sizes $L = 9$, 12 and 15, and $\beta = \frac{1}{3}L^2$.

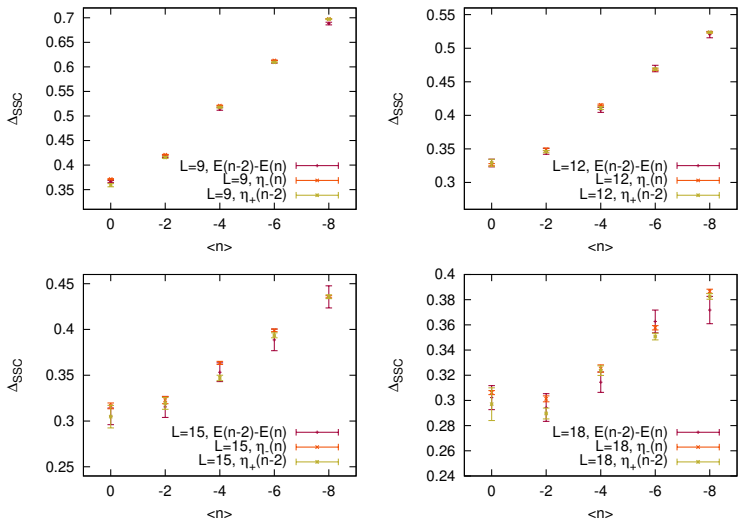

Figure 32: Three ways of pairing gap evaluation for (a) $L = 9$, (b) 12, (c) 15, and (d) 18, for doped particle number $N_{\rm p} - 2L^2 = 0, -2, -4, -6$ and -8.

noticed long warm-up and autocorrelation times to equilibrate the particle number in the vicinity of $\mu = \mu_c$.

4.3.5 Consistency check of the pairing gap

We check the consistency of our evaluation of the ground-state energy difference between different even particle-number sectors:

$$E(N_{\rm p}) - E(N_{\rm p} - 2) = \Delta_{\eta^-}(N_{\rm p}) = \Delta_{\eta^+}(N_{\rm p} - 2) \tag{132}$$

where $E(N_{\rm p})$ is the ground state energy measured within the PQMC in the $N_{\rm p}$ particle number sector; $\Delta_{\eta^-}(N_{\rm p})$ is the s-wave pairing (η^-) gap extrapolated from the time-displaced correlation function.

The imaginary-time domain β, in which we measure the time-displaced correlation function, is set to $\beta = L$ for $L = 9$, 12, 15, and 18, and to $\beta = 10$ for $L = 21$. To extrapolate the pairing gap, we use sequential fits

$$\langle \eta^+(m\tau_0 + \tau)\eta^-(m\tau_0)\rangle \propto e^{-\Delta_m \tau} \quad m = 0, 1, 2, 3... \tag{133}$$

where $\tau_0 = 1.0$ and $\tau \in [0, \tau_0)$. The gap is extrapolated as

$$\Delta_m - \Delta(m \to \infty) \propto e^{-am} \tag{134}$$

where a is optimized for the best fit.

In Fig. 32, we show that the three different ways of evaluating the gap give consistent results for $L = 9$, 12, 15, and 18 for several particle-number sectors near half-filling. In particular, one can compute the ground-state energy and take the difference or measure time-displaced correlation functions of the pair adding or removal operator. Using the energy difference generically produces bigger error bars. Here, we carry out two independent simulations and thereby have to add the errors on two extensive quantities (total energies) to estimate the error on an intensive one, the total energy difference. Hence to keep the error bar on the total energy difference, we have to scale the error on the energy per site as $1/L^2$. Even taking into account self-averaging on large system sizes, this proves to be numerically expensive.

4.4 Discussion

Our data suggest a doping-induced, continuous and direct phase transition between the QSH state and the SSC. Clearly, we cannot exclude the possibility of a weakly first-order transition in which the correlation length saturates beyond our maximum system size ($L = 24$). Our dynamically generated QSH state possesses Goldstone modes and charge-$2e$ Skyrmions of the QSH order parameter. The Goldstone modes correspond to long-wavelength fluctuations of the spin-orbit coupling and do not break time-reversal symmetry. Hence, single-particle spin-flip scattering off Goldstone modes—as present in doped quantum antiferromagnets—is not allowed. Remarkably, one can also show that $\left[\hat{\boldsymbol{c}}_{\boldsymbol{k}=0}, \hat{H}_\lambda\right] = 0$, so that at the Γ point the single-particle spectral function is unaffected by the interaction $\hat{H}_\lambda$. This is in strong contrast to quantum antiferromagnets, where Goldstone modes couple to single-particle excitations to form a narrow band of spin polarons [71, 72, 73]. These arguments suggest that Goldstone modes do not provide the glue that leads to pairing.

We interpret our results in terms of preformed pairs, Skyrmions carrying charge $2e$, that condense upon doping. Within this picture, the correlation length that diverges at the transition corresponds to the average distance between Skyrmions. While the mean-field calculation produces a first-order transition or a doping range where QSH and SSC coexist, the QMC results suggest a continuous transition across which the single-particle gap remains nonzero. This points to the very non-mean-field character of the transition.

There are many possible ways to check the interpretation of our results in terms of a proliferation of charge-$2e$ Skyrmions. We can consider an SO(2) model, as opposed to the present SO(3) model, where only two of the three QSH masses are dynamically generated. Such a model would be free of Skyrmions and one would expect a different doping-induced insulator-superconductor transition. Another possibility is to energetically disfavor the Skyrmions. Our model is very close to the DQCP, where Skyrmions play a central role and have a low energy. Enhancing the spin-current stiffness, e.g., by using a longer-ranged spin-current interaction, will render Skyrmions smaller and increase their energy. In the limit of infinite stiffness, the mean-field result should emerge.

The finite-temperature phase diagram remains to be analyzed. Such calculations could reveal pseudo-gap physics related to preformed pairs at small doping.

Finally, the condensation of charged Skyrmions has recently been proposed as a possible mechanism for superconductivity in graphene Moiré superlattice systems such as twisted bilayer graphene [74]. Although our model differs significantly from the actual graphene Moiré systems in terms of symmetries and interactions, it does capture the essence of this proposal—a correlation-induced topological insulator (broadly defined) contains Skyrmions as low-lying charged excitations, and upon doping becomes superconducting due to the condensation of charged Skyrmions. We therefore expect our study, especially regarding the universal behavior near the insulator-superconductor transition, to be relevant if Skyrmion condensation is indeed the mechanism for superconductivity in Moiré systems.

5 Phases of the (2+1) dimensional O(5) non-linear sigma model with topological term

In this Chapter, we use the half-filled zeroth Landau level in graphene as a regularization scheme to study the physics of the SO(5) non-linear sigma model subject to a Wess-Zumino-Witten topological term in 2+1 dimensions. This approach allows for negative sign free auxiliary field quantum Monte Carlo simulations. The model has a single free parameter, U_0, that monitors the stiffness. Within the parameter range accessible to negative sign free simulations, we observe an ordered phase in the large U_0 or stiff limit. Remarkably, upon reducing U_0 the magnetization drops substantially, and the correlation length exceeds our biggest system sizes, accommodating 100 flux quanta. This work can be taken as a continuum limit of our deconfined quantum critical point in QSH-SSC (or AFM-VBS) transition shown in previous chapter, when the assumption of a emergent SO(5) symmetry in the later model is taken. The results of this work can be found in Ref. [3].

5.1 Landau Level projection and sigma model

5.1.1 Dirac Landau Levels

The idea of using the projected Landau Level to study the non-linear sigma model comes from Graphene with 2 flavors of fermions. The low energy physics at half filed case is described by Dirac cones with 8 component of fermions: the one particle Hilbert space is described by the production of valley, sublattice, real spin and $2D$ Euclidean space. Hence the half filed graphene with only kinetic energy is described by:

$$\hat{H}_{Dirac} = \sum_{\boldsymbol{p}} \hat{\psi}^{\dagger}(\boldsymbol{p})[p_x \mu_z \otimes \tau_x \otimes \sigma_0 + p_y \mu_0 \otimes \tau_y \otimes \sigma_0]\hat{\psi}(\boldsymbol{p}) \tag{135}$$

where we have set the fermion velocity $v_F \equiv 1$. Here a creation operator in the momentum space is defined by:

$$\hat{\psi}^{\dagger}(\boldsymbol{p}) \equiv \hat{\psi}^{\dagger}_{\mu=(\boldsymbol{K},-\boldsymbol{K}),\tau=(\boldsymbol{A},\boldsymbol{B}),\sigma=(\uparrow,\downarrow)}(\boldsymbol{p}) \tag{136}$$

Define a canonical transformation:

$$\hat{\psi}^{\dagger} \longrightarrow \hat{\psi}^{\dagger}(\tau_y \otimes P_+ + P_-) \quad with \quad P_{\pm} \equiv \frac{1}{2}(\mu_0 + \mu_z) \tag{137}$$

the Dirac Hamiltonian of Eq.138 is transformed as:

$$\hat{H}_{Dirac} = \sum_{\boldsymbol{p}} \hat{\psi}^{\dagger}(\boldsymbol{p})[p_x \tau_x + p_y \tau_y]\hat{\psi}(\boldsymbol{p}) \tag{138}$$

the two unit matrix μ_0 and σ_0 are ignored here. Thus the global U(4) symmetry of the low energy effective theory is more clear in this basis. (The above Hamiltonian has actually an O(8) symmetry when the flavor-dependent particle hole transformation is also included, but it's not relevant to our discussion of Landau Level projection.)

Inserting an orbital magnetic field to Graphene is basically to introduce the minimal coupling so as to redefine the canonical momentum:

$$\begin{aligned} &\hat{H}_{Dirac} = \sum_{\boldsymbol{p}} \hat{\psi}^{\dagger}(\boldsymbol{p})[\Pi_x \tau_x + \Pi_y \tau_y]\hat{\psi}(\boldsymbol{p}) \\ &\boldsymbol{\Pi} \equiv \boldsymbol{p} - e\boldsymbol{A} \end{aligned} \tag{139}$$

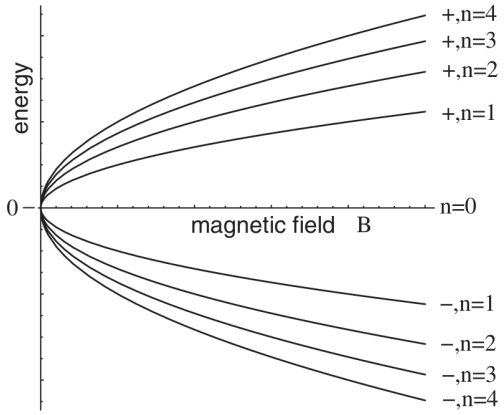

Figure 33: Eigenvalues of quantized Dirac LLs as a function of magics field B, taken from Ref. [75].

where the commutation role of the canonical momentum behaves:

$$[\Pi_x, \Pi_y] = -ie\hbar(\frac{\partial A_y}{\partial x} - \frac{\partial A_x}{\partial y}) = -i\frac{\hbar^2}{l_B^2} \tag{140}$$

the magnetic length scale here is defined as $l_B \equiv \sqrt{\frac{\hbar}{eB}}$.

Note that the square of the first quantized Hamiltonian is:

$$\begin{aligned} &(\Pi_x\tau_x + \Pi_y\tau_y)^2 \\ =&(\Pi_x)^2 + (\Pi_y)^2 - eB\tau_z \end{aligned} \tag{141}$$

Since the spacial part above commutes with the part of $B\tau_z$, the eigenstate of Dirac Landau Level (LL) follows the one of Schrodinger's Landau Level. One can easily solve the eigen equation of Eq.139, with plus and minus eigenvalues comes in pairs:

$$\epsilon_{n,\pm} = \pm\frac{\hbar}{l_B}\sqrt{2n} \tag{142}$$

A plot of the magnetic field B dependence of the eigenvalues is shown in Fig.5.1.1. Above n denotes the nth Dirac LL, with the wave function of:

$$\begin{aligned} |\psi\rangle_{n\neq 0,\pm} &= \frac{1}{\sqrt{2}}\begin{pmatrix} |n-1\rangle \\ \pm|n\rangle \end{pmatrix} \\ |\psi\rangle_{n=0} &= \begin{pmatrix} 0 \\ |n=0\rangle \end{pmatrix} \end{aligned} \tag{143}$$

Here the zeroth Dirac LL has nonzero component only in the " spin down " component of τ_z channel. $|n\rangle$ is the nth Schrodinger's Landau Level:

$$|n\rangle_a^k = (\sum_{\boldsymbol{r}} \phi_n^k(\boldsymbol{r})\hat{\psi}_{\boldsymbol{r},a}^\dagger)|0\rangle \tag{144}$$

where $a = 1, 2, 3, 4$ denotes the 4 component index spanning valley(μ) and real spin(σ) space. $\phi_n^k(\boldsymbol{r})$ indicates one of the nth Schrodinger's LL wave function by diagnosing the matrix of $(\Pi_x)^2 + (\Pi_y)^2$. The label $k = 1, 2, ...N_\phi$ indicates the ith wave function in the N_ϕ degenerate space, where N_ϕ is the number of magnetic flux through the 2D system: $N_\phi \equiv \frac{|B|V}{2\pi\hbar/e}$. The N_ϕ degeneracy comes from the momentum (angular momentum)

conservation in the choice of Landau gauge (symmetric gauge) . Including the 4 flavor component, each Dirac LL has the degeneracy of $4N_\phi$. We can see that due to the magnetic field, the Dirac LL here broke the O(8) symmetry of Eq. 138 but leaves the $U(4)$ global symmetry invariant.

Note that the notation of Dirac LL is only an approximation of the low energy limit of Graphene in orbital magnetic field. However the interesting details based on 'Hofstadter butterfly' of Graphene is not within our consideration here. Our following discussion based on projected interaction in LL only concentrate on the continues field theory.

5.1.2 Projected interactions

Now consider the case of finite fermion interaction written in generic form:

$$\hat{H} = \hat{H}_{Dirac} + \hat{H}_{Int}(\hat{\psi}^\dagger, \hat{\psi}) \tag{145}$$

When the free Dirac Hamiltonian is diagnosed in the LL basis:

$$\begin{aligned} &\hat{H}_{Dirac} = \hat{\psi}^\dagger h_{Dirac} \hat{\psi} = \sum_{k,n} \hat{c}_k^\dagger(n)\epsilon(n)\hat{c}_k(n) \\ &\hat{H}_{Int}(\hat{\psi}^\dagger, \hat{\psi}) = \hat{H}_{Int}(\sum_n \sum_k \phi_n^{k*}(\boldsymbol{r})\hat{c}_k^\dagger(n), \sum_n \sum_k \phi_n^k(\boldsymbol{r})\hat{c}_k(n)) \end{aligned} \tag{146}$$

where the creation operator in terms of a LL state is: $\hat{c}_k^\dagger(n) \equiv \sum_{\boldsymbol{r}} \phi_n^k(\boldsymbol{r})\hat{\psi}_{\boldsymbol{r}}^\dagger$, and $\hat{\psi}_{\boldsymbol{r}}^\dagger = \sum_n \sum_k \phi_n^{k*}(\boldsymbol{r})\hat{c}_k^\dagger(n)$.

We consider that limit of large magnetic field and small interacting energy scale, which perturb the half filed kinetic band (all the Dirac LL with negative eigenvalues are filed and the zeroth LL is half filed). Hence it is safe to reduce the single particle Hilbert space of Eq.146 to degrees of freedom which only contains the zeroth LL, with a Hamiltonian includes only interacting part, and re-defined fermion creation-annihilation operators:

$$\begin{aligned} &\hat{\psi}^\dagger(\boldsymbol{r}) \equiv \sum_k {\phi_{(n=0)}^k}^*(\boldsymbol{r})\hat{c}_k^\dagger(n=0) \\ &\hat{H}_{Int}(\hat{\psi}^\dagger, \hat{\psi}) = \hat{H}_{Int}(\sum_k {\phi_{(n=0)}^k}^*(\boldsymbol{r})\hat{c}_k^\dagger(n=0), \sum_k \phi_{(n=0)}^k(\boldsymbol{r})\hat{c}_k(n=0)) \end{aligned} \tag{147}$$

This projection is exact under first order perturbation, and the dimension of single particle Hilbert space is reduced from infinity to $4N_\phi$. Note that the projected operators $\hat{\psi}_{\boldsymbol{r}}^\dagger$ does not follow the canonical fermion commutation role since Eq. 147 only includes the summation over zeroth LL.

The interacting Hamiltonian that we consider to generate the non-linear sigma model reads:

$$\begin{aligned} \hat{H} = \int_V d^2\boldsymbol{r} \Bigg(&\frac{U_0}{2}[\hat{\psi}^\dagger(\boldsymbol{r})\hat{\psi}(\boldsymbol{r}) - C(\boldsymbol{r})]^2 \\ &- \frac{U}{2}\sum_{i=1}^{5}[\hat{\psi}^\dagger(\boldsymbol{r})O^i\hat{\psi}(\boldsymbol{r})]^2 \Bigg) \end{aligned} \tag{148}$$

which is proposed by the work of Ippoliti et al. [56]. We consider the case of $U > 0$ here. Limited in the zeroth LL, now we write a simplified form of fermion annihilation operator in Eq. 147 recalling the component index : $\hat{\psi}_a(\boldsymbol{r}) = \sum_{k=1}^{N_\phi} \phi_k(\boldsymbol{r})\hat{c}_{a,k}$. The

background $C(\boldsymbol{r}) \equiv 2\sum_{k=1}^{N_\phi} |\phi_k(\boldsymbol{r})|^2$ ensures the particle-hole symmetry. Now we have a Hamiltonian of continues field theory but with finite degrees of freedom.

For $i = 1 \cdots 5$, O^i, are mutually anti-commuting matrices. A convenient choice reads:

$$\tau_x \otimes \mathbb{I}_2, \tau_y \otimes \mathbb{I}_2, \tau_z \otimes \vec{\tau} \quad i = 1, 2, ...5. \tag{149}$$

Thus we see that our interaction of Eq. (148) has an exact O(5) symmetry, due to the anti-commutation of the five matrices. The 10 matrices $L^{ij} = -\frac{i}{2}[O^i, O^j]$, $i, j = 1 \cdots 5$, are the generators of the SO(5) group and commute with the Hamiltonian. On the other hand, the Z_2 symmetry of the O(5) group is easily shown applying a Particle-Hole transformation:

$$\begin{aligned} &PH\hat{\psi}_a(\boldsymbol{r})PH^{-1} = \hat{\psi}_a^\dagger(\boldsymbol{r}) \\ &PH[\hat{\psi}^\dagger(\boldsymbol{r})O^i\hat{\psi}(\boldsymbol{r})]PH^{-1} = -\hat{\psi}^\dagger(\boldsymbol{r})O^i\hat{\psi}(\boldsymbol{r}) \end{aligned} \tag{150}$$

which reverse the sign in front of all the five fermion bilinears. The fact that all the 5 matrices O^i are traceless is necessary for above calculation.

5.1.3 Sigma model

Consider the interaction without the term of U_0, the most simple mean field solution of Eq.148 in the half filed case is to take a polarized direction in the O(5) space, say O^5. Since the failing of fermion commutation role $[\hat{\psi}(\boldsymbol{r}), \hat{\psi}(\boldsymbol{r'})] \neq 0$, a convenient choice would be a ferromagnetic saddle point $m\hat{\psi}^\dagger(\boldsymbol{r})O^i\hat{\psi}(\boldsymbol{r})$, requiring $m = \langle\hat{\psi}^\dagger(\boldsymbol{r})O^i\hat{\psi}(\boldsymbol{r})\rangle$. Crucially

$$\int_V d^2\boldsymbol{r}\hat{\psi}_a^\dagger(\boldsymbol{r})\hat{\psi}_b(\boldsymbol{r}) = \sum_{k=1}^{N_\phi} \hat{c}_{a,k}^\dagger \hat{c}_{b,k} \tag{151}$$

Thus all the canonical degree's of freedom of zeroth LL in the ferromagnetic saddle point acquire a finite gap $\Delta_{sp} \propto m$. This simple mean field wave function is a half filed Slater determinate:

$$|\Psi\rangle = \prod_{k=1}^{N_\phi} \hat{c}_{2,k}^\dagger \hat{c}_{3,k}^\dagger |0\rangle \tag{152}$$

since we took the 5th matrix in Eq. (149).

The many body solution of the interacting Hamiltonian will become much more complicated as along as more than one component of masses is considered in Eq.149. In the case that two or three masses ($O(2)$ or $O(3)$ symmetric) are considered, strong magnetic instabilities is observed [76]. Mean field wave function of Eq. (152) will fail completely in this case, but system still has insulating ground state with spontaneous broken symmetry, leading to a "valence bond solid"(VBS) or " anti-ferromagnetic "(AFM) state. The low lying excitation of these states are O(2) or O(3) golden-stone modes.

It is surprising that, when the number of masses is larger than or equal to four, strong space-time fluctuation of the $O(n)$ order parameter may destroy the order: not only Goldstone mode, but also a geometric term which depends on the topology by which the order parameter cover the space-time contributes to the Boltzmann weight in statistics. We are mainly interested in the O(5) case in our study. Ref.[28] shows in a Lagrangian based calculation that, by integrating out the fermionic degrees of freedom in the Hubbard–Stratonovich decomposed form of Eq. 148 (such that there

are 5 component order parameters which are coupled to the fermion bilinears),

$$S^{LL} = \int_0^\beta d\tau \left(-\sum_{k=1}^{N_\phi} \boldsymbol{c}_k^\dagger(\tau)\partial_\tau \boldsymbol{c}_k(\tau) + \int_V d^2\boldsymbol{x}(\frac{|\boldsymbol{\varphi}(\boldsymbol{x},\tau)|^2}{2Ul_B^2} - \boldsymbol{\varphi}(\boldsymbol{x},\tau)\cdot\boldsymbol{\psi}^\dagger(\boldsymbol{x},\tau)\boldsymbol{O}\boldsymbol{\psi}(\boldsymbol{x},\tau)) \right) \tag{153}$$

one get the purely bosonic action which only contains the 5 bosonic field:

$$S = \frac{1}{g}\int d^3x(\nabla\boldsymbol{\varphi})^2 + S_{\mathrm{WZW}}. \tag{154}$$

Note that the projection onto the lowest level reads $\boldsymbol{\psi}_a(\boldsymbol{x}) = \sum_{k=1}^{N_\phi}\phi_k(\boldsymbol{x})\boldsymbol{c}_{a,k}$, with $\boldsymbol{c}_{a,k}$ the variable which follows grassmann algebra.

Above topological WZW term reads:

$$\begin{aligned} &S_{\mathrm{WZW}} = 2\pi i W[\varphi_a] \\ &W[\varphi_a] = \frac{3}{8\pi^2}\int_0^1 d\mu \int d^2\boldsymbol{r}\int d\tau \epsilon_{abcde}\varphi_a\partial_x\varphi_b\partial_y\varphi_c\partial_\tau\varphi_d\partial_\mu\varphi_e \end{aligned} \tag{155}$$

where μ is an additional parameter introduced for the integration, and $\boldsymbol{\varphi}(\mu,\boldsymbol{r},\tau)$ is a continues function which connects between the physical field $\vec{\varphi}(\boldsymbol{r},\tau)$ at $\mu = 1$ and a fixed polarized field at $\mu = 0$. Note that above integration of fermionic degree's of freedom is based on the space-time fluctuating bosonic field, but a gaped fermionic spectrum is still necessary for the integration.

Without the topological term S_{WZW}, action of Eq. (154) is the well known sigma model which has two attractive fixed point at strong ($1/g \longrightarrow \infty$) and weak coupling ($1/g \longrightarrow 0$) limit, separated by a Wilson-Fisher fixed point at an intermediate g_c. This captures a quantum phase transition between an O(n) symmetry broken state and an para-magnetic insulator at zero temperature, e.g. the O(n) quantum rotor model, or equivalently, the classical phase transition at finite temperature. The so called "stiffness" $1/g$ is the only controlling parameter in this field theory.

In the limit of large stiffness, the WZW term should not play a role since the order parameters tend to be polarized, such that the action is reduced. In this case the system will flow to the same symmetry broken fixed point of the sigma model without topological term. On the other hand, in the small stiffness case, the action which includes S_{WZW} may not have a disordered ground state. Knowing the equivalence of two anomalous dimensions (of AFM and VBS) within high numerical precision, A. Nahum[50] expect that a $SO(5)$ symmetric CFT which is represented by Eq.154 is a candidate field theory for deconfined quantum critical point (DQCP). To describe a 'AFM to VBS' phase transition, symmetry breaking terms which explicitly break the O(5) symmetry is necessarily to be added to the action.

Action of Eq. 154 can not be directly mapped to the one of two-component Abelian Higgs model mentioned in previous chapter, although both theory captures the point that topological defect of one order parameter carries the charge of the dual one. A key difference is that, the $NCCP^1$ field theory does not require a O(5) symmetry. It may have a critical point where both correlation functions of AFM and VBS order parameters have a power law decay : generally the two anomalous dimensions can be different. The question of whether or not the critical point of $NCCP^1$ is asymptotically O(5) symmetric could be identical to : for the action of Eq.154, is an additional term which corresponds to a higher order symmetry breaking field irrelevant or not in the renormalization group limit.

Note that the above two versions of $O(5)$ symmetry breaking terms are significantly different to each other: the anisotropy term which drives the system to AFM or VBS fixed point is certainly relevant under RG. This term goes:

$$S = \alpha \int d^3x (\sum_{i=1,3} \varphi^i \varphi^i - \sum_{i=4,5} \varphi^i \varphi^i) \tag{156}$$

While the higher order symmetry breaking term which could be irrelevant under RG should be written as some cross terms between AFM and VBS order parameters.

The action of Eq.154 has the same form as what we have for QSH-SSC transition. This is actually not so surprising given the similar anti-commuting algebra of Dirac masses. Recall O(5) symmetric Dirac action mentioned in the chapter of QSH-SSC transition:

$$S_{Dirac} = \int d\tau \int d^2\boldsymbol{x} [c^\dagger(\boldsymbol{x},\tau)(\gamma_0\gamma_\mu\partial_\mu)c(\boldsymbol{x},\tau) + \boldsymbol{\phi}(\boldsymbol{x},\tau)\cdot c^\dagger(\boldsymbol{x},\tau)\boldsymbol{O}c(\boldsymbol{x},\tau)] \tag{157}$$

where $\mu = 0, 1, 2$. We have set the Fermi velocity to unity here.

The differences between Dirac system with a finite velocity and the system which is projected into zeroth LL are :

1. Matrix formulations. As mentioned in previous chapter, the 5 anti-commuting mass of AFM an VBS in 2D Dirac system follows:

$$Tr^8(\gamma^1\gamma^2 O^I O^J O^K O^L O^N) = 8i\epsilon_{IJKLN} \tag{158}$$

If Nambu spinor is included, e.g. in the case of QSH-SSC competition, above formalism is generalized to 16×16 matrix. However, as the derivation shown in the appendix, the bosonic action after integrating out the fermions will be the same.

When projected to the zeroth LL, the structure of 4×4 matrices are:

$$Tr^4(O^I O^J O^K O^L O^N) = 4\epsilon_{IJKLN} \tag{159}$$

Our choice of Eq. 149 in current work is an example. A calculation in Ref. [77] explicitly shows that the WZW term of the 5 component order parameter is equivalent to the one derived from Dirac fermions.

2. Stiffness of sigma model. In 2D Dirac systems in terms of free Dirac fermions coupled to bosonic order parameters in terms of Yukawa coupling, a calculation by Abanov and Wiegmann [45] shows that after integrating out the fermions, the 'stiffness' $(1/g)$ of sigma model in Eq. 154 is proportional to the fermionic single particle gap. The calculation holds exactly only in the limit of small but finite fermionic gap. More precisely, it depends on the single particle gap in the unit of fermion velocity. In the case of zeroth LL, it's a bit tricky since there is no fermion velocity. If one only has the U term of Eq.148, the single particle gap, which is proportional to U, simply re-scales the bosonic velocity of sigma model without changing the stiffness.

Now we recall the interacting term of $\frac{U_0}{2}[\hat{\psi}^\dagger(\boldsymbol{r})\hat{\psi}(\boldsymbol{r}) - C(\boldsymbol{r})]^2$ in Eq. (148), which is invariant under $U(4)$ transformation. This term does not change the symmetry of Hamiltonian, but tunes the "stiffness" $(1/g)$ of sigma model[78]. We will see later that it is shown numerically. U_0 is our only tuning parameter in the following numerical calculation.

3. The Dirac formalism of Eq.157 is hard to be solved numerically, since it's Hilbert space has infinite dimension. On the other hand, it can be an effective action of a lattice Hamiltonian, e.g. the QSH-SSC transition of previous section. However, the

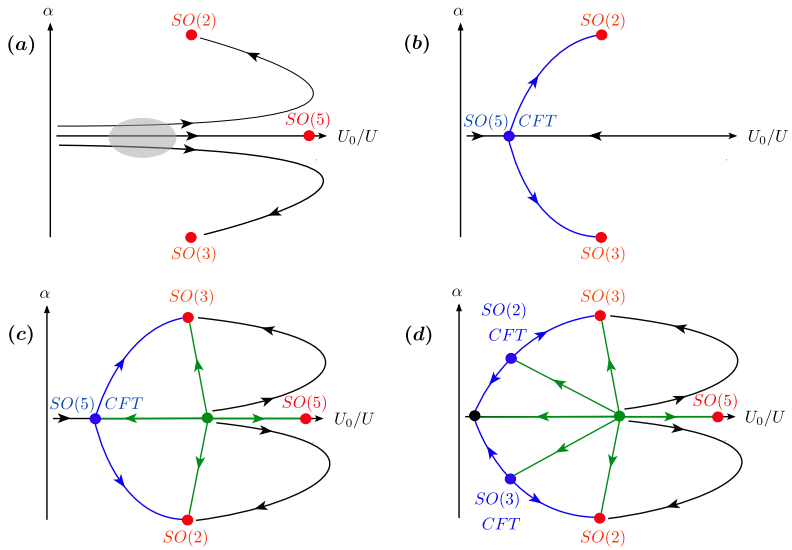

Figure 34: Possible RG flows in the U_0 versus α phase. α corresponds to the amplitude of a term that breaks down the O(5) symmetry to SO(3) $\times$ SO(2). The horizontal line corresponds to the $\alpha = 0$ or to O(5) symmetry. Red bullets, corresponds to phases where the symmetry group is spontaneously broken. The black bullet is an O(5) disordered phase. Blue (green) bullets denote critical (multi-critical) points. In scenario (a) the O(5) model orders and the shaded region depicts a slow RG flow (see text). In (b) the O(5) model remains critical. In (c) the O(5) model has an ordered and critical phase separated by a multi-critical point. Finally, in (d) the O(5) model shows an order-disorder transition.

O(5) symmetry is not an exact symmetry of lattice models, in the sense that a symmetry breaking term which doesn't respect the O(5) symmetry is necessarily involved in the Dirac action, as well as in the bosonic action of Eq.154. The zeroth LL formalism, on the other hand, is able to be simulated based on Hamiltonian of Eq.148 with a finite Hilbert space which does not break the O(5) symmetry.

5.1.4 RG scenario

Now we consider a phase transition which is tuned by the second axis : an anisotropy which breaks the O(5) symmetry. In the picture of Hamiltonian a term of $\alpha(\sum_{i=1}^{2}[\hat{\psi}^\dagger(\boldsymbol{r})O^i\hat{\psi}(\boldsymbol{r})]^2 - \sum_{i=3}^{5}[\hat{\psi}^\dagger(\boldsymbol{r})O^i\hat{\psi}(\boldsymbol{r})]^2)$ would play this role, where α is the relevant operator which breaks the symmetry. Schematic RG flows for an enhanced O(5) symmetry that is broken down to SO(3) $\times$ SO(2) are shown in Fig. 34. Here U_0/U does not change and symmetry, and plays the role of stiffness. If the O(5) symmetric model at $\alpha = 0$ is always ordered, the nature of AFM-VBS transition is always first order [Fig.34(a)] . The spin-flop transition corresponding to the field-driven reorientation of the easy axis falls into this category. In this case the O(5) symmetric line always flow to the strong coupling $1/g \longrightarrow \infty$ limit, thus the transition tuned by α is not captured by any divergence of correlation length.

The second possibility is that a critical phase is pinned by the topological term, regardless of stiffness. This scenario is shown in Fig. 34(b). As mentioned before, a fixed point which is relevant in the direction of anisotropy but irrelevant in the direction of $1/g$ exists. Thus a power law decaying of correlation function, captured by the same

scaling dimension would always be found at all the range of U_0/U. As an example for this scenario, we can consider the one-dimensional DQC between a dimer and Néel state in the XXZ model considered in Refs. [79, 80] and realized in [81]. The critical point has a U(1) symmetry that is broken by the umklapp operator that tunes through the transition. However in our $O(n)$ sigma model this scenario is unlikely to hold in the limit of large stiffness: the topological defect would be expired but to large free energy.

As a third possibility, the enhanced-symmetry model may have a relevant tuning parameter U_0 – and associated (multi) critical point – that does not break the enhanced symmetry. Fig. 34(c) describes a scenario where the ordered state gives way to a critical phase. In this case, tuning α leads to first order or continuous transitions depending upon the value of U_0. Finally, in Fig. 34(d) U_0 drives an order-disorder transition. Aside from fine tuning, the transition from the SO(3) to SO(2) broken symmetry states is first order or separated by a disordered phase.

5.2 QMC implementation

5.2.1 Momentum space interaction

To perform a numerical simulation of Eq. (148), recall that due to the projection to the zeroth LL:

$$\hat{\psi}_a(\boldsymbol{r}) = \sum_{k=1}^{N_\phi} \phi_k(\boldsymbol{r}) \hat{c}_{a,k} \tag{160}$$

where the operators which annihilate(create) single LL obeys fermion canonical commutation role:

$$\left\{\hat{c}^\dagger_{k,a}, \hat{c}_{k',a'}\right\} = \delta_{a,a'}\delta_{k,k'}, \;\; \left\{\hat{c}_{k,a}, \hat{c}_{k',a'}\right\} = 0. \tag{161}$$

while since the zeroth LL does not span the hole Hilbert space, operators $\hat{\psi}_a(\boldsymbol{r})$ does not satisfy the canonical commutation role. To perform QMC we have to formulate the interaction based on canonical operators.

As aforementioned, the wave-function $\phi_k(\boldsymbol{r})$, of Zeroth LL of Graphene is identical to the lowest LL of free nonrelativistic electrons in the 2D plane pieced by magnetic field:

$$\hat{H}_0 = \frac{1}{2m}\left(\hat{\boldsymbol{P}} - e\boldsymbol{A}(\boldsymbol{r})\right)^2. \tag{162}$$

We choose Landau gauge, such that $\boldsymbol{A}(\boldsymbol{r}) = B(0, x, 0)$ ($\boldsymbol{r} = (x, y, z)$), translations along the y direction leave the Hamiltonian invariant such that the momentum in this axis, p_y, is a good quantum number. On a torus of size $L_x \times L_y$ the wave function of the first Landau level reads:

$$\phi_{p_y}(\boldsymbol{r}) = \frac{1}{\sqrt{L_y}} \frac{1}{\sqrt{l_B\sqrt{\pi}}} e^{-(x/l_B - \mathrm{sign}(B) p_y l_B)^2/2} e^{i p_y y}. \tag{163}$$

Here the magnetic length scale is defined as $l_B^2 = \frac{\phi_0}{2\pi|B|}$, with $\phi_0 = \frac{h}{e}$, and the number of magnetic fluxes piercing the system, $N_\phi = \frac{|B|V}{\phi_0}$, is an integer so as to guarantee uniqueness of the wave function. Finally the momentum in the y-direction is given $p_y = \frac{2\pi n}{L_y}$ with $n \in 1, \cdots, N_\phi$. Note that no we used p_y as labeling of degenerate wave-function k in Eq. (160). Defining the Fourier transform of the four component spinor:

$$\hat{\boldsymbol{\psi}}^\dagger_{\boldsymbol{p}} = \frac{1}{\sqrt{V}} \int_V d^2\boldsymbol{r} e^{i\boldsymbol{p}\cdot\boldsymbol{r}} \hat{\boldsymbol{\psi}}^\dagger(\boldsymbol{r}) \tag{164}$$

Real space Hamiltonian of Eq. (148) is transformed as:

$$\begin{aligned}\hat{H} &= \sum_{i=0}^{5}\int_V d^2\boldsymbol{r}\frac{U_i}{2}[\hat{\psi}_a^\dagger(\boldsymbol{r})O_{ab}^i\hat{\psi}_b(\boldsymbol{r}) - C(\boldsymbol{r})\delta_{i,0}]^2 \\ &= \sum_{i=0}^{5}\frac{U_i}{2}\sum_{\boldsymbol{q}}\sum_{\boldsymbol{q'}}\int_V d^2\boldsymbol{r}(\frac{1}{V}e^{i\boldsymbol{q}\cdot\boldsymbol{r}}\hat{N}^i(\boldsymbol{q}))(\frac{1}{V}e^{i\boldsymbol{q'}\cdot\boldsymbol{r}}\hat{N}^i(\boldsymbol{q'})) \\ &= \frac{1}{2V}\sum_{i=0}^{5}\sum_{\boldsymbol{q}}\hat{N}^i(\boldsymbol{q})U_i\hat{N}^i(-\boldsymbol{q})\end{aligned} \tag{165}$$

To write the interaction in a compact form we labeled the interaction pre-factor as $U_i = -U$ for $i = 1\cdots5$. Here, O^0, is the unit matrix and $\hat{\psi}^\dagger(\boldsymbol{r})O^i\hat{\psi}(\boldsymbol{r}) = \frac{1}{V}\sum_{\boldsymbol{q}}e^{-i\boldsymbol{q}\cdot\boldsymbol{r}}\hat{N}^i(\boldsymbol{q})$ for $i = 1\cdots5$ and $\hat{\psi}^\dagger(\boldsymbol{r})\hat{\psi}(\boldsymbol{r}) - C(\boldsymbol{r}) = \frac{1}{V}\sum_{\boldsymbol{q}}e^{-i\boldsymbol{q}\cdot\boldsymbol{r}}\hat{N}^0(\boldsymbol{q})$.

Neglecting the constant background term at $i = 0$, the *density* operators $\hat{N}^i(\boldsymbol{q})$, can be expressed in terms of the canonical operators $\hat{\boldsymbol{c}}_{p_y}^\dagger$:

$$\begin{aligned}\hat{N}^i(\boldsymbol{q}) &= \sum_{\boldsymbol{p}}\hat{\psi}_{\boldsymbol{p}}^\dagger\boldsymbol{O}^i\hat{\psi}_{\boldsymbol{p}-\boldsymbol{q}} \\ =&\frac{1}{V}\sum_{\boldsymbol{p}}\int_V\int_{V'}d^2\boldsymbol{r}d^2\boldsymbol{r'}e^{i\boldsymbol{p}\cdot\boldsymbol{r}}e^{-i(\boldsymbol{p}-\boldsymbol{q})\cdot\boldsymbol{r'}}\sum_{k_1}\hat{\boldsymbol{c}}_{k_1}^\dagger\phi_{k_1}^*(\boldsymbol{r})\boldsymbol{O}^i\sum_{k_2}\hat{\boldsymbol{c}}_{k_2}\phi_{k_2}(\boldsymbol{r'}) \\ =&\frac{1}{2\sqrt{\pi}}e^{-l_B^2\boldsymbol{q}^2/4}\sum_{p_y}e^{iq_xp_yl_B^2}\hat{\boldsymbol{c}}^\dagger_{p_y+\frac{q_y}{2}}\boldsymbol{O}^i\hat{\boldsymbol{c}}_{p_y-\frac{q_y}{2}}\end{aligned} \tag{166}$$

With the substitution $k = p_y + \frac{q_y}{2}$ and

$$\begin{aligned}\hat{n}^i(\boldsymbol{q}) =&\sum_{k=1}^{N_\phi}\sum_{a,b=1}^{4}F(\boldsymbol{q})e^{\frac{i}{2}(2k-q_y)l_B^2q_x}(\hat{c}_{a,k}^\dagger O_{a,b}^i\hat{c}_{b,k-q_y} \\ &-2\delta_{q_y,0}\delta_{i,0})\end{aligned} \tag{167}$$

where the background term $2\delta_{q_y,0}\delta_{i,0}$ can easily be verified by Fourier transform the real space background $C(\boldsymbol{r})$ (see main text). Now the Hamiltonian reads:

$$\hat{H} = \frac{1}{8\pi V}\sum_{i=0}^{5}\sum_{\boldsymbol{q}}\hat{n}^i(\boldsymbol{q})U_i\hat{n}^i(-\boldsymbol{q}). \tag{168}$$

In the above, $a(\mathrm{b}) = 1, 2, 3$ and 4 is the flavor index, and $F(\boldsymbol{q}) \equiv e^{-\frac{1}{4}(q_x^2+q_y^2)l_B^2}$. As we will shown in the next subsection, this exponential decaying factor is essential for the QMC simulation since it provides a natural cutoff for the momenta $\boldsymbol{q}$. Finally, setting the magnetic unit length to unity such that $\frac{2\pi}{V} = \frac{1}{N_\phi}$ we obtain:

$$\hat{H} = \frac{1}{16\pi^2N_\phi}\sum_{i=0}^{5}\sum_{\boldsymbol{q}}\hat{n}^i(\boldsymbol{q})U_i\hat{n}^i(-\boldsymbol{q}) \tag{169}$$

5.2.2 Fierz identity and absence of the negative sign problem

To avoid the negative sign problem in the QMC simulations we use the Fierz identity to rewrite Eq. (165) as:

$$H = \frac{1}{2N_\phi}\sum_{i=0}^{3}\sum_{\boldsymbol{q}}\hat{n}_{-\boldsymbol{q}}^ig^i\hat{n}_{\boldsymbol{q}}^i \tag{170}$$

Instead of the original density operators in Eq. (167), the $n^i(i = 0, 1, 2, 3)$ operators are based on 4 matrix:

$$\mathbb{I}_4, \tau_x \otimes \mathbb{I}_2, \tau_y \otimes \mathbb{I}_2, \tau_z \otimes \mathbb{I}_2. \tag{171}$$

Eq. (170) is identical to Eq. (165) when $\frac{g^0}{8\pi^2} = U_0 + U$, $\frac{g^1}{8\pi^2} = \frac{g^2}{8\pi^2} = -2U$, and $\frac{g^3}{8\pi^2} = 2U$. Here we consider the SO(5) symmetric point and set $U_i = -U$ for $i \in 1, \cdots, 4$. The absence of sign problem holds for the region of $U_0 \geq -U$, follows from the work of Ref. [82] and is discussed in detail in reference [56]. The above matrix structure also gives an explicit $SU(2)$ symmetry which holds for each Hubbard-Stratonovich field configuration.

5.2.3 Trotter errors

Since $n(\boldsymbol{q})^\dagger = n(-\boldsymbol{q})$, the exponential of operators at each time slice is given by:

$$\begin{aligned} & e^{-\frac{\Delta\tau}{2N_\phi}(\hat{n}^i_{\boldsymbol{q}} g^i \hat{n}^i_{-\boldsymbol{q}} + \hat{n}^i_{-\boldsymbol{q}} g^i \hat{n}^i_{\boldsymbol{q}})} \\ =& e^{-\frac{\Delta\tau}{4N_\phi}[g^i(\hat{n}^i_{\boldsymbol{q}} + \hat{n}^i_{-\boldsymbol{q}})^2 - g^i(\hat{n}^i_{\boldsymbol{q}} - \hat{n}^i_{-\boldsymbol{q}})^2]} \end{aligned} \tag{172}$$

The QMC implementation is followed by HS decomposing the "perfect square" terms above.

Similar to the model of QSH-SSC transition which is discussed in previous chapter, interacting operators at different momentum does not commute with each other. Thus to ensure hemiticity, again we use a symmetric Trotter decomposition:

$$Z = \mathrm{Tr}\,[\prod_{m=1}^{N} e^{-\frac{\Delta\tau}{2}\hat{H}_m} \prod_{n=N}^{1} e^{-\frac{\Delta\tau}{2}\hat{H}_n}]^{L_\tau} \tag{173}$$

where $\hat{H}_m$ corresponds to the $N = 2 \times 4 \times N_q$ operators $\pm\frac{g^i}{4N_\phi}(\hat{n}^i_{\boldsymbol{q}} \pm \hat{n}^i_{-\boldsymbol{q}})^2$. N_q is the number of momentum points used for the simulation. As we will see below N_q scales as N_ϕ. The difference between current case and the QSH model is that, the non-commutation relation here holds non-locally. We will see that here the systemic err of free energy density is not scaling invariant but scales proportionally to N_ϕ.

For two operators $\hat{H}_1$ and $\hat{H}_2$ the leading order error produced in the symmetric Trotter decomposition reads:

$$\begin{aligned} & e^{-\frac{\Delta\tau}{2}\hat{H}_1} e^{-\Delta\tau\hat{H}_2} e^{-\frac{\Delta\tau}{2}\hat{H}_1} \\ =& e^{-\Delta\tau(\hat{H}_1+\hat{H}_2) + \frac{\Delta\tau^3}{12}[2\hat{H}_1 + \hat{H}_2, [\hat{H}_1, \hat{H}_2]]} + \mathcal{O}(\Delta\tau^4) \end{aligned} \tag{174}$$

Iterating the above formula gives:

$$\prod_{m=1}^{N} e^{-\frac{\Delta\tau}{2}\hat{H}_m} \prod_{n=N}^{1} e^{-\frac{\Delta\tau}{2}\hat{H}_n} = \quad e^{-\Delta\tau((\sum_{m=1}^{N}\hat{H}_m) + \hat{\lambda})} + \mathcal{O}(\Delta\tau^4) \tag{175}$$

where

$$\begin{aligned} \hat{\lambda} \equiv -\frac{\Delta\tau^2}{12}(& \sum_{m=1}^{N-1} \sum_{m'=m+1}^{N} [2\hat{H}_m + \hat{H}_{m'}, [\hat{H}_m, \hat{H}_{m'}]] \\ & + \sum_{m=1}^{N-1} \sum_{m'=m+1}^{N} \sum_{m''=m+1}^{N} [\hat{H}_{m'}, [\hat{H}_m, \hat{H}_{m''}]](1 - \delta_{m',m''})) \end{aligned} \tag{176}$$

and $\delta_{m',m''}$ the Kronecker delta. Using time dependent perturbation theory, we then obtain:

$$\begin{aligned}&\left(\prod_{m=1}^{N} e^{-\frac{\Delta\tau}{2}\hat{H}_m}\prod_{n=N}^{1} e^{-\frac{\Delta\tau}{2}\hat{H}_n}\right)^{L_\tau}\\ =&e^{-\beta\hat{H}} - e^{-\beta\hat{H}}\int_0^\beta d\tau e^{\tau\hat{H}}\hat{\lambda}e^{-\tau\hat{H}} + \mathcal{O}(\Delta\tau^3)\end{aligned} \tag{177}$$

with $L_\tau = \frac{\beta}{\Delta\tau}$ the number of time slices. $\hat{\lambda}$ is measure of the leading order error on the free energy density:

$$\begin{aligned}f_{QMC} \equiv& -\frac{1}{\beta V}\ln \mathrm{Tr}\,(\prod_{m=1}^{N} e^{-\frac{\Delta\tau}{2}\hat{H}_m}\prod_{n=N}^{1} e^{-\frac{\Delta\tau}{2}\hat{H}_n})^{L_\tau}\\ =&f + \frac{1}{\beta V}\int_0^\beta d\tau\langle e^{\tau\hat{H}}\hat{\lambda}e^{-\tau\hat{H}}\rangle + \mathcal{O}(\Delta\tau^3)\\ =&f + \frac{1}{V}\langle\hat{\lambda}\rangle + \mathcal{O}(\Delta\tau^3)\\ =&f + \frac{1}{2\pi N_\phi}\langle\hat{\lambda}\rangle + \mathcal{O}(\Delta\tau^3)\end{aligned} \tag{178}$$

In the above we have set $l_B = 1$ so as to replace V by N_ϕ, and $f = -\frac{1}{\beta V}\ln \mathrm{Tr}\, e^{-\beta\hat{H}}$. Since the interacting operators for different masses i do not commute with each other, the Trotter decomposition breaks the SO(5) symmetry of Hamiltonian (a SU(2) symmetry is left due to the Fierz identity in Eq. (170)).

To evaluate the expectation value of $\hat{\lambda}$, we first evaluate the commutator of two density operators:

$$\begin{aligned}&[\hat{n}^i(\boldsymbol{q_1}), \hat{n}^j(\boldsymbol{q_2})]\\ =&F(\boldsymbol{q_1})F(\boldsymbol{q_2})\sum_k \hat{\boldsymbol{c}}_k^\dagger\{e^{\frac{i}{2}(2k-(q_{1y}+q_{2y}))l_B^2(q_{1x}+q_{2x})}\\ &(2\cos(\theta_{\boldsymbol{q_1},\boldsymbol{q_2}})[O_i,O_j] + 2i\sin(\theta_{\boldsymbol{q_1},\boldsymbol{q_2}})\{O_i,O_j\})\}\hat{\boldsymbol{c}}_{k-(q_{1y}+q_{2y})}\\ =&\frac{F(\boldsymbol{q_1})F(\boldsymbol{q_2})}{F(\boldsymbol{q_1}+\boldsymbol{q_2})}\{n^{[O_i,O_j]}(\boldsymbol{q_1}+\boldsymbol{q_2})2\cos(\theta_{\boldsymbol{q_1},\boldsymbol{q_2}})\\ &+n^{\{O_i,O_j\}}(\boldsymbol{q_1}+\boldsymbol{q_2})2i\sin(\theta_{\boldsymbol{q_1},\boldsymbol{q_2}})\}\end{aligned} \tag{179}$$

where $\theta_{\boldsymbol{q_1},\boldsymbol{q_2}} = \frac{l_B^2}{2}(q_{1y}q_{2x} - q_{1x}q_{2y})$. Since the density operators do not commute we can estimate the magnitude of the Trotter error as follows. Let $||\hat{A}|| \equiv \max_{|\Psi\rangle,|||\Psi\rangle||=1}||\hat{A}|\Psi\rangle||$. Since the Hamiltonian $\sum_m H_m$ is an extensive quantity, $||\sum_m H_m|| \propto N_\Phi$. Here m runs over a set of order N_Φ momenta, hence implies that typically, $H_m \propto N_\Phi^0$. Using this to estimate the systematic error, yields the result:

$$f_{QMC} = f + \mathcal{O}\left(\Delta\tau^2 N_\Phi^2\right). \tag{180}$$

Hence, to keep the Trotter error under control we have to scale $\Delta\tau$ as $1/N_\Phi$.

The Trotter error in our model has a different scaling behavior, than for models with only local interaction such as the Hubbard model. For local interactions $||\lambda||$ scales as N_Φ, such the systematic error on the free energy density is size independent.

An improved estimator is introduced, based on the SO(5) invariant structure factor:

$$S(\boldsymbol{q}) = \frac{1}{N_\phi}\sum_{i=1}^{5}\langle\hat{n}^i_{\boldsymbol{q}}\hat{n}^i_{\boldsymbol{-q}}\rangle. \tag{181}$$

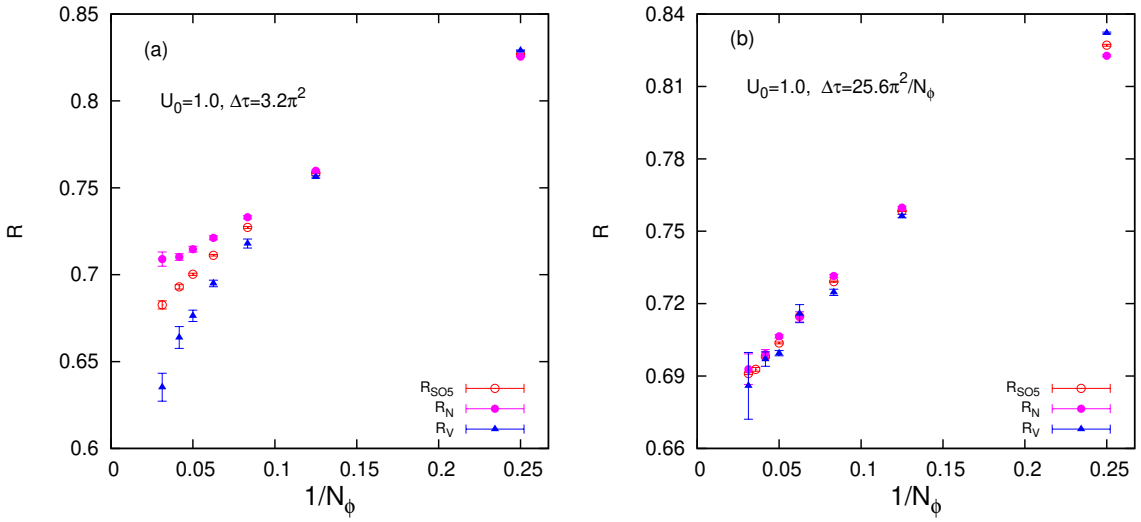

Figure 35: Correlation ratio R of Neel, VBS order and the improved estimator for a fix $\Delta\tau$ as $3.2\pi^2$ (a), and for a linear scaling of $\Delta\tau = 25.6\pi^2/N_\phi$ (b). The simulation is based on $U_0 = 1.0$, of system sizes $N_\phi = 4, 8, 12, 16, ...32$, with $\beta = 1$.

The magnetization and correlation ratio used for the scaling analysis in the main part of the paper is based on the above structure factor.

Fig. 35 shows a numerical comparison of the correlation ratio for multiple system sizes. In Fig. 35 (a) we consider a constant $\Delta\tau$ while in Fig. 35 (b) we scale $\Delta\tau$ with the volume: $\Delta\tau = 25.6\pi^2/N_\phi$. As mentioned previously, our Trotter decomposition breaks the SO(5) symmetry such that a convenient measure of the finite time step systematic error is the discrepancy between the Néel and VBS order parameters. At constant $\Delta\tau = 3.2\pi^2$ the correlation ratio defined from the Néel, VBS and SO(5) order parameters progressively differ as a function of system size. On the other hand, for simulations where we keep $\Delta\tau N_\phi$ constant, see Fig. 35 (b), no $SO(5)$ symmetry breaking up to $N_\phi = 32$ is apparent. In all our simulations we have kept $\Delta\tau N_\phi$ constant.

5.2.4 Cutoff and computational difficulty

The effective interacting strength in Eq. (170) is controlled by a momentum dependent function $F(\boldsymbol{q})$ in Eq. (167):

$$F(\boldsymbol{q}) = e^{-\frac{1}{4}(q_x^2+q_y^2)l_B^2} \tag{182}$$

The exponential decay of the interacting strength gives a natural cutoff in the momentum space. In particular, we we can consider momenta satisfying $F(\boldsymbol{q}) > F_{min}$. As shown in Fig. 36, for $N_\phi = 4, 8$ and 12 at $U_0 = U = 1$, the cutoff dependence of the correlation ratio is negligible up to $F_{min} = 0.01$. In our calculations, we have chosen $F_{min} = 0.01$. Setting $l_B = 1$ implies that the number of $\boldsymbol{q}$-vectors we consider for a given cutoff scales as N_ϕ.

Taking all the above into account yields a computational effort that scales as $N_\phi^5\beta$ where β is the inverse temperature. This should be compared to the generic $N_\phi^3\beta$ scaling for say the Hubbard model. The above explains why our simulations are limited to $N_\phi = 100$.

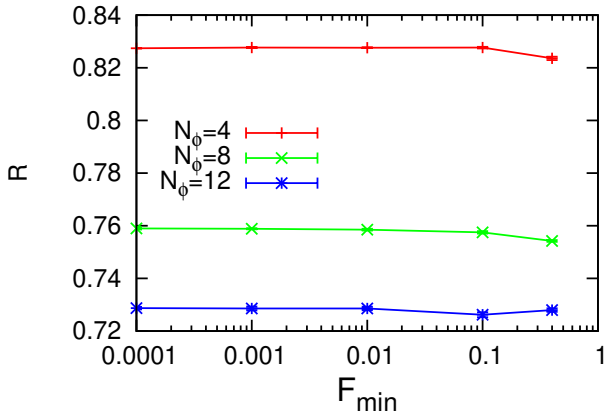

Figure 36: Correlation ratio as a function of F_{min} for $N_\phi = 4, 8$ and 12, at $U_0 = U = 1, \beta = 160\pi^2, \Delta\tau = 3.2\pi^2$.

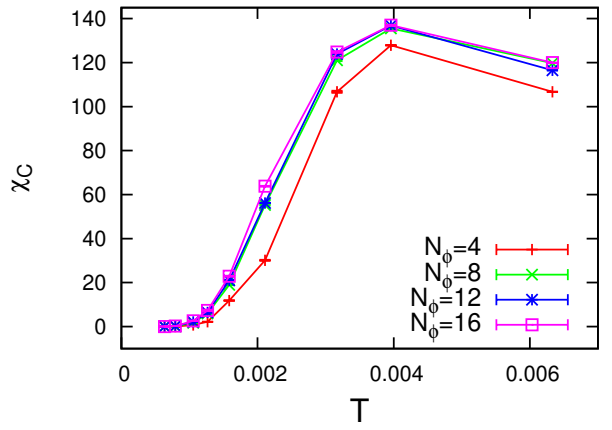

Figure 37: Temperature dependence of the uniform charge susceptibility χ_C for $U_0 = -1$.

5.3 QMC results

For the simulations we set the energy scale by choosing $U = 1$, the length scale by choosing $l_B = 1$ and vary U_0 and the volume N_ϕ. We found that an inverse temperature of $\beta = 160\pi^2$ suffices to obtain ground state properties on our largest system sizes, $N_\phi = 100$. We have used the finite temperature auxiliary field algorithm [35, 36, 19] of the algorithms for lattice fermions (ALF)-library [31].

5.3.1 Charge Susceptibility

As mentioned before, to map to the non-linear sigma model, the ground state is necessary to be an insulating state. In Fig. 37 we plot the uniform charge susceptibility,

$$\chi_C = \frac{\beta}{N_\phi}(\langle \hat{n}_{\boldsymbol{q}=0}\hat{n}_{\boldsymbol{q}=0}\rangle - \langle \hat{n}_{\boldsymbol{q}=0}\rangle\langle \hat{n}_{\boldsymbol{q}=0}\rangle). \tag{183}$$

The charge fluctuations decay exponentially upon reducing the temperature as expected for an insulating state of matter. Since $\hat{\boldsymbol{\psi}}^\dagger(\boldsymbol{x})O^i\hat{\boldsymbol{\psi}}(\boldsymbol{x})$ are mass terms, any non-vanishing expectation value of these fermion bi-linears, φ_i, will lead to a charge

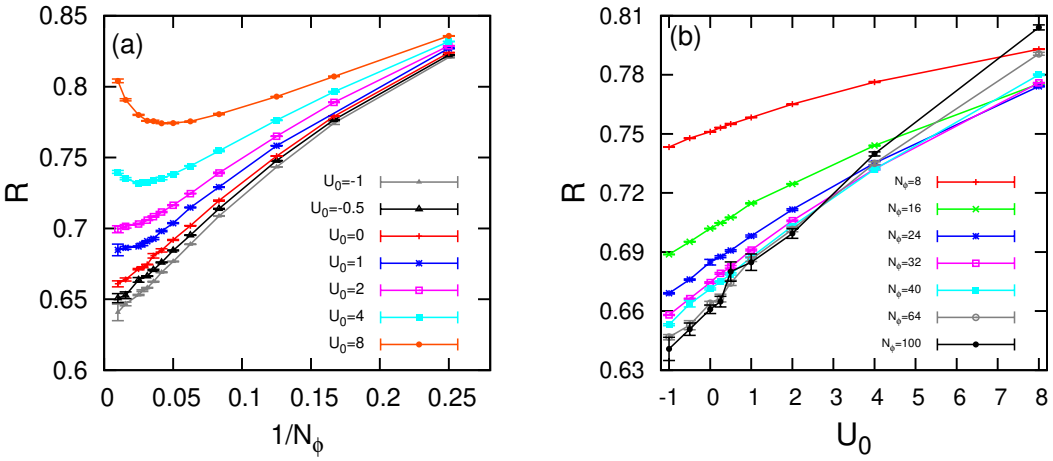

Figure 38: Correlation ratio R as a function of $1/N_\phi$ (a) and U_0 (b).

gap. Owing to the SO(5) symmetry the single particle gap is proportional to the norm of this five component vector, $|\boldsymbol{\varphi}|$.

5.3.2 Order parameter and Correlation ratio

We compute the order parameter correlation function

$$S(\boldsymbol{q}) = \frac{1}{N_\phi} \sum_{i=1}^{5} \langle \hat{n}^i_{\boldsymbol{q}} \hat{n}^i_{-\boldsymbol{q}} \rangle. \tag{184}$$

For our ordering wave vector $\boldsymbol{Q} = (0, 0)$ here, the local moment reads

$$m = \sqrt{\frac{1}{N_\phi} S(\boldsymbol{Q})} \tag{185}$$

and it is convenient to define a renormalization group invariant quantity

$$R \equiv 1 - \frac{S(\boldsymbol{Q} + \Delta\boldsymbol{q})}{S(\boldsymbol{Q})} \tag{186}$$

with $|\Delta\boldsymbol{q}| = \frac{2\pi}{\sqrt{N_\phi}}$. In the ordered (disordered) phase R converges to unity (zero) and the local moment takes a finite (vanishing) value. At a critical point, the correlation ratio converges to a universal value.

In Fig. 38(a) we plot the correlation ratio R as a function of system size for various values of U_0. For system sizes up to $N_\phi = 20$ all curves scale downwards and would suggest a critical or disordered phase. Beyond $N_\phi = 20$ and for large values of U_0 the correlation ratio changes behavior and grows. The length scale at which this crossover occurs can naturally be interpreted as a measure of the correlation length. In Fig. 38(b) we replot the correlation ratio as a function of U_0. The data is consistent with a crossing at $U_0 \simeq 3$. Below this value, R does not scale to zero, as already seen in Fig. 38(a), and hence signals a phase where the correlation length exceeds our system sizes. For these large values of U_0, a finite size extrapolation of the square of the local moment (see Fig. 39) is consistent with a finite value (see inset of Fig. 39).

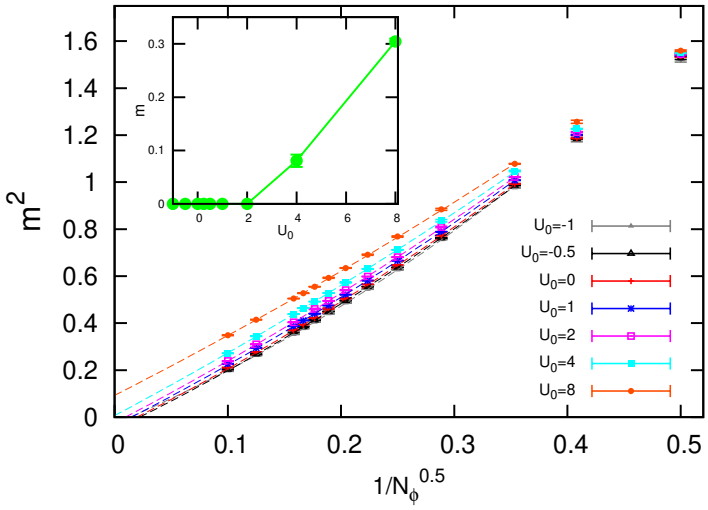

Figure 39: O(5) order parameter as a function of $1/\sqrt{N_\phi}$. The dashed lines and the inset is the extrapolation via the fitting form $m(N_\phi)^2 = m^2_{N_\phi\to\infty} + a/\sqrt{N_\phi} + b/N_\phi$. Negative extrapolated values of m^2 suggest a critical or disordered state. In both cases the polynomial, in inverse linear length, fitting form is not justified.

5.3.3 Scaling analysis

When a critical state is assumed, the O(5) order parameter should form a power law scaling behaviour:

$$m = aN_\phi^{-\frac{\eta+z}{4}} \tag{187}$$

We performed a finite size scaling based on the above equation, with assuming the dynamical exponent $z = 1$. Since no scaling correction term is assumed on top of Eq. (187), we gradually tossed small system sizes used for the fit. Surprisingly, we didn't observe a strong drift of η exponent as a function of minimal size of fit. On the other hand, η exponent drops down dramatically as a function of U_0. Since a minimal size $N_{min} = 16$ give an acceptable $\chi^2/D.O.F$ for all of the U_0 in our calculation, we show η exponent as a function of U_0 in Fig. 40 based on $N_{min} = 16$.

Apart from the last point ($U_0 = 4$) in Fig.40, which is already known as an ordered state due to the correlation ratio, a power law assumption of Eq.187 sames to be valid. However, a drift of η exponent as a function of stiffness is hard to understand: unless there exists a continues line of infinite number of fixed points in the case of 2+1D. Back to the RG scenario of Fig. 34(c), if the parameter range of weak coupling ($1/g$) flow to one fixed point of CFT, the anomalous dimension has to acquire the same value. A possible explanation is that, a large and finite correlation length ξ, decays gradually as a function of stiffness. Although ξ is still larger than our largest system size $N_\phi = 100$ when $U_0 < 8$, it may lead to a violation of our fitting procedure.

Hence we introduced another way of fitting the order parameter:

$$m = m_0 + aN_\phi^{-\frac{\eta+z}{4}} \tag{188}$$

This is based on the assumption that we are always close to the fixed point collision point, in the sense that we always has a finite correlation length ξ, which depends on

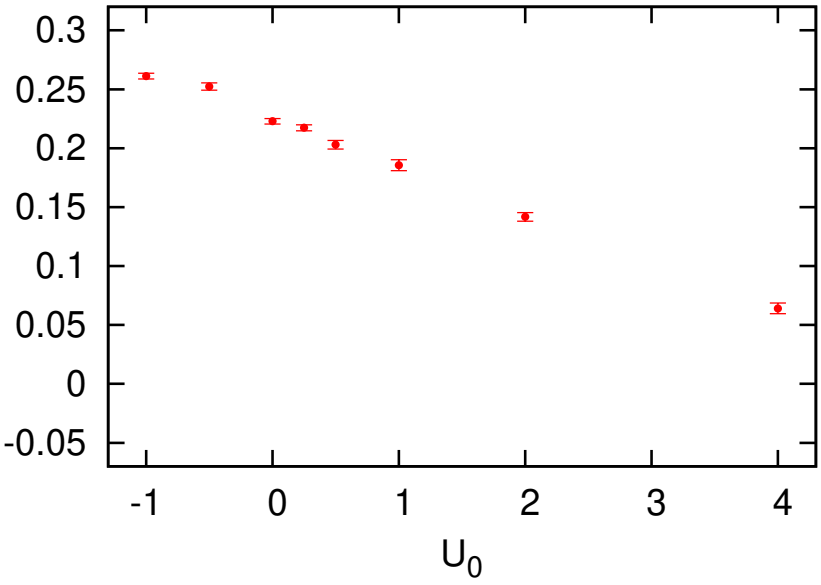

Figure 40: Fit of η exponent as a function of minimal size took into account, for several U_0 in $[-1, 4]$ (a), and η exponent as a function of U_0 (b), taken $N_{min} = 16$. Blue dots of the DMRG calculation in (b) are taken from ref [56].

U_0. As we can see from Table 4, the χ^2/DOF of fit are acceptable, when all the system sizes are included. The η exponent is robust as function of U_0, except the point of $U_0 = 8$. On the other hand, the extrapolated magnetization become nonzero within when $U_0 \geq 0.25$.

5.4 Discussion

In Fig. 34 we show possible RG flows in the U_0 versus α plane where α corresponds to the amplitude of a term that breaks down the SO(5) symmetry to SO(3) $\times$ SO(2).

Fig. 34(a) corresponds a scenario where the topological term is irrelevant and the model orders for all values of the stiffness. Taken at face value, our results do not support this point of view. However we cannot exclude the possibility that an ordered phase with small magnetic moment will occur on larger system sizes. In this case, the

U_0	$\langle m \rangle_0$	η	χ^2/DOF
-1.0	0.03(1)	0.33(2)	1.51
-0.5	0.01(1)	0.28(2)	1.32
0.0	0.03(1)	0.29(2)	1.78
0.25	0.028(7)	0.27(1)	0.92
0.5	0.04(1)	0.28(2)	0.25
1.0	0.05(1)	0.28(2)	1.17
2.0	0.064(7)	0.26(2)	0.98
4.0	0.11(1)	0.26(2)	1.75
8.0	0.27(1)	0.38(2)	1.11

Table 4: Collective fit using Eq. (188).

transition as a function of α from the SO(3) to SO(2) broken symmetries corresponds to a spin-flop transition.

In contrast in Fig. 34(b) we assume that the SO(5) model corresponds to a CFT. In this case, α is a relevant parameter, and the transition from SO(3) to SO(2) broken symmetry phases is continuous with an emergent SO(5) CFT at the critical point. This SO(5) CFT could be a candidate theory for DQCP. Again in light of our data, this scenario seems unlikely since at large values of U_0 our data supports an ordered phase.

In Fig. 34(c) we assume that the observed ordered phase gives way to a critical phase corresponding to an SO(5) CFT. Adding the α axis implies that along the SO(5) line we have a multi-critical point as well as a critical one. Note that this two fixed point scenario has been suggested by a ϵ expansion of an effective theory at the boundary of an $3+1$ D SPT state [83]. Our data actually favors this scenario: below $U_0 = U_0^c \simeq 3$ the correlation ratio does not seem to scale to zero, and is hence consistent with a critical phase. If such is the case, the nature of the transition between SO(3) and SO(2) broken symmetry states, with emergent SO(5) symmetry, depends upon the value of U_0 and is either continuous or first order. There are a number of models that show a transition from SO(2) (VBS/SSC) to SO(3) (AFM/QSH) broken symmetry phases and that favor continuous or weakly first order quantum phase transitions. For instance, 3D loop models [50] ($\eta_{\rm Neel} = 0.259(6)$, $\eta_{\rm VBS} = 0.25(3)$), the J-Q model, [17, 42] as well as transitions between quantum spin Hall insulators and s-wave superconductors, ($\eta_{\rm QSH} = 0.21(5)$, $\eta_{\rm SSC} = 0.22(6)$) [84] all seem to show similar exponents and are believed to belong to the class of DQCP with emergent spinons coupled to a non-compact U(1) gauge field. Compelling evidence of emergent SO(5) symmetry has been put forward for the loop model [27]. However, the value of the anomalous dimension lies at odds with conformal bootstrap bounds, $\eta > 0.52$ [51], for emergent SO(5) symmetry. Systematic drift in the exponents has been observed in [50]. Within the present context one can understand the above in terms fix-point collision put forward in [54, 85, 86, 87]. Consider a third axis – the dimension – and assume that the sketch of Fig. 34(c) is realized *close* to the physical dimension $d = 2$ but that before approaching $d = 2$ the multi-critical and critical points collide and develop a complex component. In this case we are back to the spin-flop transition of Fig. 34(a) but with the important insight that the RG flow becomes arbitrarily slow due to proximity of a fix-point collision. The shaded region in Fig. 34(a) schematically depicts the region where the RG flow becomes very slow.

Proximity to a critical point motivates fitting the QMC data to the form: $m = m_0 + aN_\phi^{-\frac{\eta+z}{4}}$. In the region where our correlation length exceeds the size of our system we obtain a good fit with robust anomalous dimension $\eta = 0.28(2)$ under the assumption of $z = 1$ (see the SM). The agreement with the aforementioned QMC results is remarkable. We note that this exponent is much larger than the one of the $3D$ classical O(5) critical point, with $\eta = 0.036(6)$ [88]. We conclude this section by noting that Ref. [32] introduces a fermion model showing a DQCP with emergent SO(5) symmetry and that has exponents that comply with the bootstrap bounds. This model could be a realization of the SO(5) CFT conjectured in Fig. 34(c).

Fig. 34(d) describes the possibility of an order-disorder transition along the SO(5) line. Note however that on the accessible system sizes, we cannot resolve the length scale associated with the disordered state. This scenario excludes a DQCP with emergent SO(5) symmetry, and the transition from the disordered to ordered phases involve SO(3) or SO(2) critical points. As shown in Fig. 37 the insulating phase has vanishing charge susceptibility.

The existence and nature of an SO(5) symmetric disordered phase is intriguing. Starting from Dirac fermions any band insulating state necessarily involves SO(5) symmetry breaking. Hence in the conjectured phase diagram of Fig. 34(d) the disordered phase is not adiabatically connected to a band insulator. In fact, if the disordered phase preserves the particle-hole symmetry, the arguments of Ref. [54] rule out *any* gaped phase (even a topological one), because the particle-hole symmetry forbids the SO(5) Hall-conductance argued to be necessary in any such insulator.

5.5 Conclusions

Our data on systems up to $N_\Phi = 100$ show that the O(5) non-linear sigma model exhibits an ordered phase in the limit of large stiffness. Remarkably (and within the accessible parameter range where negative sign free AFQMC simulations can be carried out), we observe another regime characterized by a correlation length that exceeds our system size. Given the aforementioned body of work on DQC and insights from the conformal bootstrap approach, our results find a natural interpretation by assuming that the model lies close to a fix-point with small complex component [54, 85, 86] such that the RG flow becomes very slow and shows pseudo-critical behavior. Clearly larger system sizes are desirable so as to confirm this point of view. Although very appealing, as implemented the Landau level projection approach comes with a computational effort that scales as $N_\phi^5\beta$ as opposed to $N_\phi^3\beta$ for the generic Hubbard model. Further improvements to the code will have to be implemented so as to reach bigger flux values. The method can also be applied to the O(4) model with θ-term at $\theta = \pi$ by setting one mass term to zero. This will have impact on our understanding of easy plane de-confined quantum critical points with emergent O(4) symmetry.

6 Conclusion and Outlook

We would like to briefly summarize what we have done in this thesis. We investigated several models with exotic quantum critical points, which are in principle beyond the Landau-Ginzburg paradigm. An extremely attractive topic in condensed matter physics is the interplay between correlation effects and topology. As an example, the field theories that we consider in the thesis require the topological contribution of field configurations to the statistical weight. We successfully formulated the exotic field theories on the basis of interacting fermions and performed large scale calculations based on sign-problem-free auxiliary field quantum Monte Carlo method. It is amazing to see that through numerical simulations, even a student with poor knowledge of field theories could find something unusual in the eyes of an theoretician.

We found a dynamically generated quantum spin hall insulator (QSH) as described in Chapter. 3. Remarkably, that phase gives way to a Dirac Semi-metal (DSM) phase via a Gross-Neveu transition and to an s-wave superconductor (SSC) via a deconfined quantum critical point (DQCP). The direct and continuous nature of QSH-SSC transition relies on the fact that the skyrmion configurations of the QSH order parameter carries twice the electron charge, and vortex defects of the SSC order parameter carry spinons. This DQCP display significant difference compare to the one between an anti-ferromagnetic state and a valence-bond solid phase: since the broken U(1) charge conservation is an exact symmetry of our lattice Hamiltonian, our phase transition does not allow any quadruple monopole configurations which are irrelevant only at the critical point along AFM-VBS transition. Therefore, only one divergent length scale exists in our case.

SSC generation can be triggered not only by tuning the interaction but also by doping. We describe the doping induced QSH-SSC transition in Chapter. 4. This is the first time of a sign-problem-free simulation of a doping induced insulator-superconductor phase transition. It has a very different critical point compared to DQCP, in the sense that the chemical potential plays the role of skyrmion fugacity. Remarkably, it is reminiscent of the twisted bilayer graphene system around magnetic angle: an understanding of the superconducting state beyond BCS theory could be built on the charged skyrmions of dynamically generated topological insulator.

In Chapter. 5 we investigated the $2+1$D nonlinear sigma model based on a Hamiltonian of enlarged global symmetry where the UV regulator is given by the Landau level instead of the lattice. The low energy effective field theory of the sigma model supported by topological WZW term is given. This is the first time that a continuous field theory is directly simulated using a quantum Monte Carlo method. The $O(5)$ symmetry between order parameters, which is possible to be an emergent symmetry of the DQCP in the low energy limit, is not broken by our Hamiltonian. We found numerically a stable critical phase in the 'weak coupling' case.

Our examples of DQCP based on QSH-SSC transition at half filling and the sigma model in Dirac landau levels are strongly connected to the notion of quantum anomaly. Surprisingly, it seems to be related to the statistics of particles: although we are using fermionic models to capture bosonic field theory, the fact that we have gaped fermionic degrees of freedom is important (or necessary) for our monopole-free realization of the deconfined quantum critical point. On the other hand, the bosonic approach of DQCP necessarily involves a Z_4 dangerously irrelevant symmetry breaking field from lattice regularization. Thus the fermionic approach has an essential meaning. Although fermion statistics leads to a βL^{3d} scaling in our auxiliary field approach, it is also

necessary, in the sense that simulations based on bosonic statistics can not capture the correct physics.

7 Appendix

7.1 Charged skyrimion of QSH

We show the details of deriving the charge response of QSH skyrimion configuration here. It follows from an explicit integration of fermionic degrees of freedom from an action of Dirac fermions coupled to bosonic order parameters, as shown in Ref. [37].

We start from the case of an action based on the effective low energy theory on Graphene in the Nambu basis, such that the 16 component of Dirac fermions are written in the basis of Valley, sublattice, real spin, and Bogoliubov-de Gennes (BdG) index:

$$S = \begin{pmatrix} \psi^\dagger & \psi \end{pmatrix} \begin{pmatrix} A & B \\ B^\dagger & -A^T \end{pmatrix} \begin{pmatrix} \psi \\ \psi^\dagger \end{pmatrix} \tag{189}$$

We take the Nambu notation of $\Psi(\boldsymbol{x},\tau) \equiv \begin{pmatrix} \psi(\boldsymbol{x},\tau) & \psi^\dagger(\boldsymbol{x},\tau) \end{pmatrix}$, such that the Hilbert space read: $\mathbb{R}^2 \otimes \mathbb{C}^2_{valley} \otimes \mathbb{C}^2_{orbital} \otimes \mathbb{C}^2_{spin} \otimes \mathbb{C}^2_{BdG}$.

If one only needs to show the charge response from skyrmion configuration of QSH order parameter, only 8 dimensional Hilbert space (without BdG index) is enough. We will discuss the reason latter. Now the action reads:

$$S = S_0 + S_Y \tag{190}$$

where the S_0 denotes the part of free Dirac action:

$$\begin{aligned} S_0 = \int d\tau \int d^2\boldsymbol{x} \Psi^\dagger(\boldsymbol{x},\tau)[(\frac{\partial}{\partial\tau} + ieA_0\tau_z) \\ +(\gamma_0\gamma_1 \otimes \tau_0(\frac{\partial}{\partial x_1} + ieA_1\tau_z) + \gamma_0\gamma_2 \otimes \tau_z(\frac{\partial}{\partial x_2} + ieA_2\tau_z))]\Psi(\boldsymbol{x},\tau) \end{aligned} \tag{191}$$

and S_Y denotes the coupling between bosonic order parameter and fermionic degrees of freedom:

$$S_Y = \int d\tau \int d^2\boldsymbol{x} m \sum_{I=1}^{3} N^I(\boldsymbol{x},\tau) \cdot \Psi^\dagger(\boldsymbol{x},\tau) M^I \Psi(\boldsymbol{x},\tau) \tag{192}$$

We take the example of three QSH masses:

$$\begin{aligned} M^1 \equiv M^x_{QSH} = i\gamma_0\gamma_3\gamma_5 \otimes \sigma_x \otimes \tau_z \quad M^2 \equiv M^y_{QSH} = i\gamma_0\gamma_3\gamma_5 \otimes \sigma_y \otimes \tau_0 \\ M^3 \equiv M^z_{QSH} = i\gamma_0\gamma_3\gamma_5 \otimes \sigma_z \otimes \tau_z \end{aligned} \tag{193}$$

Here $A_\mu(\boldsymbol{x},\tau)$ is the 'Charge' gauge field in the sense that above action is invariant under flavor independent U(1) charge transformation locally:

$$\Psi(\boldsymbol{x},\tau) \to e^{ie\theta(\boldsymbol{x},\tau)\mathbb{1}_4 \otimes \sigma_0 \otimes \tau_z} \Psi(\boldsymbol{x},\tau), \qquad A_\mu(\boldsymbol{x},\tau) \to A_\mu(\boldsymbol{x},\tau) - \partial_\mu\theta(\boldsymbol{x},\tau) \tag{194}$$

where left part of above transformation is simply $\psi(\boldsymbol{x},\tau) \to e^{ie\theta(\boldsymbol{x},\tau)}\psi(\boldsymbol{x},\tau)$.

Note that the Dirac Gamma matrices are defined as:

$$\gamma_0 = \mu_0 \otimes \tau_z, \quad \gamma_1 = \mu_z \otimes \tau_y, \quad \gamma_2 = \mu_0 \otimes \tau_x, \quad \gamma_3 = \mu_x \otimes \tau_y, \quad \gamma_5 = \mu_y \otimes \tau_y \tag{195}$$

where $\boldsymbol{\mu}$ and $\boldsymbol{\tau}$ are the Pauli matrices in the space of Valley and sublattice. For simplification in later calculation we define:

$$\Gamma_0 \equiv \mathbb{1}_{16} \quad \Gamma_1 \equiv \gamma_0\gamma_1 \otimes \sigma_0 \otimes \tau_0 \quad \Gamma_2 \equiv \gamma_0\gamma_2 \otimes \sigma_0 \otimes \tau_z \tag{196}$$

We set unit of $e = 1$ and $t = 1$, and perform Fourier transformation into the Momentum and Frequency space:

$$\begin{aligned} S = & \frac{1}{V_b}\sum_{\omega}\sum_{\boldsymbol{k}}[\Psi^\dagger(\boldsymbol{k},\omega)(i\omega + i\Gamma_1 k^x + \Gamma_2 k^y)\Psi(\boldsymbol{k},\omega) \\ & + \frac{m}{V_b}\sum_{\omega_b}\sum_{\boldsymbol{q}}\vec{N}(\boldsymbol{q},\omega_b)\cdot\Psi^\dagger(\boldsymbol{k}+\boldsymbol{q},\omega_b+\omega)\vec{M}\Psi(\boldsymbol{k},\omega) \\ & + \frac{i}{V_b}\sum_{\omega_b}\sum_{\boldsymbol{q}}A_\mu(\boldsymbol{q},\omega_b)\Psi^\dagger(\boldsymbol{k}+\boldsymbol{q},\omega_b+\omega)\Gamma_\mu\tau_z\Psi(\boldsymbol{k},\omega)] \end{aligned} \tag{197}$$

where $V_b \equiv \beta L_x L_y$. Thus the partition function reads:

$$\begin{aligned} Z &= \int\prod_{\boldsymbol{k},\omega} D(\Psi^\dagger(\boldsymbol{k},\omega),\Psi(\boldsymbol{k},\omega))e^{-S} \\ &= \int\prod_{\underline{k}} D(\Psi^\dagger(\underline{k}),\Psi(\underline{k}))e^{-\sum_{\underline{k_1}}\sum_{\underline{k_2}}\Psi^\dagger(\underline{k_1})(h_0+h_1)_{\underline{k_1},\underline{k_2}}\Psi(\underline{k_2})} \end{aligned} \tag{198}$$

where $\underline{k} \equiv (\boldsymbol{k},\omega)$. We ignore the fluctuation of third component: $N^3(\boldsymbol{x},\tau) = N^3$ and $N^1(N^2) << N_3$. h_0 and h_1 are written as:

$$\begin{aligned} (h_0)_{\underline{k_1},\underline{k_2}} &= [(i\omega_1 + i(\Gamma_1 k_1^x + \Gamma_2 k_1^y))\delta_{\underline{k_1},\underline{k_2}} + mN^3M^3\delta_{\underline{k_1},\underline{k_2}}]\frac{1}{V_b} \\ (h_1)_{\underline{k_1},\underline{k_2}} &= [m\sum_{I=1}^{2}N^I(\boldsymbol{k_1}-\boldsymbol{k_2},\omega_1-\omega_2)M^I + iA^\mu(\boldsymbol{k_1}-\boldsymbol{k_2},\omega_1-\omega_2)\Gamma_\mu\tau_z]\frac{1}{V_b^2} \\ (h_0)^{-1}_{\underline{k_1},\underline{k_2}} &= [\frac{i\omega_1 - i(\Gamma_1 k_1^x + \Gamma_2 k_1^y) - mN^3M^3}{-\omega_1^2 - |\boldsymbol{k_1}|^2 - m^2(N^3)^2}\delta_{\underline{k_1},\underline{k_2}}]V_b \end{aligned} \tag{199}$$

Recall the generalized Grassmann integration:

$$\begin{aligned} & \int d\psi^\dagger d\psi \exp\begin{pmatrix}\psi^\dagger & \psi\end{pmatrix}(M)_{2N\times 2N}\begin{pmatrix}\psi \\ \psi^\dagger\end{pmatrix} \\ =& 2^N\sqrt{\det M} \end{aligned} \tag{200}$$

which holds only when matrix M is written in the formalism of Eq.189. Now we need to perform the expansion to third order:

$$\begin{aligned} S_{eff} &\approx -\ln\sqrt{\det(h_0+h_1)} \\ &= -\frac{1}{2}\operatorname{Tr}\ln(h_0+h_1) \\ &= -\frac{1}{2}\operatorname{Tr}(h_0^{-1}h_1 - \frac{1}{2}h_0^{-1}h_1h_0^{-1}h_1 + \frac{1}{3}h_0^{-1}h_1h_0^{-1}h_1h_0^{-1}h_1 - ...) - \frac{1}{2}\operatorname{Tr}h_0 \end{aligned} \tag{201}$$

Note that above expansion only holds for a gaped system, in the sense that matrix h_0 is has no zero eigenvalue. One can easily check that the first order term above is traceless. The contribution from the second order term will be introduced latter. The

topological term that we are interested in is from the third order expansion:

$$
\begin{aligned}
&-\frac{1}{6}\,\mathrm{Tr}\,[h_0^{-1}h_1h_0^{-1}h_1h_0^{-1}h_1]\\
=&-\frac{1}{6V_b^3}\sum_{\underline{k_1}}\sum_{\underline{k_2}}\sum_{\underline{k_3}}\sum_{\underline{k_4}}\sum_{\underline{k_5}}\sum_{\underline{k_6}}G_+(\underline{k_1})G_-(\underline{k_1})G_+(\underline{k_3})G_-(\underline{k_3})G_+(\underline{k_5})G_-(\underline{k_5})\\
&\mathrm{Tr}^{16}(i\underline{k_1^\alpha}\Gamma_\alpha-mN^3M^3)\delta_{\underline{k_1},\underline{k_2}}[m\sum_{I=1}^{2}N^I(\underline{k_2}-\underline{k_3})M^I+iA^\beta(\underline{k_2}-\underline{k_3})\Gamma_\beta\tau_z]\\
&(i\underline{k_3^\delta}\Gamma_\delta-mN^3M^3)\delta_{\underline{k_3},\underline{k_4}}[m\sum_{J=1}^{2}N^J(\underline{k_4}-\underline{k_5})M^J+iA^\epsilon(\underline{k_4}-\underline{k_5})\Gamma_\epsilon\tau_z]\\
&(i\underline{k_5^\eta}\Gamma_\eta-mN^3M^3)\delta_{\underline{k_5},\underline{k_6}}[m\sum_{I=K}^{2}N^K(\underline{k_6}-\underline{k_1})M^K+iA^\kappa(\underline{k_6}-\underline{k_1})\Gamma_\kappa\tau_z]\\
=&-\frac{1}{6V_b^3}\sum_{\underline{k_1}}\sum_{\underline{k_3}}\sum_{\underline{k_5}}\frac{-1}{\omega_1^2+|\boldsymbol{k_1}|^2+m^2(N^3)^2}\frac{-1}{\omega_3^2+|\boldsymbol{k_3}|^2+m^2(N^3)^2}\frac{-1}{\omega_5^2+|\boldsymbol{k_5}|^2+m^2(N^3)^2}\\
&(m^3\epsilon_{\alpha\delta\kappa}\epsilon_{IJ3}iA^\kappa(-\underline{k_1}+\underline{k_5})(\underline{k_1^\alpha}-\underline{k_3^\alpha})(\underline{k_3^\alpha}-\underline{k_5^\alpha})N^I(\underline{k_1}-\underline{k_3})N^J(\underline{k_3}-\underline{k_5})N^3\mathrm{Tr}^{16}(\mathbb{1}_{16})\\
&+m^3\epsilon_{\delta\eta\beta}\epsilon_{JK3}iA^\beta(-\underline{k_3}+\underline{k_1})(\underline{k_3^\delta}-\underline{k_5^\alpha})(\underline{k_5^\delta}-\underline{k_1^\alpha})N^J(\underline{k_3}-\underline{k_5})N^K(\underline{k_5}-\underline{k_1})N^3\mathrm{Tr}^{16}(\mathbb{1}_{16})\\
&+m^3\epsilon_{\alpha\eta\epsilon}\epsilon_{IK3}iA^\epsilon(-\underline{k_5}+\underline{k_3})(\underline{k_1^\alpha}-\underline{k_3^\alpha})(\underline{k_5^\delta}-\underline{k_1^\alpha})N^I(\underline{k_1}-\underline{k_3})N^K(\underline{k_5}-\underline{k_1})N^3\mathrm{Tr}^{16}(\mathbb{1}_{16}))
\end{aligned}
\tag{202}
$$

We wrote the fermion Green's function as $G_\pm(\underline{k})\equiv\frac{1}{i\omega\pm E_{\boldsymbol{k}}}$, where $E_{\boldsymbol{k}}=\sqrt{|\boldsymbol{k}|^2+(mN^3)^2}$. Note the difference between Tr and Tr^{16} (trace over only 16 flavor index) above. In in the expansion of last step, the only traceless terms are those products over three N field as well as single A field, since:

$$
\begin{aligned}
&\Gamma_1\Gamma_2M^1M^2M^3=-\mathbb{1}_8\otimes\tau_z\\
&\{M^I,M^J\}=0\quad I\neq J\\
&\{\Gamma_1,M^I\}=0,\quad\{\Gamma_2,M^I\}=0,\quad[\Gamma_0,M^I]=0
\end{aligned}
\tag{203}
$$

Allowing long wave length expansion of $\underline{k_1}\sim\underline{k_3}\sim\underline{k_5}$, with a simplified notation as $\underline{k_{13}}\equiv\underline{k_1}-\underline{k_3}$ ..., we get :

$$
\begin{aligned}
&-\frac{16}{6V_b^3}\sum_{\underline{k_1}}\sum_{\underline{k_3}}\sum_{\underline{k_5}}G_+(\underline{k_1})G_-(\underline{k_1})G_+(\underline{k_3})G_-(\underline{k_3})G_+(\underline{k_5})G_-(\underline{k_5})\\
&(i\epsilon_{\alpha\delta\kappa}\epsilon_{IJ3}A^\kappa(-\underline{k_{15}})\underline{k_{13}^\alpha}\ \underline{k_{35}^\delta}N^I(\underline{k_{13}})N^J(\underline{k_{35}})N^3\\
&+i\epsilon_{\delta\eta\beta}\epsilon_{JK3}A^\beta(-\underline{k_{31}})\underline{k_{35}^\delta}\ \underline{k_{51}^\eta}N^J(\underline{k_{35}})N^K(\underline{k_{51}})N^3\\
&+i\epsilon_{\alpha\eta\epsilon}\epsilon_{IK3}A^\epsilon(-\underline{k_{53}})\underline{k_{13}^\alpha}\ \underline{k_{51}^\eta}N^I(\underline{k_{13}})N^K(\underline{k_{51}})N^3)\\
\approx&\frac{16}{6V_b^3}\sum_{\underline{k}}\sum_{\underline{p}}\sum_{\underline{q}}(G_+(\underline{k})G_-(\underline{k}))^3 3i\epsilon_{\alpha\delta\kappa}\epsilon_{IJ3}A^\kappa(-\underline{p}-\underline{q})\underline{p^\alpha}N^I(\underline{p})\underline{q^\delta}N^J(\underline{q})N^3\\
=&8i\int d\underline{x}(\frac{1}{(2\pi)^3}\int d\underline{k}(G_+(\underline{k})G_-(\underline{k}))^3)\epsilon_{\alpha\delta\kappa}\epsilon_{IJ3}A^\kappa(\underline{x})(\frac{\partial}{\partial x_\alpha}N^I(\underline{x}))(\frac{\partial}{\partial x_\delta}N^J(\underline{x}))N^3
\end{aligned}
\tag{204}
$$

The $\frac{1}{V_b}\sum_{\boldsymbol{k}}$ is substituted by $\frac{1}{(2\pi)^3}\int d\boldsymbol{k}$ above. Note that we took the limit of $\boldsymbol{q}\to\boldsymbol{0}$

and $\boldsymbol{p} \to \mathbf{0}$, but we have to integrate over $\boldsymbol{k}$:

$$\begin{aligned} &\frac{1}{(2\pi)^3}\int_{|\underline{k}|=0}^{\infty} d\underline{k}\frac{8m^3}{[G_+(\underline{k})G_-(\underline{k})]^3} \\ &\frac{1}{(2\pi)^3}\int_{|\underline{k}|=0}^{\infty} d\underline{k}\frac{8m^3}{[\omega_1^2+|\boldsymbol{k}|^2+m^2(N^3)^2]^3} \\ =&\frac{1}{4\pi}\frac{1}{(N^3)^3} \end{aligned} \tag{205}$$

It is interesting to know that above integration is m independent . Re-defining the normalized spin current field $\vec{n} \equiv \frac{\vec{N}}{N_3}$, Eq. 204 becomes:

$$\begin{aligned} &\frac{1}{4\pi}\int d^2\boldsymbol{x}\int d\tau\epsilon_{\alpha\delta\kappa}\epsilon_{IJ3}iA^{\kappa}(\underline{x})(\frac{\partial}{\partial x_\alpha}n^I(\underline{x}))(\frac{\partial}{\partial x_\delta}n^J(\underline{x}))n^3 \\ =&i\frac{1}{4\pi}\epsilon_{\alpha\delta\kappa}\int d^2\boldsymbol{x}\int d\tau A^{\kappa}(\underline{x})n^3\boldsymbol{e_z}\cdot(\partial_\alpha\vec{n}\times\partial_\delta\vec{n}) \end{aligned} \tag{206}$$

In general the O(3) basis does not need to be pinned, thus the above formula becomes:

$$S_c = i\frac{1}{4\pi}\epsilon_{\alpha\delta\kappa}\int d^2\boldsymbol{x}\int d\tau A^{\kappa}(\underline{x})\vec{n}\cdot(\partial_\alpha\vec{n}\times\partial_\delta\vec{n}) \tag{207}$$

knowing the charge current coupled to the gauge field is defined as:

$$J^\mu = -i\frac{\delta S_c}{\delta A^\mu} \tag{208}$$

Combining this with Eq. 207, we get the charge response:

$$J^\mu(\boldsymbol{x},\tau) = 2\frac{1}{8\pi}\epsilon_{\alpha\delta\mu}\vec{n}\cdot(\partial_\alpha\vec{n}\times\partial_\delta\vec{n}) \tag{209}$$

where the electron charge density that we are interested in is simply the zeroth component :

$$\begin{aligned} J^0(\boldsymbol{x},\tau) &\equiv \frac{1}{2}\langle\Psi^\dagger(\boldsymbol{x},\tau)\tau_z\Psi(\boldsymbol{x},\tau)\rangle \\ &= \frac{1}{Z}\int D(\psi^\dagger,\psi)e^{-S(A^\mu=0)}(\psi^\dagger(\boldsymbol{x},\tau)\psi(\boldsymbol{x},\tau)) \end{aligned} \tag{210}$$

Note that Eq. 209 does not include the integration over space-time. It's a local response between the charge current and the curvature of $O(3)$ QSH order parameter.

The zero component of current is basically the electron charge density. Integrating over the 2D space on a certain time slice we get the relation between the response charge and skyrimion number:

$$\begin{aligned} &N_e \equiv \int d^2\boldsymbol{x}J^0(\boldsymbol{x},\tau) = 2Q \\ &Q \equiv \frac{1}{8\pi}\epsilon_{\alpha\delta 0}\int d^2\boldsymbol{x}\vec{n}\cdot(\partial_\alpha\vec{n}\times\partial_\delta\vec{n}) \end{aligned} \tag{211}$$

where Q is the Potragain index in terms of QSH order parameter in any imaginary time slice. Above formula only includes the $2d$ integration over space.

Apart from skyrimions, another kind of topological defect called 'meron' vortices is also interesting, especially for a many body Hamiltonian which does not respect the $SU(2)$ spin rotational symmetry. An example of a 'meron' configuration is:

$$\begin{aligned} (n_1,n_2,n_3) =&(x/|r|,y/|r|,0) \qquad |r| \longrightarrow \infty \\ &(0,0,1) \qquad\qquad\quad |r| = 0 \end{aligned} \tag{212}$$

with a smooth extrapolation of three component vectors from $|r| = 0$ to $|r| \longrightarrow \infty$. Hence from the view of topology, this configuration simply introduces a half integer of Potragain index :

$$\begin{aligned} Q &\equiv \frac{1}{8\pi}\epsilon_{\alpha\delta 0}\int d^2\boldsymbol{x}\vec{n}\cdot(\partial_\alpha\vec{n}\times\partial_\delta\vec{n}) = \frac{1}{2} \\ N_e &= 2Q = 1 \end{aligned} \tag{213}$$

which carries integer values of electron charge. Above identity follows from the fact that Eq. 209 holds locally.

Odd number of vortices make the far away $|r| \longrightarrow \infty$ limit ill defined. To have a well defined field theory, with a uniform order parameter polarization in the $|r| \longrightarrow \infty$ limit, one needs even numbers of vortices (anti-vortices) in the system. On the other hand, the Kramers degeneracy due to the time reversal symmetry hold for any vector order parameter configurations, thus the charge response due to the topological defects will be quantized to only even numbers when the boundary is well defined.

On the other hand, we don't discuss the energy scales of skyrmions or meron vortices : whether they are low energy excitations or not. They may depends on the details of the many body Hamiltonian.

The key point of long wave length approximation in Eq.204 requires:

$$|\underline{k_1} - \underline{k_3}| << m \tag{214}$$

On a lattice we need:

$$L >> \frac{1}{m} \tag{215}$$

In this sense, we need fat Skyrimions which has sizes much larger than inverse stiffness.

Note that we didn't write down details of the second order expansion in Eq.201. It corresponds to the relation between the stiffness of sigma model with the mass of Dirac fermions. Following the well known calculation of Abanov and Wiegmann [45], it gives the term of

$$S_N = \int d^2\boldsymbol{x}d\tau\frac{1}{g}(\partial_\mu\vec{n})^2 \tag{216}$$

where $1/g \approx m$.

We notice that in Eq. 191, 192 there are no off diagonal elements in the matrices of Nambu basis. Thus why we made things complicated rather than keeping the 8×8 matrices ? The reason is to direct generalize above calculation to response function of other order parameters.

Recall the five matrices including three QSH masses and two SSC masses:

$$\begin{aligned} &M^1 \equiv M^x_{QSH} = i\gamma_0\gamma_3\gamma_5\otimes\sigma_x\otimes\tau_z \quad M^2 \equiv M^y_{QSH} = i\gamma_0\gamma_3\gamma_5\otimes\sigma_y\otimes\tau_0 \\ &M^3 \equiv M^z_{QSH} = i\gamma_0\gamma_3\gamma_5\otimes\sigma_z\otimes\tau_z \quad M^4 \equiv M^x_{SSC} = i\gamma_0\gamma_2\gamma_3\otimes\sigma_y\otimes\tau_x \\ &M^5 \equiv M^y_{SSC} = i\gamma_0\gamma_2\gamma_3\otimes\sigma_y\otimes\tau_y \end{aligned} \tag{217}$$

The 5 matrices follows the rule that each two of them anticommute with each other:

$$\begin{aligned} &\{\Gamma^I, M^J\} = 0 \qquad (I = 1,2) \\ &\{M^I, M^J\} = 0 \qquad (I \neq J) \\ &\Gamma^1\Gamma^2M^1M^2M^3M^4M^5 = -i\mathbb{1}_{16} \\ &Tr^{16}(\Gamma^1\Gamma^2M^IM^JM^KM^LM^N) = -16i\epsilon_{IJKLN} \qquad I = 1,2,3,4,5 \end{aligned} \tag{218}$$

One can take any three masses out of the five. Take M^z_{QSH}, M^x_{SSC} and M^y_{SSC} as an example, Eq. 191, 192 becomes:

$$\begin{aligned} S_0 =& \int d\tau \int d^2\boldsymbol{x}\Psi^\dagger(\boldsymbol{x},\tau)[(\frac{\partial}{\partial\tau}+ieA_0X) \\ &+(\gamma_0\gamma_1\otimes\tau_0(\frac{\partial}{\partial x_1}+ieA_1X)+\gamma_0\gamma_2\otimes\tau_z(\frac{\partial}{\partial x_2}+ieA_2X))]\Psi(\boldsymbol{x},\tau) \\ S_Y =& \int d\tau\int d^2\boldsymbol{x}m\sum_{I=3}^{5}N^I(\boldsymbol{x},\tau)\cdot\Psi^\dagger(\boldsymbol{x},\tau)M^I\Psi(\boldsymbol{x},\tau) \end{aligned} \tag{219}$$

Here the U(1) gauge field A_μ is not the previous 'charge' gauge field, since the 16×16 matrix X now is defined as :

$$X\equiv\frac{i}{2}[M^1,M^2]=\mathbb{1}_4\otimes\sigma_z\otimes\tau_z \tag{220}$$

In current case the local $U(1)$ charge transformation is redefined:

$$\Psi(\boldsymbol{x},\tau)\to e^{ie\theta(\boldsymbol{x},\tau)\mathbb{1}_4\otimes\sigma_z\otimes\tau_z}\Psi(\boldsymbol{x},\tau),\qquad A_\mu(\boldsymbol{x},\tau)\to A_\mu(\boldsymbol{x},\tau)-\partial_\mu\theta(\boldsymbol{x},\tau) \tag{221}$$

This new transformation contains also no off-diagonal elements in Nambu basis. Combine Eq.220 with Eq.218 one get:

$$Tr^{16}(\Gamma^1\Gamma^2M^IM^JM^KX)=-16\epsilon_{IJK}\qquad I=3,4,5 \tag{222}$$

Follow the same role of integration, one notice that above formula has the same algebra of Eq. 203. Thus one get the general version of Eq. 209:

$$J^0_{\sigma^z}(\boldsymbol{x},\tau)=\frac{1}{4\pi}\epsilon_{\alpha\delta0}\int d^2\boldsymbol{x}\vec{n}\cdot(\partial_\alpha\vec{n}\times\partial_\delta\vec{n}) \tag{223}$$

and Eq.211:

$$\begin{aligned} N_{\sigma^z}\equiv&\int d^2\boldsymbol{x}J^0_{\sigma^z}(\boldsymbol{x},\tau)=2Q \\ Q\equiv&\frac{1}{8\pi}\epsilon_{\alpha\delta0}\int d^2\boldsymbol{x}\vec{n}\cdot(\partial_\alpha\vec{n}\times\partial_\delta\vec{n}) \end{aligned} \tag{224}$$

where $\vec{n}\equiv(\frac{N_3,N_4,N_5}{\sqrt{N_3^2+N_4^2+N_5^2}})$, and $J^0_{\sigma^z}$ is not the electron charge density but:

$$\begin{aligned} J^0_{\sigma^z}(\boldsymbol{x},\tau)\equiv&\frac{1}{2}\langle\Psi^\dagger(\boldsymbol{x},\tau)X\Psi(\boldsymbol{x},\tau)\rangle \\ =&\frac{1}{Z}\int D(\psi^\dagger,\psi)e^{-S(A_\mu=0)}(\psi^\dagger(\boldsymbol{x},\tau)\sigma_z\psi(\boldsymbol{x},\tau)) \end{aligned} \tag{225}$$

Now we turn to the argument of a S-wave superconducting vortices. It is same as the QSH meron of Eq.212 up to a unitary transformation in the 5 component order parameter space:

$$\begin{aligned} (n_1,n_2,n_3,n_4,n_5)=&(0,0,0,x/|r|,y/|r|) \qquad |r|\longrightarrow\infty \\ &(0,0,n_3,0,0) \qquad\qquad\qquad\quad |r|=0 \end{aligned} \tag{226}$$

in the constraint of $n_1=n_2=0$ ($\sqrt{n_3^2+n_4^2+n_5^2}=1$). As long as we require the O(3) vector to be continuously distributed, above configuration gives the contribution of half a Pontryagin index in the space of n_3,n_4,n_5.

$$Q=\frac{1}{8\pi}\epsilon_{\alpha\delta\mu}\int d^2\boldsymbol{x}\vec{n}\cdot(\partial_\alpha\vec{n}\times\partial_\delta\vec{n})=\frac{1}{2} \tag{227}$$

Hence

$$N_{\sigma^z} \equiv \int d^2\boldsymbol{x} J^0_{\sigma^z}(\boldsymbol{x},\tau) = 1 \tag{228}$$

One is allowed to perform a O(3) global transformation in Eq.219 in the space of n_1, n_2, n_3. In another word the 'core' of vortex does not need to be pinned in the polarized direction of n_3:

$$\vec{N_\sigma} = \frac{(n_1, n_2, n_3)}{\sqrt{n_1^2 + n_2^2 + n_3^2}} \tag{229}$$

where

$$\vec{N_\sigma} \equiv \int d^2\boldsymbol{x} \frac{1}{Z} \int D(\psi^\dagger, \psi) e^{-S(A_\mu = 0)} (\psi^\dagger(\boldsymbol{x},\tau)\vec{\sigma}\psi(\boldsymbol{x},\tau)) \tag{230}$$

In our spin $\frac{1}{2}$ system we have $S_x = \frac{1}{2}\sigma_x$...:

$$\int d^2\boldsymbol{x} \langle \psi^\dagger(\boldsymbol{x},\tau)\vec{S}\psi(\boldsymbol{x},\tau\rangle = \frac{1}{2}\frac{(n_1, n_2, n_3)}{\sqrt{n_1^2 + n_2^2 + n_3^2}} \tag{231}$$

Hence, when spin SU(2) rotational symmetry is not explicitly broken, a free spin 1/2 'spinon' which has two fold degeneracy lies in the core of a SSC vortex.

7.2 WZW term

In this section we show the derivation of Wess-Zumino-Witten (WZW) topological term based on integrating out the fermionic degrees of freedom in a action of Dirac fermions coupled to a 5 component order parameter in $2+1$D. The calculation is a brute-force generalization of last section.

We take the action of fermion-boson coupling:

$$S = S_0 + S_Y \tag{232}$$

where

$$S_0 = \int d\tau \int d^2\boldsymbol{x} \Psi^\dagger(\boldsymbol{x},\tau)(\frac{\partial}{\partial\tau} + (\gamma_0\gamma_1 \otimes \tau_0 \frac{\partial}{\partial x_1} + \gamma_0\gamma_2 \otimes \tau_z \frac{\partial}{\partial x_2}))\Psi(\boldsymbol{x},\tau) \tag{233}$$

as well as the Yukawa coupling term

$$S_Y = \int d\tau \int d^2\boldsymbol{x} m \sum_{I=1}^{5} N^I(\boldsymbol{x},\tau) \cdot \Psi^\dagger(\boldsymbol{x},\tau) M^I \Psi(\boldsymbol{x},\tau) \tag{234}$$

We can still take the 5 dirac masses as shown in Eq. 217, as well as the same anti-commuting relation in Eq. 218:

$$\begin{aligned}
&\{\Gamma^I, M^J\} = 0 \qquad (I = 1, 2) \\
&\{M^I, M^J\} = 0 \qquad (I \neq J) \\
&\Gamma^1\Gamma^2 M^1 M^2 M^3 M^4 M^5 = -i\mathbb{1}_{16} \\
&Tr^{16}(\Gamma^1\Gamma^2 M^I M^J M^K M^L M^N) = -16i\epsilon_{IJKLN}
\end{aligned} \tag{235}$$

In momentum and frequency space above action reads:

$$\begin{aligned}
S = \frac{1}{V_b}\sum_\omega \sum_{\boldsymbol{k}} [&\Psi^\dagger(\boldsymbol{k},\omega)(i\omega + i\gamma_0\gamma_1 \otimes \tau_0 k_x + i\gamma_0\gamma_2 \otimes \tau_z k_y)\Psi(\boldsymbol{k},\omega) \\
&+ \frac{m}{V_b}\sum_{\omega_b}\sum_{\boldsymbol{q}} \vec{N}(\boldsymbol{q},\omega_b) \cdot \Psi^\dagger(\boldsymbol{k}+\boldsymbol{q}, \omega_b + \omega)\vec{M}\Psi(\boldsymbol{k},\omega)]
\end{aligned} \tag{236}$$

Thus the partition function reads:

$$\begin{aligned} Z &= \int \prod_{\boldsymbol{k},\omega} D(\Psi^\dagger(\boldsymbol{k},\omega),\Psi(\boldsymbol{k},\omega))e^{-S} \\ &= \int \prod_{\underline{k}} D(\Psi^\dagger(\underline{k}),\Psi(\underline{k}))e^{-\sum_{\underline{k_1}}\sum_{\underline{k_2}}\Psi^\dagger(\underline{k_1})(h_0+h_1)_{\underline{k_1},\underline{k_2}}\Psi(\underline{k_2})} \end{aligned} \tag{237}$$

here we perform the expansion similar to last section: $N^5(\boldsymbol{x},\tau) = N^5$ and $N^I(I = 1,2,3,4) \ll N_5$. h_0 and h_1 are written as:

$$\begin{aligned} (h_0)_{\underline{k_1},\underline{k_2}} &= [(i\omega_1 + i(\Gamma_1 k_1^x + \Gamma_2 k_1^y))\delta_{\underline{k_1},\underline{k_2}} + mN^5M^5\delta_{\underline{k_1},\underline{k_2}}]\frac{1}{V_b} \\ (h_1)_{\underline{k_1},\underline{k_2}} &= [m\sum_{I=1}^{4} N^I(\boldsymbol{k_1}-\boldsymbol{k_2},\omega_1-\omega_2)M^I]\frac{1}{V_b^2} \\ (h_0)^{-1}_{\underline{k_1},\underline{k_2}} &= [\frac{i\omega_1 - i(\Gamma_1 k_1^x + \Gamma_2 k_1^y) - mN^5M^5}{-\omega_1^2 - |\boldsymbol{k_1}|^2 - m^2(N^5)^2}\delta_{\underline{k_1},\underline{k_2}}]V_b \end{aligned} \tag{238}$$

We take the grassmann integration of Eq. 200. Instead of the last section, now we need to perform the expansion to fourth order:

$$\begin{aligned} S_{eff} &\approx -\ln\sqrt{\det(h_0+h_1)} \\ &= -\frac{1}{2}\operatorname{Tr}\ln(h_0+h_1) \\ &= -\frac{1}{2}\operatorname{Tr}(h_0^{-1}h_1 - \frac{1}{2}h_0^{-1}h_1h_0^{-1}h_1 + \frac{1}{3}h_0^{-1}h_1h_0^{-1}h_1h_0^{-1}h_1 - \frac{1}{4}h_0^{-1}h_1h_0^{-1}h_1h_0^{-1}h_1h_0^{-1}h_1) - \frac{1}{2}\operatorname{Tr}h_0 \end{aligned} \tag{239}$$

We write the fermion Green's function as $G_\pm(\underline{k}) \equiv \frac{1}{i\omega \pm E_{\boldsymbol{k}}}$, where $E_{\boldsymbol{k}} = \sqrt{|\boldsymbol{k}|^2 + (mN^5)^2}$.

The topological term comes from the third order expansion:

$$
\begin{aligned}
&\frac{1}{8}\,\mathrm{Tr}\,[h_0^{-1}h_1h_0^{-1}h_1h_0^{-1}h_1h_0^{-1}h_1] \\
=&\frac{1}{8V_b^4}\sum_{\underline{k_1}}\sum_{\underline{k_2}}\sum_{\underline{k_3}}\sum_{\underline{k_4}}\sum_{\underline{k_5}}\sum_{\underline{k_6}}\sum_{\underline{k_7}}\sum_{\underline{k_8}} G_+(\underline{k_1})G_-(\underline{k_1})G_+(\underline{k_3})G_-(\underline{k_3})G_+(\underline{k_5})G_-(\underline{k_5})G_+(\underline{k_7})G_-(\underline{k_7}) \\
&Tr^{16}(i\underline{k_1^\alpha}\Gamma_\alpha - mN^5M^5)\delta_{\underline{k_1},\underline{k_2}}[m\sum_{I=1}^{4}N^I(\underline{k_2}-\underline{k_3})M^I] \\
&\quad(i\underline{k_3^\beta}\Gamma_\beta - mN^5M^5)\delta_{\underline{k_3},\underline{k_4}}[m\sum_{J=1}^{4}N^J(\underline{k_4}-\underline{k_5})M^J] \\
&\quad(i\underline{k_5^\gamma}\Gamma_\gamma - mN^5M^5)\delta_{\underline{k_5},\underline{k_6}}[m\sum_{K=1}^{4}N^K(\underline{k_6}-\underline{k_7})M^K] \\
&\quad(i\underline{k_7^\delta}\Gamma_\delta - mN^5M^5)\delta_{\underline{k_7},\underline{k_8}}[m\sum_{L=1}^{4}N^L(\underline{k_8}-\underline{k_1})M^L] \\
=&\frac{1}{8V_b^4}\sum_{\underline{k}}\sum_{\underline{p}}\sum_{\underline{q}}\sum_{\underline{s}} G_+(\underline{k})G_-(\underline{k})G_+(\underline{k}+\underline{p})G_-(\underline{k}+\underline{p})G_+(\underline{k}+\underline{p}+\underline{q})G_-(\underline{k}+\underline{p}+\underline{q}) \\
&G_+(\underline{k}+\underline{p}+\underline{q}+\underline{s})G_-(\underline{k}+\underline{p}+\underline{q}+\underline{s}) \\
&Tr^{16}(i\underline{k}^\alpha\Gamma_\alpha - mN^5M^5)[m\sum_{I=1}^{4}N^I(-\underline{p})M^I] \\
&\quad(i(\underline{k}^\beta+\underline{p}^\beta)\Gamma_\beta - mN^5M^5)[m\sum_{J=1}^{4}N^J(-\underline{q})M^J] \\
&\quad(i(\underline{k}^\gamma+\underline{p}^\gamma+\underline{q}^\gamma)\Gamma_\gamma - mN^5M^5)[m\sum_{K=1}^{4}N^K(-\underline{s})M^K] \\
&\quad(i(\underline{k}^\delta+\underline{p}^\delta+\underline{q}^\delta+\underline{s}^\delta)\Gamma_\delta - mN^5M^5)[m\sum_{L=1}^{4}N^L(\underline{p}+\underline{q}+\underline{s})M^L]
\end{aligned}
\tag{240}
$$

We've used Einstein notation for $\beta(\gamma,\delta)$ indices but not for $I(J,K,L)$ indices. In the approximation of long wave length limit: $|\underline{p}|\to 0$, etc, above formula reduces to:

$$
\begin{aligned}
\approx&\frac{-16i}{8V_b^4}[\sum_{\underline{k}}(G_+(\underline{k})G_-(\underline{k}))^4]\sum_{\underline{p}}\sum_{\underline{q}}\sum_{\underline{s}} i\epsilon_{\beta\gamma\delta}\epsilon_{IJKL}\underline{p^\beta}\ \underline{q^\gamma}\ \underline{s^\delta} \\
&\sum_{I,J,K,L}N^I(-\underline{p})N^J(-\underline{q})N^K(-\underline{s})N^L(\underline{p}+\underline{q}+\underline{s}) \\
=&K\int d\tau d^2\boldsymbol{x}\sum_{I,J,K,L} i\epsilon_{\beta\gamma\delta}\epsilon_{IJKL}\frac{\partial}{\partial x_\beta}N^I(\boldsymbol{x},\tau)\frac{\partial}{\partial x_\gamma}N^J(\boldsymbol{x},\tau)\frac{\partial}{\partial x_\delta}N^K(\boldsymbol{x},\tau)N^L(\boldsymbol{x},\tau)
\end{aligned}
\tag{241}
$$

where terms with single $\underline{k}$ component are odd functions and will vanish after integration. We again used the commutation role in Eq. 218. We can perform the integration:

$$
\begin{aligned}
K=&\frac{1}{(2\pi)^3}\int_{|\underline{k}|=0}^{\infty}d\underline{k}\frac{2m^5}{(\omega_1^2+|\boldsymbol{k}|^2+m^2(N^3)^2)^4} \\
=&\frac{1}{32\pi}\frac{1}{(N^3)^4}
\end{aligned}
\tag{242}
$$

take this prefactor back to Eq. 240, we get the effective action:

$$\begin{aligned} S_{eff} =& i\frac{1}{32\pi}\int d\tau d^2\boldsymbol{x} \sum_{I,J,K,L} \epsilon_{\beta\gamma\delta}\epsilon_{IJKL}\frac{\partial}{\partial x_\beta}n^I(\boldsymbol{x},\tau)\frac{\partial}{\partial x_\gamma}n^J(\boldsymbol{x},\tau)\frac{\partial}{\partial x_\delta}n^K(\boldsymbol{x},\tau)n^L(\boldsymbol{x},\tau) \\ =& i\frac{3}{16\pi}\int d\tau d^2\boldsymbol{x} \sum_{I,J,K,L} \epsilon_{IJKL}\partial_\tau n^I(\boldsymbol{x},\tau)\partial_x n^J(\boldsymbol{x},\tau)\partial_y n^K(\boldsymbol{x},\tau)n^L(\boldsymbol{x},\tau) \end{aligned} \tag{243}$$

This is the effective action where the 5 component vector fluctuates around one polarized direction. Recall the $2+1d$ WZW term:

$$\begin{aligned} S =& \frac{2\pi i}{vol(S_4)}\int d\tau d^2\boldsymbol{x}\int_0^1 du\epsilon^{abcde}n^a\partial_x n^b\partial_y n^c\partial_\tau n^d\partial_u n^e \\ =& \frac{3i}{4\pi}\int d\tau d^2\boldsymbol{x}\int_0^1 du\epsilon^{abcde}n^a\partial_x n^b\partial_y n^c\partial_\tau n^d\partial_u n^e \end{aligned} \tag{244}$$

where an extra coordinate u need to be introduced such that $n^a(\tau,\boldsymbol{x},u)$ at $u=1$ equals the physical vector $n^a(\tau,\boldsymbol{x})$, whereas at $u=0$ it extrapolates to a fixed value (say $0,0,0,0,1$).

Note that the action is independent of smooth path of extrapolation in the parameter space of u. We can take the simple example of using a straight line to link: $\boldsymbol{n}(u=1)=(n^1,n^2,n^3,n^4,1)$ and $\boldsymbol{n}(u=0)=(0,0,0,0,1)$, such that the action of Eq. 245 goes back to Eq. 243 due to a simple integration: $\int_0^1 duu^3=\frac{1}{4}$.

$$\begin{aligned} S =& \frac{2\pi i}{vol(S_4)}\int d\tau d^2\boldsymbol{x}\int_0^1 du\epsilon^{abcde}n^a\partial_x n^b\partial_y n^c\partial_\tau n^d\partial_u n^e \\ =& \frac{3i}{4\pi}\int d\tau d^2\boldsymbol{x}\int_0^1 du\epsilon^{abcde}n^a\partial_x n^b\partial_y n^c\partial_\tau n^d\partial_u n^e \end{aligned} \tag{245}$$

List of Figures

List of Tables

Acknowledgements

First of all, I would like to thank Fakher Assaad, the supervisor of my thesis. He gave me this great opportunity as doctoral student; and the extremely interesting projects that he suggested to me are treasures. Moreover, the discussions and suggestions (no matter for details or ideas) during the past years are very important to me.

The great atmosphere of this research group in Wuerzburg is also a great help to me. Especially I would like thank my colleges Toshihiro Sato, Martin Hohenadler and Francesco Parisen Toldin, who had collaboration with me on research topics and provided most of the discussions and guidance. I am also grateful to my office mates and colleges during the PhD: Johannes Hofmann, Stefan Beyl, Manuel Weber, Jonas Schwab, Marcin Raczkowski, Florian Goth, Emilie Huffman, Maksim Ulybyshev, Bimla Danu, Jefferson Stafusa, and Zihong Liu. The helps that I got cover wide range: from computer techniques to condensed matter; from physics to real life.

I would also like to thank Wenan Guo, my previous supervisor of Master thesis as well as Yuhai Liu, my previous college in Beijing Normal University. I got a lot of important helps from them during collaborations from them, even after I left from BNU. Thank my collaborators Michael P. Zaletel, Roger S. K. Mong, and Chong Wang for important ideas.

I am grateful to Toshihiro Sato, Bimla Danu, Jefferson Stafusa, Marcin Raczkowski and Francesco Parisen Toldin for proofreading of chapters in the thesis. Thank Jonas Schwab and Florian Goth for the correction of German version of abstract.

Last but not least, I would like to thank my parents for their support during my PhD period, although at most of the time we could not stay together.

References

[1] Yuhai Liu, Zhenjiu Wang, Toshihiro Sato, Martin Hohenadler, Chong Wang, Wenan Guo, and Fakher F Assaad. Superconductivity from the condensation of topological defects in a quantum spin-hall insulator. *Nature Commun.*, 10(1):2658, June 2019.

[2] Zhenjiu Wang, Yuhai Liu, Toshihiro Sato, Martin Hohenadler, Chong Wang, Wenan Guo, and Fakher F. Assaad. Doping-induced quantum spin hall insulator to superconductor transition, 2020.

[3] Zhenjiu Wang, Michael P. Zaletel, Roger S. K. Mong, and Fakher F. Assaad. Phases of the (2+1) dimensional so(5) non-linear sigma model with topological term, 2020.

[4] Steven Weinberg. *Critical Phenomena for Field Theorists*, pages 1–52. Springer US, Boston, MA, 1978.

[5] J. Bardeen, L. N. Cooper, and J. R. Schrieffer. Theory of superconductivity. *Phys. Rev.*, 108:1175–1204, Dec 1957.

[6] Subir Sachdev. *Quantum Phase Transitions*. American Cancer Society, 2007.

[7] J. Rogel-Salazar. Quantum phase transitions, 2nd edn., by s. sachdev. *Contemporary Physics*, 53(1):77–77, 2012.

[8] David J. Gross and André Neveu. Dynamical symmetry breaking in asymptotically free field theories. *Phys. Rev. D*, 10:3235–3253, Nov 1974.

[9] J M Kosterlitz and D J Thouless. Ordering, metastability and phase transitions in two-dimensional systems. *Journal of Physics C: Solid State Physics*, 6(7):1181, 1973.

[10] F. D. M. Haldane. O(3) nonlinear σ model and the topological distinction between integer- and half-integer-spin antiferromagnets in two dimensions. *Phys. Rev. Lett.*, 61(8):1029–1032, Aug 1988.

[11] Todadri Senthil, Leon Balents, Subir Sachdev, Ashvin Vishwanath, and Matthew P. A. Fisher. Deconfined criticality critically defined. *Journal of the Physical Society of Japan*, 74(Suppl):1–9, 2005.

[12] C. Mudry. *Lecture Notes on Field Theory in Condensed Matter Physics*. World Scientific Publishing Company, 2014.

[13] Z. Y. Meng, T. C. Lang, S. Wessel, F. F. Assaad, and A. Muramatsu. Quantum spin liquid emerging in two-dimensional correlated dirac fermions. *Nature*, 464(7290):847–851, 04 2010.

[14] J. D. Jackson. From lorenz to coulomb and other explicit gauge transformations, 2002.

[15] Jie Lou, Anders W. Sandvik, and Leon Balents. Emergence of u(1) symmetry in the 3d xy model with Z_q anisotropy. *Phys. Rev. Lett.*, 99:207203, Nov 2007.

[16] Zi-Xiang Li, Yi-Fan Jiang, Shao-Kai Jian, and Hong Yao. Fermion-induced quantum critical points. *Nature Communications*, 8(1), Aug 2017.

[17] Anders W. Sandvik. Evidence for deconfined quantum criticality in a two-dimensional heisenberg model with four-spin interactions. *Phys. Rev. Lett.*, 98:227202, Jun 2007.

[18] Marcin Raczkowski and Fakher F. Assaad. Phase diagram and dynamics of the SU(n) symmetric kondo lattice model. *Phys. Rev. Research*, 2:013276, Mar 2020.

[19] F.F. Assaad and H.G. Evertz. World-line and determinantal quantum monte carlo methods for spins, phonons and electrons. In H. Fehske, R. Schneider, and A. Weiße, editors, *Computational Many-Particle Physics*, volume 739 of *Lecture Notes in Physics*, pages 277–356. Springer, Berlin Heidelberg, 2008.

[20] Anders W. Sandvik. Computational studies of quantum spin systems, 2011.

[21] A. K. Geim and K. S. Novoselov. The rise of graphene, 2007.

[22] Igor F. Herbut, Vladimir Juričić, and Bitan Roy. Theory of interacting electrons on the honeycomb lattice. *Phys. Rev. B*, 79:085116, Feb 2009.

[23] C. L. Kane and E. J. Mele. Quantum spin hall effect in graphene. *Phys. Rev. Lett.*, 95(22):226801, Nov 2005.

[24] S. Raghu, Xiao-Liang Qi, C. Honerkamp, and Shou-Cheng Zhang. Topological mott insulators. *Phys. Rev. Lett.*, 100(15):156401, 2008.

[25] Ryan Thorngren, Ashvin Vishwanath, and Ruben Verresen. Intrinsically gapless topological phases, 2020.

[26] M. P. A. Fisher, P.B. Weichman, G. Grinstein, and D. S. Fisher. *Phys. Rev. B*, 40:546, 1989.

[27] Adam Nahum, P. Serna, J. T. Chalker, M. Ortuño, and A. M. Somoza. Emergent so(5) symmetry at the néel to valence-bond-solid transition. *Phys. Rev. Lett.*, 115:267203, Dec 2015.

[28] Junhyun Lee and Subir Sachdev. Wess-zumino-witten terms in graphene landau levels. *Phys. Rev. Lett.*, 114:226801, Jun 2015.

[29] Anders W. Sandvik and Juhani Kurkijärvi. Quantum monte carlo simulation method for spin systems. *Phys. Rev. B*, 43:5950–5961, Mar 1991.

[30] Lei Wang, Ye-Hua Liu, and Matthias Troyer. Stochastic series expansion simulation of the $t - v$ model. *Phys. Rev. B*, 93:155117, Apr 2016.

[31] Martin Bercx, Florian Goth, Johannes S. Hofmann, and Fakher F. Assaad. The ALF (Algorithms for Lattice Fermions) project release 1.0. Documentation for the auxiliary field quantum Monte Carlo code. *SciPost Phys.*, 3:013, 2017.

[32] Zi-Xiang Li, Shao-Kai Jian, and Hong Yao. Deconfined quantum criticality and emergent so(5) symmetry in fermionic systems. 2019.

[33] Zhenjiu Wang, Fakher F. Assaad, and Francesco Parisen Toldin. Finite-size effects in canonical and grand-canonical quantum monte carlo simulations for fermions. *Phys. Rev. E*, 96:042131, Oct 2017.

[34] K. S. Novoselov, A. K. Geim, S. V. Morozov, D. Jiang, M. I. Katsnelson, I. V. Grigorieva, S. V. Dubonos, and A. A. Firsov. Two-dimensional gas of massless dirac fermions in graphene. *Nature*, 438(7065):197–200, 11 2005.

[35] R. Blankenbecler, D. J. Scalapino, and R. L. Sugar. Monte carlo calculations of coupled boson-fermion systems. *Phys. Rev. D*, 24:2278–2286, Oct 1981.

[36] S. White, D. Scalapino, R. Sugar, E. Loh, J. Gubernatis, and R. Scalettar. Numerical study of the two-dimensional hubbard model. *Phys. Rev. B*, 40:506–516, Jul 1989.

[37] Tarun Grover and T. Senthil. Topological spin hall states, charged skyrmions, and superconductivity in two dimensions. *Phys. Rev. Lett.*, 100:156804, Apr 2008.

[38] T. Senthil, Leon Balents, Subir Sachdev, Ashvin Vishwanath, and Matthew P. A. Fisher. Quantum criticality beyond the landau-ginzburg-wilson paradigm. *Phys. Rev. B*, 70:144407, Oct 2004.

[39] T. Senthil, Ashvin Vishwanath, Leon Balents, Subir Sachdev, and Matthew P. A. Fisher. Deconfined quantum critical points. *Science*, 303(5663):1490–1494, 2004.

[40] Martin P. Gelfand, Rajiv R. P. Singh, and David A. Huse. Zero-temperature ordering in two-dimensional frustrated quantum heisenberg antiferromagnets. *Phys. Rev. B*, 40:10801–10809, Dec 1989.

[41] Munehisa Matsumoto, Chitoshi Yasuda, Synge Todo, and Hajime Takayama. Ground-state phase diagram of quantum heisenberg antiferromagnets on the anisotropic dimerized square lattice. *Phys. Rev. B*, 65:014407, Nov 2001.

[42] Hui Shao, Wenan Guo, and Anders W. Sandvik. Quantum criticality with two length scales. *Science*, 352(6282):213–216, 2016.

[43] Michael Levin and T. Senthil. Deconfined quantum criticality and néel order via dimer disorder. *Phys. Rev. B*, 70:220403, Dec 2004.

[44] M. Hohenadler, Z. Y. Meng, T. C. Lang, S. Wessel, A. Muramatsu, and F. F. Assaad. Quantum phase transitions in the kane-mele-hubbard model. *Phys. Rev. B*, 85:115132, Mar 2012.

[45] A.G. Abanov and P.B. Wiegmann. Theta-terms in nonlinear sigma-models. *Nuclear Physics B*, 570(3):685 – 698, 2000.

[46] Francesco Parisen Toldin, Martin Hohenadler, Fakher F. Assaad, and Igor F. Herbut. Fermionic quantum criticality in honeycomb and π-flux hubbard models: Finite-size scaling of renormalization-group-invariant observables from quantum monte carlo. *Phys. Rev. B*, 91:165108, Apr 2015.

[47] Yuichi Otsuka, Seiji Yunoki, and Sandro Sorella. Universal quantum criticality in the metal-insulator transition of two-dimensional interacting dirac electrons. *Phys. Rev. X*, 6:011029, Mar 2016.

[48] Nikolai Zerf, Luminita N. Mihaila, Peter Marquard, Igor F. Herbut, and Michael M. Scherer. Four-loop critical exponents for the gross-neveu-yukawa models. *Phys. Rev. D*, 96:096010, Nov 2017.

[49] Fakher F. Assaad and Igor F. Herbut. Pinning the order: The nature of quantum criticality in the hubbard model on honeycomb lattice. *Phys. Rev. X*, 3:031010, Aug 2013.

[50] Adam Nahum, J. T. Chalker, P. Serna, M. Ortuño, and A. M. Somoza. Deconfined quantum criticality, scaling violations, and classical loop models. *Phys. Rev. X*, 5:041048, Dec 2015.

[51] David Poland, Slava Rychkov, and Alessandro Vichi. The conformal bootstrap: Theory, numerical techniques, and applications. *Rev. Mod. Phys.*, 91:015002, Jan 2019.

[52] Yu Nakayama and Tomoki Ohtsuki. Necessary condition for emergent symmetry from the conformal bootstrap. *Phys. Rev. Lett.*, 117:131601, Sep 2016.

[53] A. B. Kuklov, M. Matsumoto, N. V. Prokof'ev, B. V. Svistunov, and M. Troyer. Deconfined criticality: Generic first-order transition in the su(2) symmetry case. *Phys. Rev. Lett.*, 101:050405, Aug 2008.

[54] Chong Wang, Adam Nahum, Max A. Metlitski, Cenke Xu, and T. Senthil. Deconfined quantum critical points: Symmetries and dualities. *Phys. Rev. X*, 7:031051, Sep 2017.

[55] V. Gorbenko, S. Rychkov, and B. Zan. Walking, Weak first-order transitions, and Complex CFTs. *ArXiv e-prints*, July 2018.

[56] Matteo Ippoliti, Roger S. K. Mong, Fakher F. Assaad, and Michael P. Zaletel. Half-filled landau levels: A continuum and sign-free regularization for three-dimensional quantum critical points. *Phys. Rev. B*, 98:235108, Dec 2018.

[57] M. A. Metlitski and R. Thorngren. Intrinsic and emergent anomalies at deconfined critical points. *Phys. Rev. B*, 98(8):085140, August 2018.

[58] Anders W. Sandvik. Stochastic series expansion method with operator-loop update. *Phys. Rev. B*, 59:R14157–R14160, Jun 1999.

[59] Anders W. Sandvik, Valeri N. Kotov, and Oleg P. Sushkov. Thermodynamics of a gas of deconfined bosonic spinons in two dimensions. *Phys. Rev. Lett.*, 106:207203, May 2011.

[60] Toshihiro Sato, Martin Hohenadler, and Fakher F. Assaad. Dirac fermions with competing orders: Non-landau transition with emergent symmetry. *Phys. Rev. Lett.*, 119:197203, Nov 2017.

[61] Lukas Janssen, Igor F. Herbut, and Michael M. Scherer. Compatible orders and fermion-induced emergent symmetry in dirac systems. *Phys. Rev. B*, 97:041117, Jan 2018.

[62] M. Hohenadler, Z. Y. Meng, T. C. Lang, S. Wessel, A. Muramatsu, and F. F. Assaad. Quantum phase transitions in the kane-mele-hubbard model. *Phys. Rev. B*, 85:115132, Mar 2012.

[63] R. Coldea, S. M. Hayden, G. Aeppli, T. G. Perring, C. D. Frost, T. E. Mason, S.-W. Cheong, and Z. Fisk. Spin waves and electronic interactions in la_2cuo_4. *Phys. Rev. Lett.*, 86:5377–5380, Jun 2001.

[64] D. J. Scalapino. A common thread: The pairing interaction for unconventional superconductors. *Rev. Mod. Phys.*, 84:1383–1417, Oct 2012.

[65] P. W. Anderson. The resonating valence bond state in la2cuo4 and superconductivity. *Science*, 235(4793):1196–1198, 1987.

[66] P.A. Lee, N. Nagaosa, and X.G. Wen. Doping a mott insulator: Physics of high-temperature superconductivity. *Rev. Mod. Phys.*, 78:17, 2006.

[67] P. Di Francesco, P. Mathieu, and D. Senechal. *Conformal Field Theory*. Springer Verlag, Berlin, Heidelberg, New York, 1997.

[68] M. Imada, A. Fujimori, and Y. Tokura. Metal-insulator transitions. *Rev. Mod. Phys.*, 70:1039, 1998.

[69] M. Imada, F. F. Assaad, H. Tsunetsugu, and Y. Motome. *cond-mat/9808044*.

[70] F. F. Assaad and M. Imada. Insulator-metal transition in the one and two-dimensional hubbard models. *Phys. Rev. Lett*, 76:3176, 1996.

[71] Gerardo Martinez and Peter Horsch. Spin polarons in the t-j model. *Phys. Rev. B*, 44:317–331, Jul 1991.

[72] R. Preuss, W. Hanke, and W. von der Linden. Quasiparticle dispersion of the 2d hubbard model: From an insulator to a metal. *Phys. Rev. Lett.*, 75:1344–1347, Aug 1995.

[73] Marcin Raczkowski, Robert Peters, Thị Thu Phùng, Nayuta Takemori, Fakher F. Assaad, Andreas Honecker, and Javad Vahedi. The hubbard model on the honeycomb lattice: from static and dynamical mean-field theories to lattice quantum monte carlo simulations. *arXiv:1908.04307*, 2019.

[74] Nick Bultinck, Eslam Khalaf, Shang Liu, Shubhayu Chatterjee, Ashvin Vishwanath, and Michael P. Zaletel. Ground state and hidden symmetry of magic-angle graphene at even integer filling. *Phys. Rev. X*, 10:031034, Aug 2020.

[75] M. O. Goerbig. Electronic properties of graphene in a strong magnetic field. *Rev. Mod. Phys.*, 83:1193–1243, Nov 2011.

[76] Maxim Kharitonov. Phase diagram for the $\nu = 0$ quantum hall state in monolayer graphene. *Phys. Rev. B*, 85:155439, Apr 2012.

[77] Junhyun Lee and Subir Sachdev. Wess-zumino-witten terms in graphene landau levels. *Phys. Rev. Lett.*, 114:226801, Jun 2015.

[78] S. L. Sondhi, A. Karlhede, S. A. Kivelson, and E. H. Rezayi. Skyrmions and the crossover from the integer to fractional quantum hall effect at small zeeman energies. *Phys. Rev. B*, 47:16419–16426, Jun 1993.

[79] F. D. M. Haldane. Spontaneous dimerization in the $s = \frac{1}{2}$ heisenberg antiferromagnetic chain with competing interactions. *Phys. Rev. B*, 25:4925–4928, Apr 1982.

[80] Christopher Mudry, Akira Furusaki, Takahiro Morimoto, and Toshiya Hikihara. Quantum phase transitions beyond landau-ginzburg theory in one-dimensional space revisited. *Phys. Rev. B*, 99:205153, May 2019.

[81] Manuel Weber, Francesco Parisen Toldin, and Martin Hohenadler. Competing Orders and Unconventional Criticality in the Su-Schrieffer-Heeger Model. May 2019.

[82] Zi-Xiang Li, Yi-Fan Jiang, and Hong Yao. Majorana-time-reversal symmetries: A fundamental principle for sign-problem-free quantum monte carlo simulations. *Phys. Rev. Lett.*, 117:267002, Dec 2016.

[83] Zhen Bi, Alex Rasmussen, Yoni BenTov, and Cenke Xu. Stable interacting (2 + 1)d conformal field theories at the boundary of a class of (3 + 1)d symmetry protected topological phases, 2016.

[84] Yuhai Liu, Zhenjiu Wang, Toshihiro Sato, Martin Hohenadler, Chong Wang, Wenan Guo, and Fakher F. Assaad. Superconductivity from the condensation of topological defects in a quantum spin-hall insulator. *Nature Communications*, 10(1):2658, 2019.

[85] Adam Nahum. Note on Wess-Zumino-Witten models and quasiuniversality in 2+1 dimensions. 2019.

[86] Ruochen Ma and Chong Wang. A theory of deconfined pseudo-criticality. 2019.

[87] Igor F. Herbut and Lukas Janssen. Topological mott insulator in three-dimensional systems with quadratic band touching. *Phys. Rev. Lett.*, 113:106401, Sep 2014.

[88] Qingquan Liu, Youjin Deng, Timothy M. Garoni, and Henk W.J. Blöte. The o(n) loop model on a three-dimensional lattice. *Nuclear Physics B*, 859(2):107 – 128, 2012.